Unidirectional Active Acoustic Control for Launch Vehicle Fairings

by

Carlos Gutiérrez

B.S. Mechanical Engineering
Florida International University, 1996

Submitted to the Department of Mechanical Engineering
in Partial Fulfillment of the Requirements for the Degree of
Master of Science in Mechanical Engineering

at the

Massachusetts Institute of Technology

February 2000

Signature of Author.....
Department of Mechanical Engineering
October 29, 1999

Certified by.....
John-Paul Clarke
Charles Stark Draper Assistant Professor of Aeronautics and Astronautics
Thesis Supervisor

Accepted by.....
Ain A. Sonin
Chairman, Department Committee on Graduate Studies

Unidirectional Active Acoustic Control for Launch Vehicle Fairings

by

Carlos Gutiérrez

Submitted to the Department of Mechanical Engineering
on October 29, 1999 in Partial Fulfillment of the
Requirements for the Degree of Master of Science in
Mechanical Engineering at the
Massachusetts Institute of Technology

ABSTRACT

Large amplitude vibro-acoustic loads during launch cause 40% of first day spacecraft failures. Structural-acoustic control offers the potential of reducing these loads without increasing payload mass by actively stiffening and destiffening the structure of the fairing to reduce acoustic transmission and reflection. In this thesis, two methods of structural-acoustic control for launch vehicle fairings are investigated. Both methods employ feedback control using only structural sensors and actuators to obtain global attenuation of the acoustic field within the fairing. This approach avoids the need for sensors and actuators near the payload, and is more effective at reducing the effect of disturbances than feedforward control.

The first method implements simultaneous transmission and reflection control on the structure. Individual Linear Quadratic Gaussian controllers are designed for transmission and reflection control and combined using superposition. Two separate sets of sensors are investigated: a microphone/accelerometer pair and a microphone/PVDF pair. Similar 10-1000 Hz broadband attenuation of 3.6 dB was predicted using both sensor pairs, but experimental results showed that the microphone/PVDF pair attenuated the broadband acoustics by 4.14 dB, whereas the microphone/accelerometer pair only attenuated the broadband acoustics by 2.62 dB.

The second method implements an acoustic power diode which allows acoustic energy to flow though the plate in only one direction, in this case, from the inside to the outside of the payload fairing. The diode only targeted the first structural mode due to sensor limitations. It was implemented on a symmetric acoustic chamber to show the effect of the diode depending on the end where the disturbance source was located. Although the diode effect was present, its performance was less than predicted. An attenuation of 10.56 dB at the first acoustic mode was obtained, with the possibility of even higher performance were the accelerometer to perform as predicted.

Thesis supervisor:
John-Paul Clarke
Charles Stark Draper Assistant Professor of Aeronautics and Astronautics

Acknowledgements

Funding for this research was provided by the U.S. Air Force Office for Scientific Research (AFOSR), under AASERT Grant No. F49620-96-1-0290 for the purpose of Active Acoustic Launch Load Alleviation with Capt. Brian Sanders as the AFOSR contract monitor, Charlotte Morse as the MIT senior contract administrator, SharonLeah Brown and the MIT fiscal officer and Karen Buck as the AFOSR contract monitor.

Table of Contents

List of Figures

List of Tables

Chapter 1

1. Introduction

1.1 Motivation

The purpose of this research was to find a method that reduces the internal acoustic field inside a rocket fairing during launch. Rockets transmit severe vibro-acoustic loads to their payloads, whether satellites or other types of spacecraft, during launch. These loads cause over 40% of first day spacecraft failures, and they also have several other consequences on the payloads. Of great importance among these is the structural design of the payload, since it has to be designed to survive the first few minutes of its life during launch. The reduction of these vibro-acoustic launch loads would have the double benefit of reducing the number of failures, as well as a relaxation in the design parameters to survive launch. This would lead to lower costs for the manufacturer and lower launch costs, as well as increased performance of the launch vehicle.

These vibro-acoustic loads come from three sources: aerodynamic buffeting during flight, ground reflection of the external energy generated by the rocket engines [10] and vibration of the rocket structure. As the rocket moves through the atmosphere,

noise is generated during transonic and maximum dynamic pressure flight. This acoustic energy impinges on the fairing and is transmitted to the inside. Similarly, the noise generated by the rocket engines reflects from the ground and is transmitted through the fairing. Finally, the mechanical vibration of the rocket also adds energy to the inside of the payload fairing. The ultimate effect of these three phenomena is the excitation of the reverberant acoustic field enclosed by the fairing.

Currently there is a trend in the aerospace industry to use more composite materials in structures. They have high strength and low mass, which are desirable for structural design of rockets. The use of composite materials in the construction of aerospace rockets has had the consequence of allowing more acoustic energy to be transmitted to the inside of the fairings, as the reduction in the mass of the fairing reduces the structure's resistance to acoustic transmission. The primary objective of this research is, then, to change the apparent mass of the fairing using smart materials and active control techniques to reduce the amount of energy transmitted into the fairing.

1.2 Control Techniques

The vibro-acoustic problem has been divided into two categories: transmission and reflection. The term *transmission* refers to the vibro-acoustic energy that reaches the payload cavity from the outside. The term *reflection* refers to the energy that has entered the payload and is reflected inside the payload fairing.

Transmission control can be done using passive and active techniques. Passive techniques consist of redesigning the structure, which entails changing either the mass, stiffness or damping of the structure. Among these, the addition of non-structural mass is

the most common technique used in payload fairings to reduce transmission [11]. However, launch costs limit the amount of mass, whether added mass or damping mechanisms, which can be added to a rocket, and the performance obtained from these techniques is moderate. Another passive technique is the use of a gas other than air inside the payload cavity, such as helium. [12,14] The structural-acoustic coupling is reduced due to helium's lower density, but at the same time structural vibrations can increase in amplitude due to the decrease of the aerodynamic damping. Active transmission control seeks to overcome these limitations by using feedback compensators that add active damping to the structure, which result in high damping ratios.

Transmitted energy enters the fairing via two paths. In the first, the energy goes through the support structure of the rocket and vibrates the fairing walls, thus acting on the internal acoustic field. In the second, energy generated outside of the faring impinges on the fairing making it vibrate, which in turn acts on the internal acoustic field. The transmission control problem seeks to reduce the amount of energy that is transmitted into the payload cavity.

No control technique will be completely successful in preventing energy from being transmitted into the payload cavity. The energy that does go in will be reflected off the walls of the internal cavity. Constructive interference between this reflected energy and that coming in will cause high amplitude resonances at the acoustic modes. The reflection control problems seeks to reduce the reflection of the energy, thus attenuating the amplitude of the acoustic modes.

Reflection control can also be done using passive and active techniques. Current state of the art in passive noise cancellation inside rocket fairings consists mostly of the

use of acoustic blankets [13]. These blankets, attached to the inside of the fairing, provide a damping mechanism for the acoustic energy being reflected off the inside walls of the fairing that converts the acoustic energy into heat. However, they are only effective for acoustic frequencies higher than 500Hz. This is because the blankets need to have a thickness that is a considerable fraction of the acoustic wavelength to be effective. At lower frequencies, and thus larger wavelengths, the thickness of the blankets has to increase, which in turn adds more mass to the rocket. Practical weight and size considerations have set the limit around 500Hz.

Active reflection control techniques seek to complement the use of the blankets by targeting the lower frequencies. There are two types of active acoustic control: Active Noise Control (ANC) and Active Structural Acoustic Control (ASAC). ANC [15,16,17] relies on destructive interference at the location of the sensor, (usually a microphone) between the active control acoustic waves, generated by secondary acoustic sources such as speakers, and the disturbance waves. It can cause amplifications further away from the sensor. It is well suited for cancellation of tonal disturbances and uses feedforward measurements of the noise source. These two facts make it unfeasible to use inside payload fairings since the disturbance is not tonal but rather diffuse and broadband. Also, global attenuation is required, not only attenuation at the location of the sensors.

ASAC [24,25,26] relies on actuating the fairing structure itself to control its vibration and thus attenuate the acoustic field inside. Since the whole structure is controlled, the acoustic attenuation that is obtained is global. ASAC uses only structural actuators and can use either structural or acoustic sensors. Performance using only structural sensors, which would be preferable inside a rocket fairing, is limited by the

observability of the acoustic modes by the structure. Typically, coupling between the acoustics and the structure is poor, limiting the performance obtained using this technique. Use of acoustic sensors, such as microphones, is not as desirable, but it has the distinct advantage of producing increased performance. The use of a structural membrane was investigated to avoid using acoustic sensors, although most of the work presented in this thesis was performed using microphones.

1.3 Past Work

Past work on this project at MIT has successfully identified methods that can be used to reduce transmission and reflection using a one-dimensional wave-guide. Glaese [1] developed a dereverberated coupled field model and an LQG impedance matching methodology to reduce the amplitude of the acoustic field inside the wave-guide.

Asari [2] developed a PVDF structural sensor and LQG controllers using system identification techniques to reduce transmission through an aluminum plate inside a one-dimensional acoustic test chamber designed at MIT, which is described later on in this thesis. He also implemented two LQG controllers using successive loop closure to reduce transmission through the plate and reflection inside the acoustic test chamber.

Pascal [3] developed a Finite Element Method (FEM) model of the acoustic test chamber and used it to develop controllers, and validated its use as a development tool by comparing their performance with those developed using system identification techniques. He also investigated the use of shaped and distributed sensors and actuators, in particular, a sensuator or self-sensing actuator. He compared experimental results with those obtained on the FEM model.

1.4 Current Work

This thesis presents two approaches to reducing the acoustic fields within launch vehicle fairings. The first extends the work done by Asari in transmission and reflection control by removing the implementation limitations of Asari's control design. The second applies the concept of a structure-structure power diode presented by Hyde [5] to the domain of structural-acoustic transmission and reflection control.

Asari used a PZT patch on a plate with a polyvinylidene fluoride (PVDF) sensor to control transmission and an external speaker with a microphone as a sensor to control reflection. The performance obtained was high, but a shortcoming of his design was the use of the secondary external speaker. This is undesired since it requires additional hardware that cannot be placed inside a rocket fairing. In Chapter 2, both transmission and reflection control are performed by using a single PZT patch on a plate as an actuator, and both the PVDF and the microphone as sensors.

Hyde [5] introduced the concept of one-way vibration control for isolation of two structures, in particular, a base and a payload joined together by some interface. The goal of this controller is to prevent vibrational energy to enter the payload from the base but to allow the payload's vibrational energy to be removed from it. From an energy flow point of view, this controller acts as a diode, allowing the flow of energy in only one direction, from the payload to the base. His concept of this "power diode" was extended from a structural problem to a structural-acoustic problem. Using this power diode, both transmission and reflection control are effectively performed by the same controller since

it prevents energy from going into the acoustic cavity (transmission control) while allowing the energy inside the payload cavity to exit (reflection control).

1.5 Thesis Outline

In Chapter 2, an overview of the techniques used for modeling and controller design is presented. Chapter 3 focuses on the controller design process and the predicted results obtained for simultaneous transmission and reflection control on a circular plate. Chapter 4 presents the structural-acoustic power diode design process and the predicted results. Chapter 5 presents the experimental results of the two techniques developed in Chapters 3 and 4 applied to the MIT acoustic test chamber. Conclusions as well as some guidelines for future work are presented in Chapter 6.

Chapter 2

2. Modeling and Controller Synthesis

This thesis is focused on experimental implementation of modeling and control techniques. An overview of the techniques used will be presented to familiarize the reader with the procedure used.

2.1 Modeling procedure

The block diagram in Figure 2.1 shows the basic control loop design used in this experiment. The plant, in this case the acoustic test chamber, requires the following open loop transfer functions: disturbance to performance sensors (G_{zw}), disturbance to feedback sensors (G_{yw}), control to performance sensors (G_{zu}) and control to feedback sensors (G_{yu}). The controllers can then be designed once the model of the plant has been obtained.

A measurement based technique was used to develop a mathematical model of the plant. This technique was used since it has the advantage of producing a model that includes all couplings of the various fields in the model, as well as the dynamics of the

actuators and sensors, and any gains introduced by the supporting electronics. It must be noted that this method has some disadvantages. Every time the chamber is reconfigured a new model must be made so that variations in the plant (even slight variations) that resulted from the reconfiguration are included. Also, any insight into the physics of the plant is lost since the model is basically fit to a set of measurements.

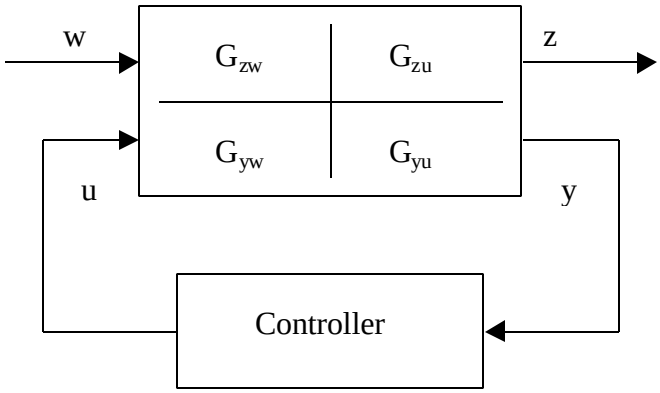

Figure 2.1 Diagram of Control Loop Design

This technique is based on the open loop measurements of the above mentioned transfer functions between inputs and outputs of the plant. Band limited white noise was used to excite the inputs: a disturbance source and the control actuator. Measurements were taken from all sensors: structural acceleration and strain sensors and acoustic sensor inside the chamber.

Once the open loop transfer functions had been measured, a state-space model of the plant is developed using the software Transfer Function ID (TFID) developed by Jacques [6]. It is based on the Frequency Domain Observability Range Space Extraction (FORSE) technique he developed by extending the Observability Range Space Extraction (ORSE) technique developed by Liu [7]. This state space model of the plant can then be used to develop controllers.

To reduce the time required for controller design the model that is developed has the least number of states necessary to accurately represent the plant. The procedure to obtain this minimum order model is iterative, and can be briefly explained as follows. The first step is to estimate the number of states in the model and tune it. Using the options in TFID, the model is reduced either by manually removing the poles that appear to be of less importance, or removing the states corresponding to the smaller Hankel singular values. After the model is reduced, it is tuned again to readjust any parameters and then compared with the measured data for accuracy. These steps are then repeated until the minimal model that is still accurate is obtained.

The FEM model developed by Pascal [2] on ANSYS was used as a complement to identify the modes of the system. The solution of the FEM model was used as an estimate to identify the structural and acoustic modes of the plate and chamber, respectively.

2.2 Controller Design

2.2.1 Linear Quadratic Gaussian (LQG) Control Design

The Linear Quadratic Gaussian (LQG) control design method was used. As its name implies, it is based on a linear model of the system, and it is composed of a regulator obtained from the Linear Quadratic Regulator (LQR) problem, and an estimator. The estimator, based on the Kalman filter, is used to estimate the states of the system based on sensor outputs, and the regulator uses these estimated states to calculate the control gain.

LQG design uses a standard state-space representation of the linear plant

$$\begin{aligned} \dot{x} &= Ax + B_u u + B_w w \\ y &= C_y x + D_{yu} u + D_{yw} w \\ z &= C_z x + D_{zu} u + D_{zw} w \end{aligned} \tag{2.1}$$

and minimizes the quadratic cost given by

$$J = \int_0^\infty (x^T Q x + u^T R u + 2u^T N x) dt \tag{2.2}$$

Q is the state penalty matrix, R is the control penalty matrix and N is the cross-coupled penalty matrix. For this problem, the cross-coupled penalty matrix N is not used, and Equation (2.2) reduces to

$$J = \int_0^\infty (x^T Q x + u^T R u) dt \tag{2.3}$$

The control gain K and the estimator filter gain L can be derived from the following Ricatti equations for S and Σ:

$$\begin{aligned} SA + A^T S + Q - SB_u R^{-1} {B_u}^T S = 0 \qquad & G = R^{-1} {B_u}^T S \\ A\Sigma + \Sigma A^T + B_w \Xi {B_w}^T - \Sigma {C_y}^T \Theta^{-1} C_y \Sigma = 0 \quad & L = \Sigma {C_y}^T \Theta^{-1} \end{aligned} \tag{2.4}$$

where Ξ is the process noise intensity and Θ is the sensor noise intensity. The controller equations are then

$$\begin{aligned} \dot{\hat{x}} &= (A - B_u K - LCy + LD_{yu} K)\hat{x} + Ly \\ u &= -K\hat{x} \end{aligned} \tag{2.5}$$

where u is the feedback signal.

2.2.2 Frequency Weighted LQG (FWLQG)

The performance of the LQR, and by extension, the LQG controller and the desired control performance are often not the same, and this discrepancy can be attributed

to the difference between the frequency domain specifications of the control system and the time domain nature of the LQR method. Using frequency weighting cost functionals [8,9], state and control penalties can be specified in the frequency domain thus obtaining a Frequency Weighted Linear Quadratic Gaussian (FWLQG) controller.

Using Parseval's Theorem, the cost functional in Equation {2.3) can be written in the frequency domain

$$J = \int_0^\infty [x^T(t)Qx(t) + u(t)^T Ru(t)]dt = \frac{1}{2p}\int_0^\infty [x^H(jw)Qx(jw) + u(jw)^H Ru(jw)]dw \qquad (2.6)$$

Since Q and R are constant in the frequency domain, the cost functional weights the states and the control equally at all frequencies. To modify these weights as a function of frequency, user specified frequency weights $W_1(jw)$ and $W_2(jw)$ are added to the cost functional

$$J = \frac{1}{2p}\int_0^\infty [x^H(jw)W_1(jw)^H W_1(jw)x(jw) + u(jw)^H W_2(jw)^H W_2(jw)u(jw)]dw \qquad (2.7)$$

To design the FWLQG controller, the frequency weights must be written back in the time domain, obtaining their state-space realization. We thus obtain

$$z_1(s) = W_1(s)x(s) \qquad where \qquad W_1(s) = C_1(sI - A_1)^{-1}B_1 + D_1 \qquad (2.8)$$

$$z_2(s) = W_2(s)u(s) \qquad where \qquad W_2(s) = C_2(sI - A_2)^{-1}B_2 + D_2 \qquad (2.9)$$

The cost functional from Equation (2.7) now becomes

$$J = \frac{1}{2p}\int_0^\infty [z_1(t)^T z_1(t) + z_2(t)^T z_2(t)]dt \qquad (2.10)$$

To use these frequency weights, the state-space realization of the system from Equation (2.1) can be augmented including these weights in the following manner

$$\begin{bmatrix} \dot{x} \\ \dot{x}_1 \\ \dot{x}_2 \end{bmatrix} = \begin{bmatrix} A & 0 & 0 \\ B_1 C_y & A_1 & 0 \\ 0 & 0 & A_2 \end{bmatrix} \cdot \begin{bmatrix} x \\ x_1 \\ x_2 \end{bmatrix} + \begin{bmatrix} B_u \\ B_1 D_u \\ B_2 \end{bmatrix} u + \begin{bmatrix} B_w \\ B_1 D_w \\ 0 \end{bmatrix} w$$

$$\begin{bmatrix} z_1 \\ z_2 \end{bmatrix} = \begin{bmatrix} D_1 C_y & C_1 & 0 \\ 0 & 0 & C_2 \end{bmatrix} \cdot \begin{bmatrix} x \\ x_1 \\ x_2 \end{bmatrix} + \begin{bmatrix} D_1 D_u \\ D_2 \end{bmatrix} u + \begin{bmatrix} D_1 D_w \\ 0 \end{bmatrix} w \tag{2.11}$$

The cost functional now becomes

$$J_{FW} = \int_0^\infty (X^T C_{aug}{}^T C_{aug} X + u^T D_{aug}{}^T D_{aug} u + 2 X^T C_{aug}{}^T D_{aug} u) dt \tag{2.12}$$

For this particular problem, only the control input frequency weight W_2 was used. The resulting state-space realization of the system is

$$\begin{bmatrix} \dot{x} \\ \dot{x}_2 \end{bmatrix} = \begin{bmatrix} A & 0 \\ 0 & A_2 \end{bmatrix} \cdot \begin{bmatrix} x \\ x_2 \end{bmatrix} + \begin{bmatrix} B_u \\ B_2 \end{bmatrix} u + \begin{bmatrix} B_w \\ 0 \end{bmatrix} w$$

$$\begin{bmatrix} z_1 \\ z_2 \end{bmatrix} = \begin{bmatrix} C_y & 0 \\ 0 & C_2 \end{bmatrix} \cdot \begin{bmatrix} x \\ x_2 \end{bmatrix} + \begin{bmatrix} D_u \\ D_2 \end{bmatrix} u + \begin{bmatrix} D_w \\ 0 \end{bmatrix} w \tag{2.13}$$

and its cost functional is, without using the cross-coupling weight

$$J_{FW} = \int_0^\infty (X^T C_{aug}{}^T C_{aug} X + u^T D_{aug}{}^T D_{aug} u) dt \tag{2.14}$$

2.3 Application

The above methods were used in the design of the controllers presented in the following chapters. Minimal mathematical models were constructed from measurements of the test chamber, and FWLQG control design techniques were used to synthesize the appropriate controllers.

Chapter 3

3. Combined Transmission and Reflection Control on a Plate

In this chapter, transmission and reflection control are simultaneously performed on a plate using two individual controllers, a structural controller and an acoustic controller. Two different sets of sensors are also used, a microphone/accelerometer pair and a microphone/PVDF pair. The attenuation obtained from each of the two configurations is similar.

3.1 Background

Transmission control involves the attenuation of the acoustic energy that enters the payload faring from the outside through the fairing itself. In the one dimensional case that is studied in this chapter, transmission control involves the attenuation of the acoustic energy that is generated by a disturbance speaker in the top chamber and enters the bottom chamber of the test setup through an aluminum plate. When a wave generated by the speaker impinges on the top of the plate, the plate responds by vibrating. Part of this energy is reflected, but this vibration also causes a pressure change on the bottom of the

plate, which becomes a pressure wave that moves through the bottom chamber. The rigidity of the plate determines the amount of energy that is transmitted through it: the higher the rigidity, the lower the energy transmitted. As a consequence of this, it is desirable to make the plate as rigid as possible. The same is true for the actual fairing.

There are two ways to increase in rigidity. The simplest is to use a thicker plate. However, this entails an increase in the mass of the structure, which is not desirable due to an increase in launch costs. Nowadays, the trend is actually moving in the opposite direction since composite structures, which are lighter, are being used to reduce weight and thus cost. The use of composites, however, increases the acoustic transmissibility of he fairing. An alternative is to use active control and smart materials, such as piezoelectric wafers, to increase the apparent rigidity of the plate.

Since no structure will be infinitely rigid or rigid enough to totally eliminate transmission, some energy will always enter the payload fairing and reverberate inside. Reflection control involves the attenuation of the intensity of the acoustic energy that is reverberating inside the acoustic chamber. Reflection control has a requirement that goes counter to the one needed for transmission control: it requires the structure to be less rigid so that more energy will be transmitted to the outside of the chamber.

Asari dealt with the reflection problem by controlling one of the boundary conditions of the waveguide. In other words, the control speaker in Figure 3.2 was used as a boundary whose condition could be altered to obtain acoustic attenuation inside the bottom chamber. The procedure was successful, although it presents a serious implementation drawback when the procedure is to be used inside an actual rocket fairing. Asari requires the use of a secondary speaker to attenuate the acoustics, which is

unfeasible inside actual rocket payload fairings. Not only would a whole array of speakers be needed, adding considerable mass, but also there is very little space available for such hardware.

To circumvent this limitation, a strategy was developed to perform simultaneous transmission and reflection control without the need for a secondary speaker. In this new approach, the plate is simultaneously stiffened and destiffened to perform transmission and reflection control. It should be expected that the performance of this setup should not be as high as that of Asari, since the plate is not designed to interact with acoustics as well as a speaker.

3.1.1 Single-Input, Multiple-Output Design

The use of two sensors and one actuator requires a single-input, multiple-output (SIMO) design. The actuator is the PZT patch on the plate, and the sensors are a microphone collocated as much as possible with the plate to measure pressure and either an accelerometer or the PVDF ring on the plate to measure the plate's motion.

Since LQG control theory will be used to develop the structural and acoustic controllers, an open loop plant is necessary. Two measurement-based models were developed with two inputs and two outputs using the technique presented in Chapter 2. In one case, the inputs were the disturbance w and the control u, and the outputs were the pressure sensor (Mic2) and an accelerometer on the plate. In the second case, the inputs were the same, but the outputs were the pressure sensor (Mic2) and the PVDF ring on the plate. A comparison of both designs will be presented at the end of the chapter, thus providing a comparison of the sensor combinations.

The models were converted to a modal form, and structural and acoustic controllers were designed based on the two models. Each controller was developed independently, that is, that successive loop closure was not used. Rather, the output of the two independent controllers was added, based on the principle of superposition, to obtain the desired transmission and reflection control. Figure 3.1 shows a diagram of the design.

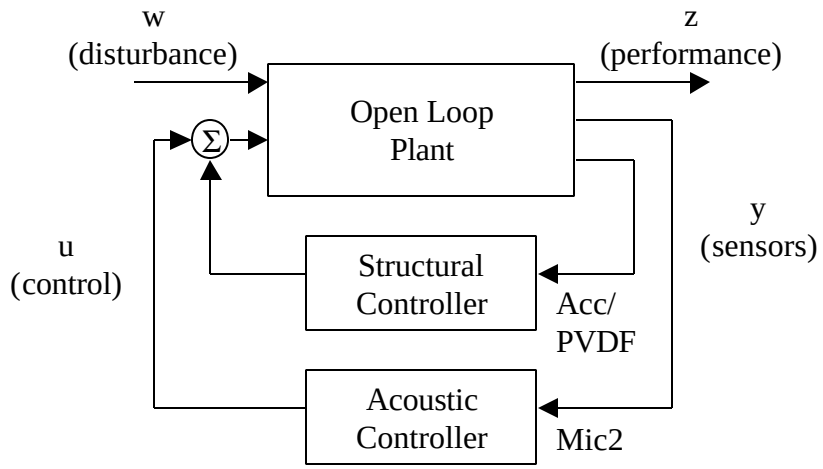

Figure 3.1 Diagram of Structural Transmission/Reflection Control

3.2 Test Chamber Description

The work presented in this chapter concentrates on computer implementation of modeling and control design methodologies for combined transmission and reflection control. A description of the experimental setup is presented below.

For the transmission and reflection control problem, a one-dimensional test chamber was used, as seen in Figure 3.2. It is 5 feet long and is made from 12-inch diameter steel pipe with ¾ inch wall thickness. The ends are closed off with flat ½ inch

thick steel plates. The chamber is made from several pipe sections. Two sections are 15 inches long, two sections are 7.5 inches long, and the two end sections are 7.5 inches long and contain each a ten inch dual voice coil subwoofer speaker that is attached to the inner walls of the sections with an aluminum ring. Because of the speaker, the effective length of the end sections is 3.5 inches, and the maximum length of the waveguide, when using all sections, is 52 inches. For this experiment, all sections were used. The joints between each section are sealed tightly with a ring of hardened RTV silicone as well as duct tape to maintain the interior chamber as acoustically isolated from the exterior as possible.

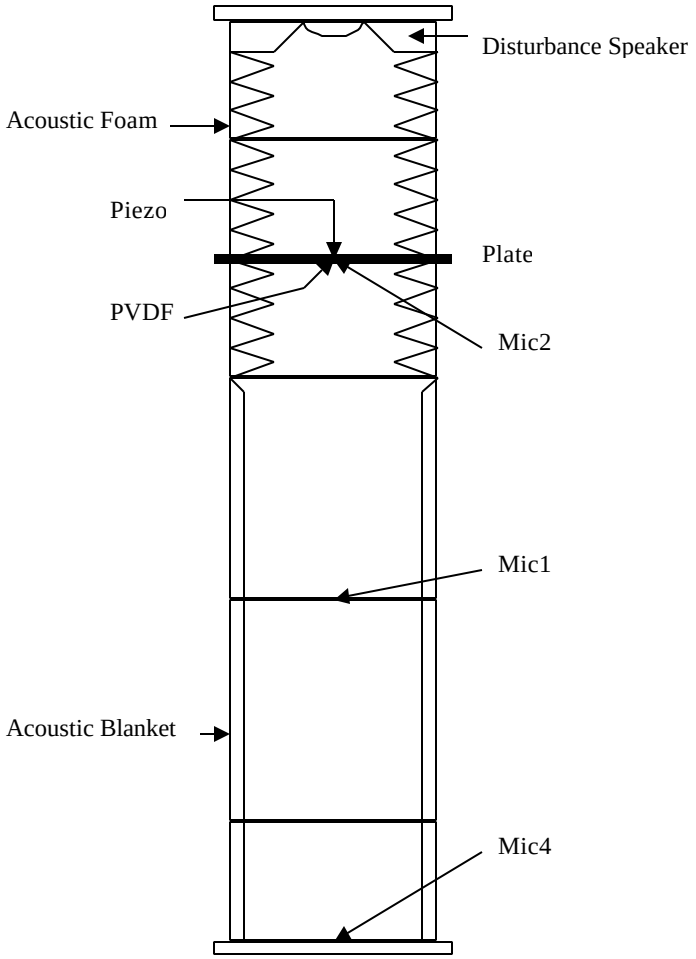

Figure 3.2 Diagram of Test Chamber for Transmission and Reflection Control

The chamber is made out of several sections for various reasons. Firstly, it was necessary to allow a single person to relocate it. Secondly, it allows for several configurations of the chamber depending on the need of the experiment. Thirdly, it also allows an access path for the cabling of the sensors and actuators that are placed inside the test chamber.

The chamber is divided by a 1/32-inch thick aluminum plate into two smaller chambers, an "exterior" chamber that is 11 inches long and an "interior" chamber that is 41 inches long. The inside of the top or exterior chamber is lined with acoustic foam to minimize reverberation and simulate an open acoustic field. The top speaker is used as a white noise disturbance source. The inside of the bottom or interior chamber is lined with a band of foam and a fiberglass blanket below it to simulate high frequency attenuation from real acoustic blankets found in rockets. The bottom speaker is not used in this experiment.

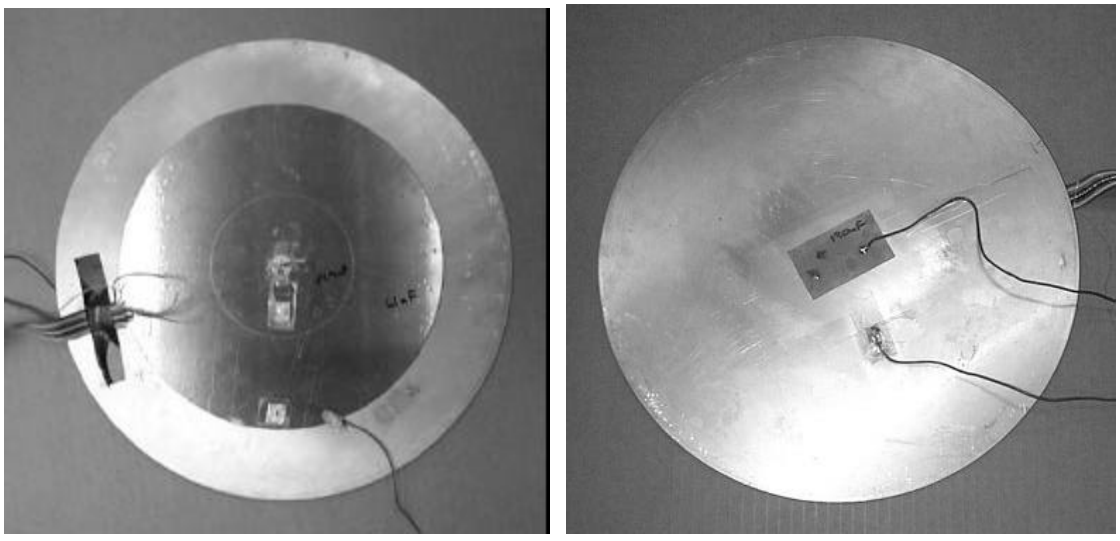

Figure 3.3 Top and Bottom Views of Plate

The plate can be seen in Figure 3.3. It is a 14-inch diameter, 1/32-inch thick aluminum plate. On one side, a rectangular PZT crystal patch is located at the center,

which is used as a structural actuator. One the other side there is an area averaging piezoelectric strain sensor made out of PVDF [2,4]. An accelerometer is also located at the center of the plate.

Five microphones are located throughout the chamber to measure the pressure. Two are located inside the top chamber, one close to the plate and another one close to the speaker. These two microphones are not necessary for the experiment and are used only to check sound levels inside the top chamber. The other three microphones are located in the bottom chamber, one below the plate (Mic2), the second one halfway through the chamber (Mic1) and the third one near the bottom speaker (Mic4). All five microphones are located on the longitudinal axis of the chamber. The microphones in the bottom chamber are either used as sensors for feedback (Mic2) or performance sensors (Mic2, Mic1 and Mic4).

The electronics used to measure, power and condition these sensors and actuators is the same as used by Asari [2].

3.3 Accelerometer and Pressure Feedback

3.3.1 Plant Identification

The first model that was used utilized the accelerometer and a microphone under the plate as feedback (Mic2). The actuator was the single PZT crystal on the plate. A model with 58 states was obtained from the measurements using the FORSE algorithm implemented in TFID software. Figure 3.4 shows a comparison of the modeled and the measured transfer function G_{yu} from the PZT to the accelerometer on the plate. It can be

seen that the model resembles the data very closely. It also ignores some of the noise that is introduced into the measured transfer function, especially the peaks introduced at 60Hz and its multiples, which correspond to feedthrough of the electrical frequency.

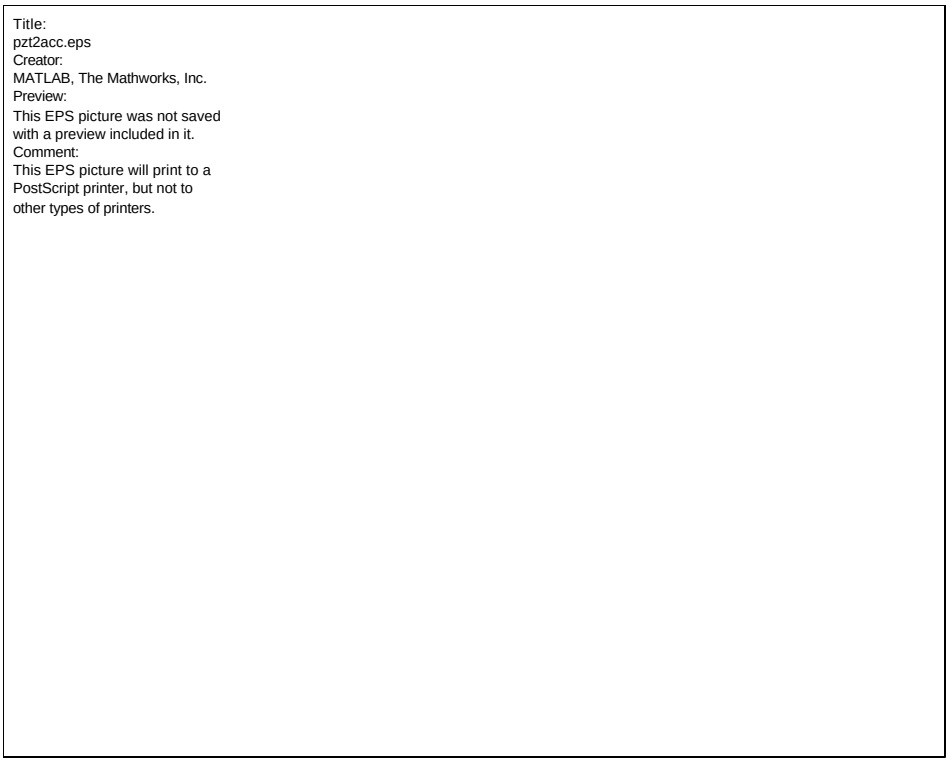

Figure 3.4 PZT to Accelerometer Model and Data Transfer Functions

Figure 3.4 also shows the location of the first three symmetric plate modes, which were targeted by the structural controller. These very observable poles are located at 79.8 Hz, 290.8 Hz and 682 Hz, respectively. The collocation of the actuator/sensor pair can also been seen by the bounded phase up to 1 kHz in the phase plot, and also by the alternating pole-zero pattern in the magnitude plot. There are other poles that appear in the transfer function that correspond to the asymmetric modes of the plate, the acoustic modes of the chambers and the speaker modes. These are less observable and thus less controllable than the symmetric plate modes.

Figure 3.5 shows the transfer function between the disturbance or top speaker and Mic2, located just under the plate. It is seen that the model and data transfer functions also correlate very well. This transfer function allows us to identify the acoustic modes. The first acoustic mode is located at 138.4 Hz, the second acoustic mode is located at 332 Hz and the third acoustic mode is at 482.9 Hz. These are the three acoustic modes that were targeted by the acoustic controller. As before, the other poles that appear in the transfer functions are higher frequency acoustic modes, speaker modes or plate modes that are also picked up by the microphones. Since the actuator and the sensor are not collocated in this case, there are some missing zeros in the transfer functions, as well as frequency roll-off as the frequency increases.

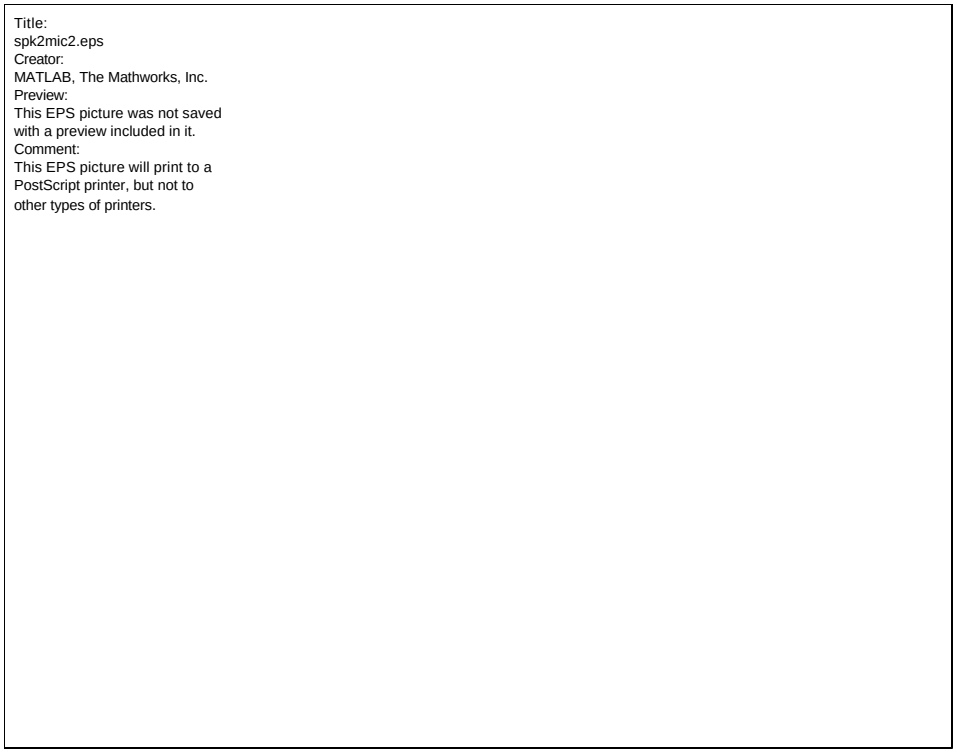

Figure 3.5 Speaker to Mic2 Model and Data Transfer Functions

3.3.2 Controller Design

Once the modes of interest, both structural and acoustic, were identified, the structural and acoustic controllers were developed. As was stated previously, the controllers were designed independently of each other and combined using superposition rather than using successive loop closure.

Superposition was chosen over successive loop closure since only one actuator is being used. The structural loop requires the stiffening of the plate modes to reduce transmission, whereas the acoustic loop requires the destiffening of the plate to reduce reflection. If successive loop closure were used as implemented by Asari, the two controllers would issue contradictory commands to the PZT. At the plate modes, the structural controller would be telling the PZT to add damping to the mode, whereas the acoustic controller would be telling the PZT to reduce the damping. Whether damping is increased or decreased will depend on the magnitude of the command issued by each controller. However, there is no simple way of determining which of the two commands will override the other, and thus the final command received by the controller.

By using superposition, each of the controllers is allowed to independently target the structural and acoustic modes, and the two signals are then combined to obtain both transmission and reflection control on the plate. Figure 3.6 shows the results obtained from each independent controller. The structural controller targets the first three structural modes at 79.8 Hz, 290.8 Hz and 682 Hz, respectively, and the acoustic controller targets the first three acoustic modes at 138.4 Hz, 332 Hz and 482.9 Hz, respectively.

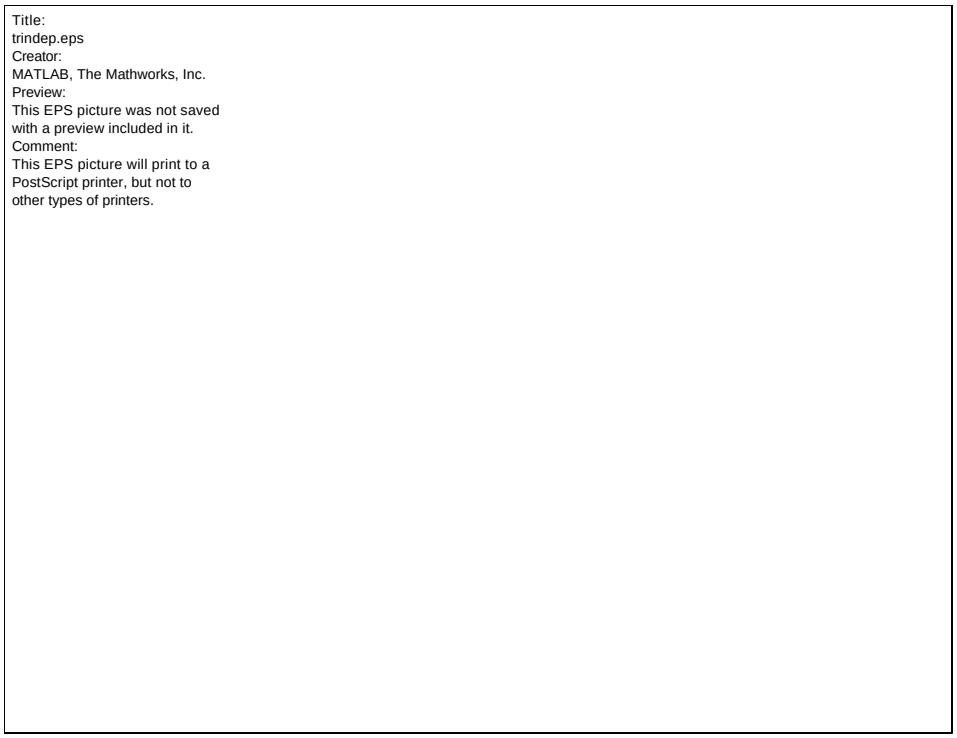

Figure 3.6 Independent Transmission and Reflection Control - Top Speaker to Mic2

Table 3.1 Attenuation for Transmission/Reflection Control using Accelerometer/Mic2

Mode	Attenuation (dB)
Structural1 - 78.9 Hz	9.64
Structural2 - 290.8 Hz	1.69
Structural3 - 682 HZ	-2.49
Acoustic1 - 138.4 Hz	3.51
Acoustic2 - 332 Hz	13.9
Acoustic3 - 482.9 Hz	4.19
Broadband (10-1000 Hz)	4.02

Table 3.1 shows the attenuation obtained at each of the modes that are targeted as well as the broadband performance from 10 Hz to 1000 Hz. Figure 3.7 shows the structural (transmission) controller and Figure 3.8 shows the Nichols plot of the structural loop transmission.

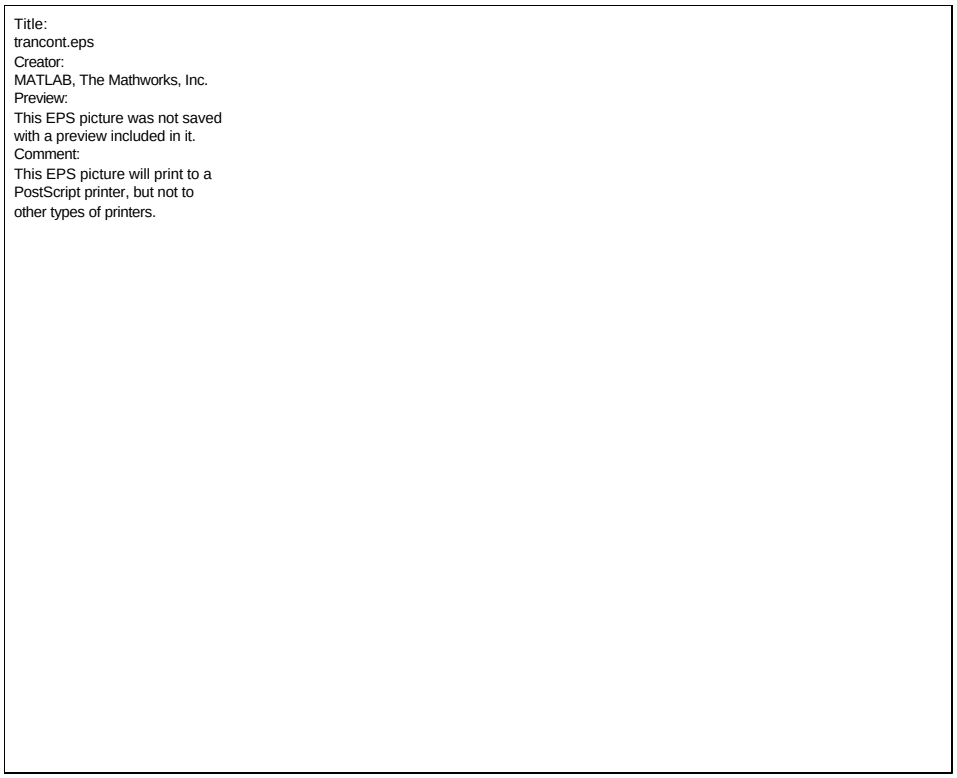

Figure 3.7 Structural (Transmission) Controller

The structural loop transmission was obtained by convolving the structural controller around the open loop transfer function G_{yu}, that is, from the PZT controller to the accelerometer. Figure 3.8 shows that there are three loops that have a magnitude greater than one, which correspond to the three structural modes that are controlled.

From the Nichols plot of the structural loop transmission, it seems that better performance could have been obtained by simply increasing the gain of the controller. However, since it was also desirable to have a stable controller this was a limiting factor in the design. Several attempts were made to increase the gain, and it was found that the loop transmission would still be stable even if an unstable controller was designed, with a corresponding increase in performance. However, this introduces complications when the controller is going to be implemented experimentally, since care has to be taken not to

destabilize the controller before the whole loop transmission has been activated. It was therefore preferable to use a stable controller at the expense of lower performance.

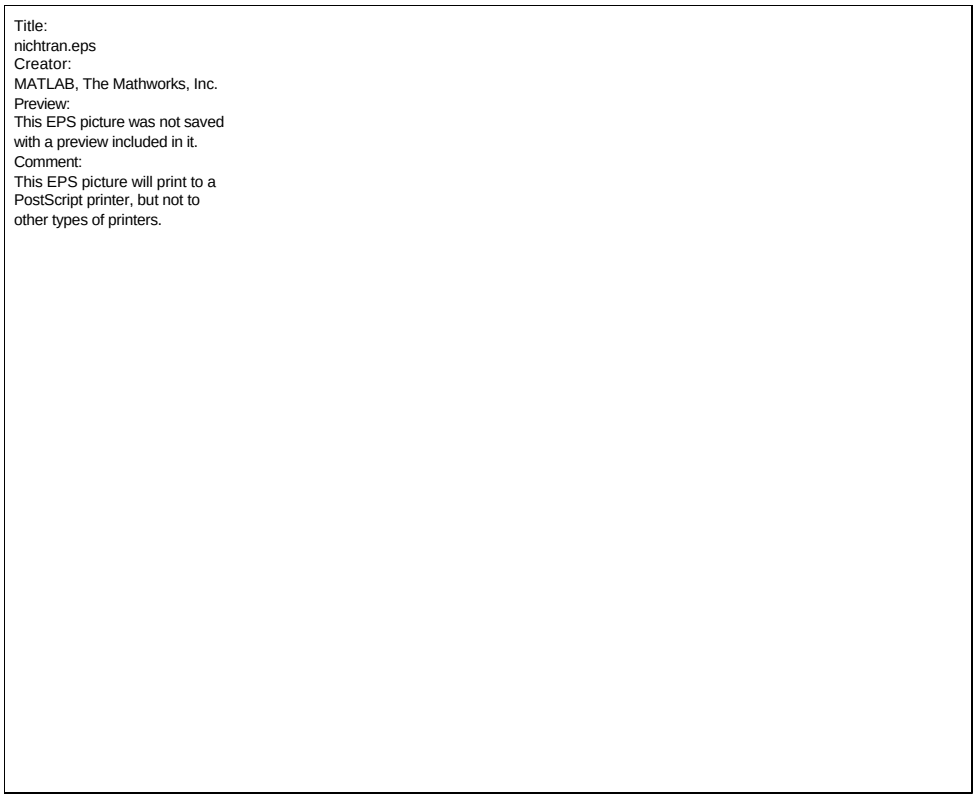

Figure 3.8 Nichols Plot of Structural Loop Transmission

Figure 3.9 shows the reflection (acoustic) controller, and Figure 3.10 shows the Nichols plot of the acoustic loop transmission. It was obtained as before, convolving the controller with the open loop transfer function G_{yu}, that is, from the PZT controller to the microphone below the plate. Figure 3.10 shows that only one loop has a magnitude greater than one, which means that one acoustic mode is being targeted mostly.

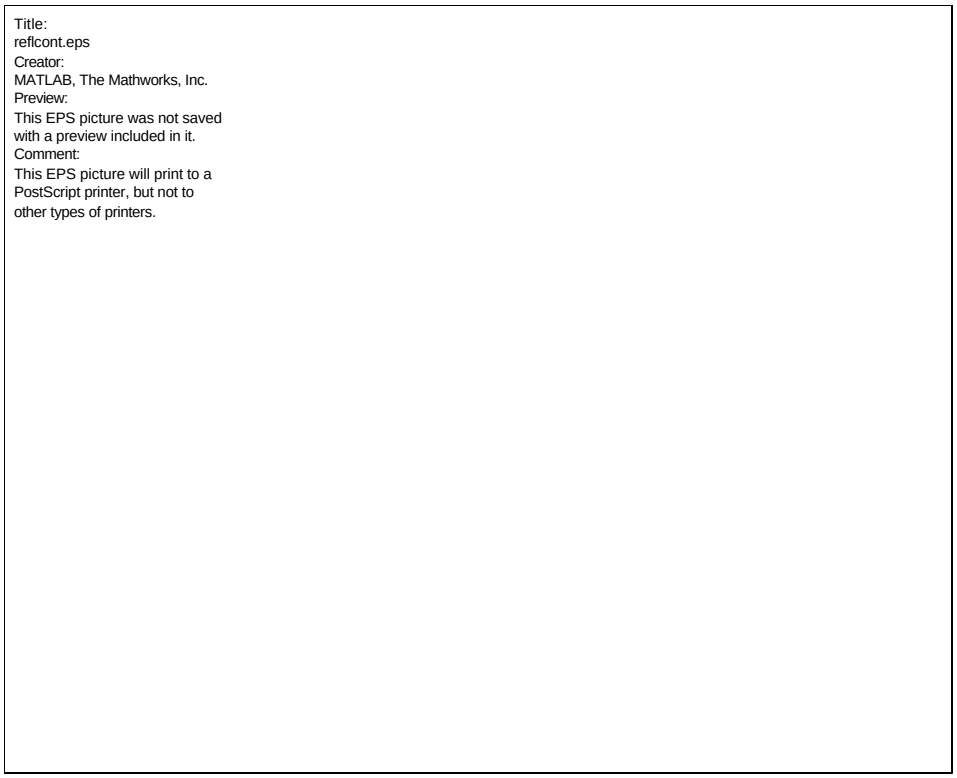

Figure 3.9 Acoustic (Reflection) Controller

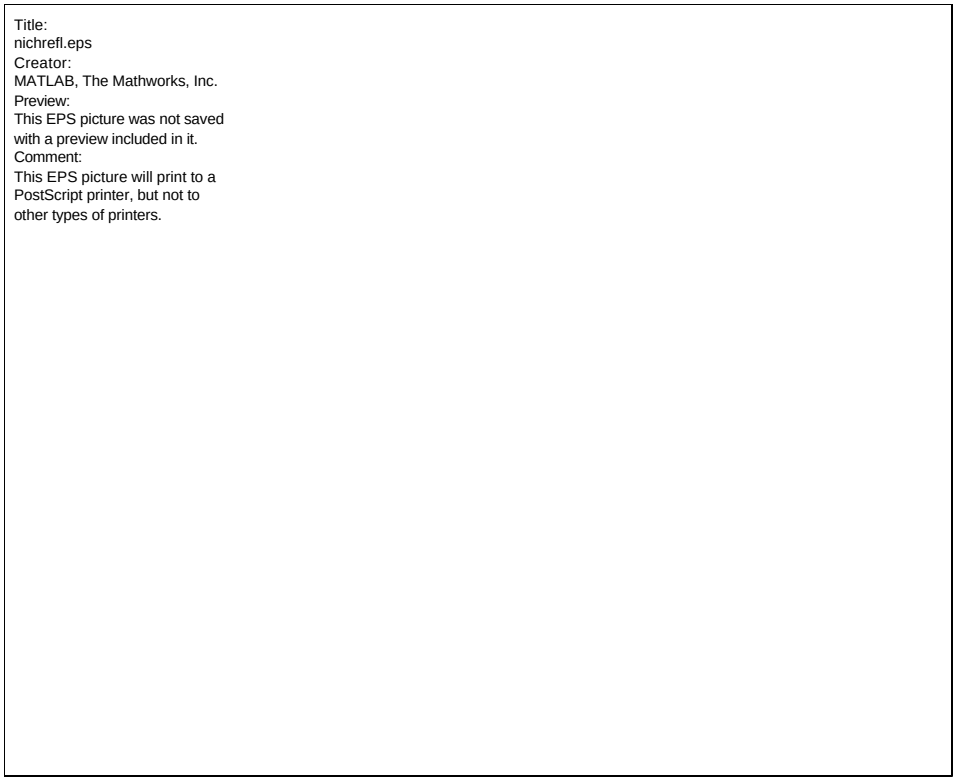

Figure 3.10 Nichols Plot of Acoustic Loop Transmission

As before, it is possible to obtain better performance from this loop by increasing the controller's magnitude at the acoustic modes of interest by changing their penalty in the LQG design. However, it lead to the same problem as before, namely, that the controller would become unstable. Several cases were tried where performance was increased with an unstable controller and a stable acoustic loop transmission, but it was preferred to use a stable controller with less performance to avoid problems during experimental implementation of the controller.

3.3.3 System Performance

The following figures show the performance of both controllers as measured by the accelerometer on the plate. The actual performance obtained from the accelerometer is not of importance, since the accelerometer is not used as a performance metric. However, the results shown in these figures can be used to understand how the structural and acoustic controllers interact and their effect on the structure.

Both Figure 3.11 and Figure 3.12 show the closed loop performance from the disturbance speaker to the accelerometer. The difference is that Figure 3.11 shows the closed loop system formed using the model plant and the controllers, whereas Figure 3.12 shows the results obtained using the measured data instead of the model plant. Equations 3.1 show the procedure to obtain these data transfer functions, as well as those seen in Figure 3.13.

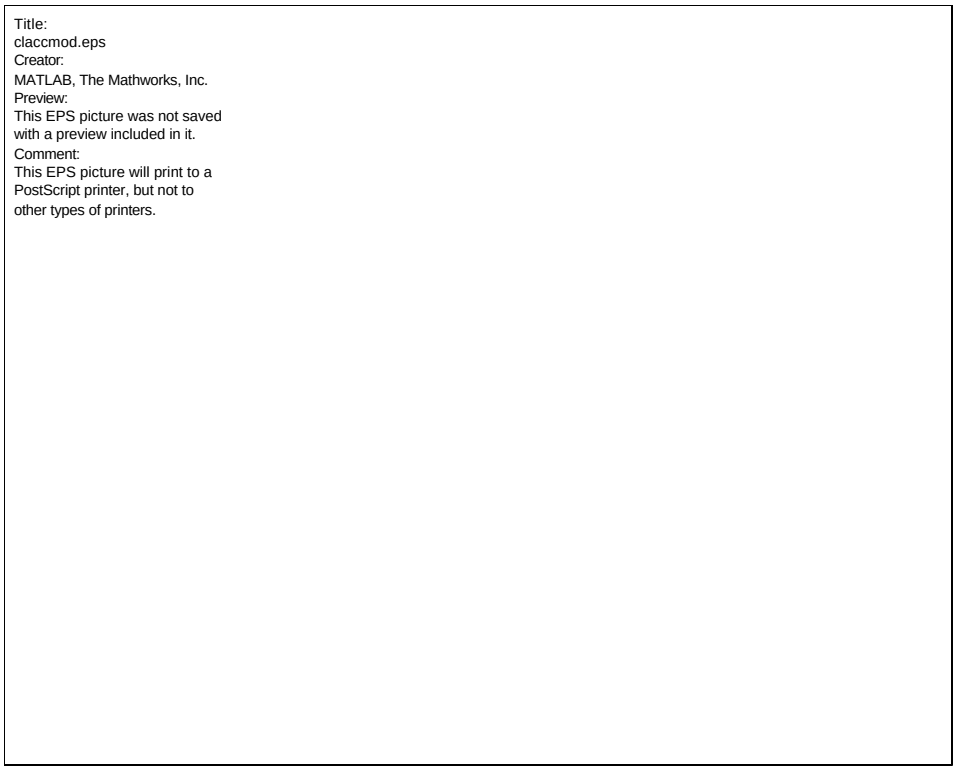

Figure 3.11 Closed Loop Model Performance - Disturbance Speaker to Accelerometer

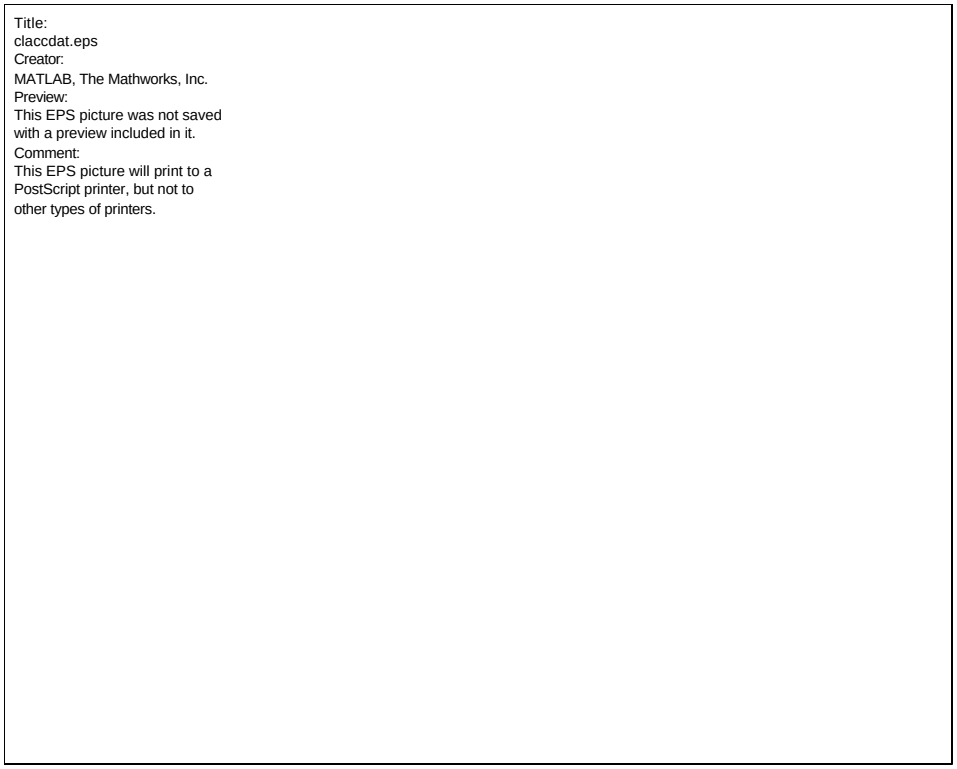

Figure 3.12 Closed Loop Data Performance - Disturbance Speaker to Accelerometer

In these equations, the measured data corresponds to *ts2a* (top speaker to accelerometer), *ts2m* (top speaker to Mic2), *p2a* (PZT to accelerometer) and *p2m* (PZT to Mic2). *ts2mict* and *ts2acct* correspond to the transfer functions obtained when only the structural controller is used, *ts2micr* and *ts2accr* correspond to the transfer functions obtained when only the reflection controller is used and *ts2micr* and *ts2accr* correspond to the transfer functions obtained when both the transmission and reflection controllers are used.

$$
\begin{aligned}
tsclt &= \frac{ts2a}{1 - p2a \cdot contt} \\
tsclr &= \frac{ts2m}{1 - p2m \cdot contr} \\
ts2mict &= ts2m + p2m \cdot tsclt \cdot contt \\
ts2acct &= ts2a + p2a \cdot tsclt \cdot contt \\
ts2micr &= ts2m + p2m \cdot tsclr \cdot contr \\
ts2accr &= ts2a + p2a \cdot tsclr \cdot contr \\
ts2mictr &= ts2m + p2m \cdot (tsclt \cdot contt + tsclr \cdot contr) \\
ts2acctr &= ts2a + p2a \cdot (tsclt \cdot contt + tsclr \cdot contr)
\end{aligned}
\tag{3.1}
$$

The performance shown in both figures is similar, although there are several instances where they differ considerably. They both show the expected behavior of the system as each of the controllers is added. When only the structural (transmission) controller is used, the modes that are attenuated are those at 79 Hz, 290 Hz and 682 Hz, the first three symmetric modes of the plate. The acoustic modes change very slightly. However, once the reflection controller is added, the first acoustic mode at 138 Hz is less attenuated, as should be expected. The plate is commanded to be more compliant to the incoming acoustic waves to attenuate them. In other words, it is trying to become better coupled with the acoustics. However, an unexpected behavior is seen for the second and

third acoustic modes, since they become attenuated, which is not expected. However, the second and third structural modes become less attenuated. Several controllers were designed giving different weights to these acoustic and structural modes, but they all demonstrated a similar behavior. It is possible that a high coupling exists between the structural and acoustic modes due to their close proximity, and that the commands issued by the controllers cause this unexpected behavior. Another instance where they differ is the appearance of the electrical resonances at 60Hz and its multiples, although this is of little consequence.

Finally, Figure 3.13 shows the closed loop performance from the disturbance speaker to the RMS value of the three performance microphones (Mic2, Mic2 and Mic4) inside the bottom chamber. This is the true performance metric of interest, since we are trying to attenuate the acoustics inside this chamber.

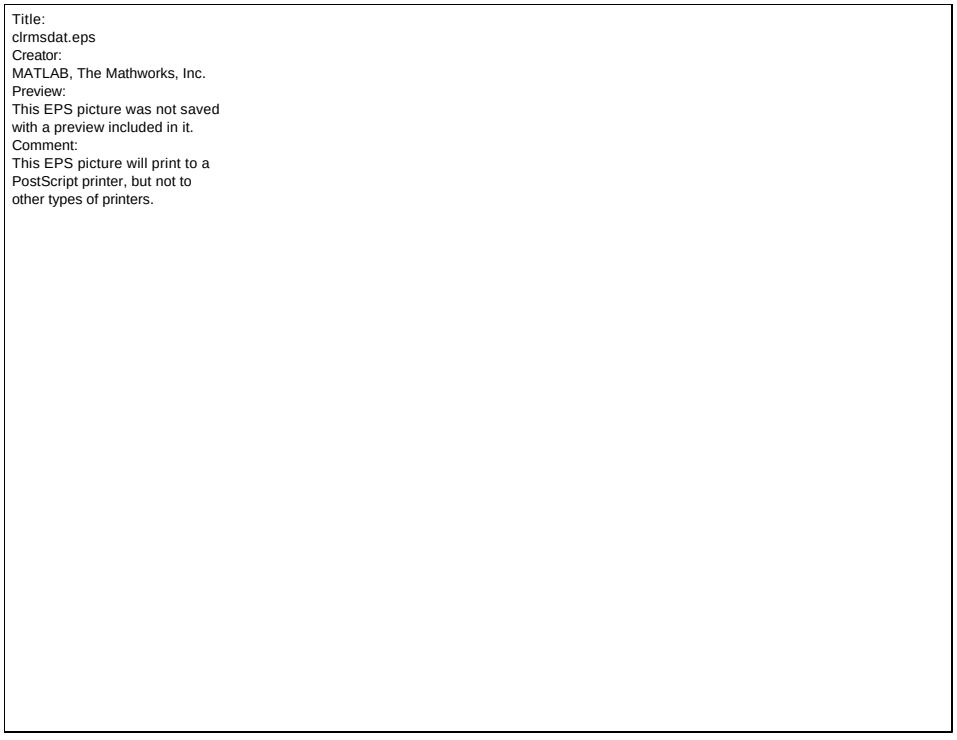

Figure 3.13 Closed Loop Data Performance - Disturbance Speaker to Microphones

Most of the results are as should be expected. The first structural mode at 79 Hz is attenuated 9.64 dB. The three acoustic modes, at 138 Hz, 332 Hz and 482 Hz, are attenuated 3.51 dB, 13.9 dB and 4.19 dB, respectively. However, the second structural mode at 290 Hz is only attenuated 1.69 dB, and the third structural mode at 682 Hz is amplified 2.49 dB.

As seen in the disturbance speaker to accelerometer transfer functions, this unexpected behavior is introduced by the acoustic controller and could not be eliminated by redesigning the acoustic controller. Despite this, a broadband attenuation of 4.02 dB was obtained.

3.4 PVDF and Pressure Feedback

This section deals with the same problem as Section 3.3, although in this case, the structural sensor was different. Previously, an accelerometer was used and now it has been substituted by the PVDF film attached to the plane. Now, instead of sensing acceleration, the strain on the plate is being sensed. The purpose of this is to compare both types of structural sensors to identify the one that is best suited for the task.

3.4.1 Plant Identification

The second model that was used utilized the PVDF and a microphone under the plate as feedback (Mic2). The actuator was the single PZT crystal on the plate. A model with 48 states was obtained from the measurements using the FORSE algorithm implemented in TFID software. Figure 3.14 shows a comparison between the measured transfer function G_{yu} from the PZT to the accelerometer on the plate. It can be seen that

the model resembles the data very closely. It also ignores some of the noise that is introduced into the measured transfer function, especially the peaks introduced at 60Hz and its multiples, which correspond to feedthrough of the electrical frequency.

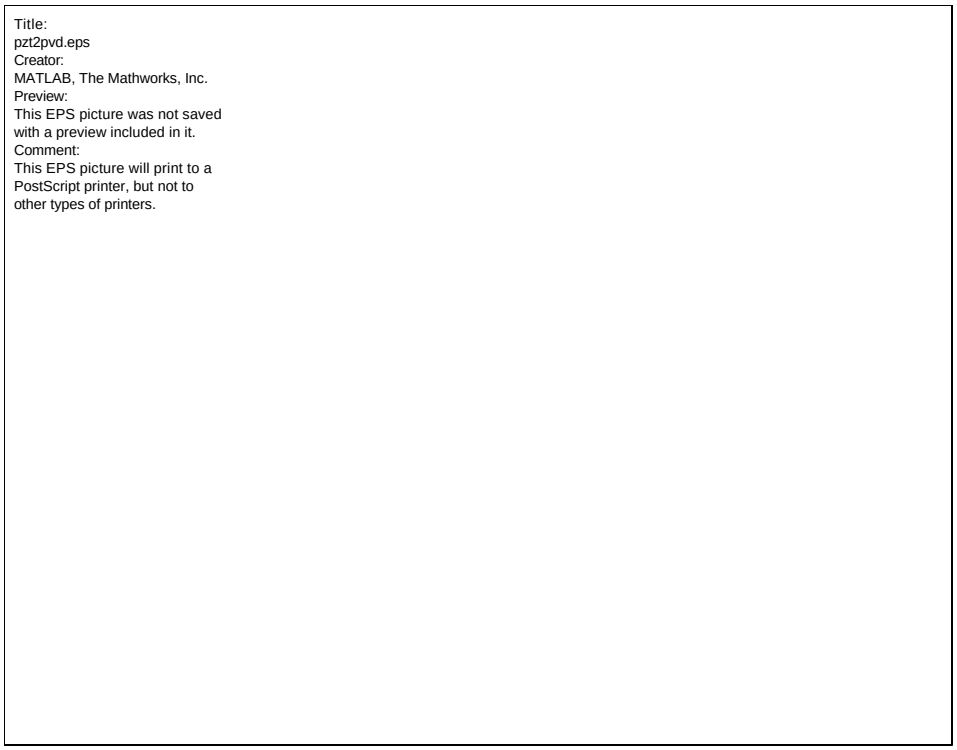

Figure 3.14 PZT to PVDF Model and Data Transfer Functions

Figure 3.14 also shows the location of the first three symmetric plate modes, which were targeted by the structural controller. These very observable poles located at 79.7 Hz, 291 Hz and 682.4 Hz, respectively. The collocation of the actuator/sensor pair can also been seen by the bounded phase of phase plot up to 1 kHz, and also by the alternating pole-zero pattern of the magnitude plot. There are other poles that appear in the transfer function that correspond to the asymmetric modes of the plate, the acoustic modes of the chambers and the speaker modes. These are less observable and thus less controllable than the symmetric plate modes.

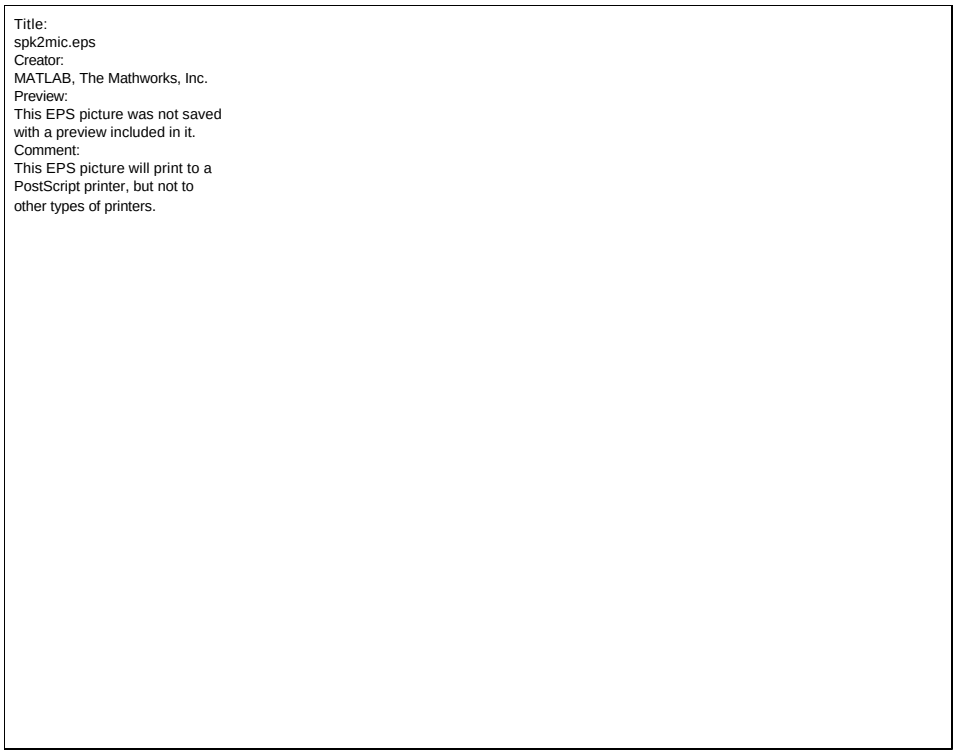

Figure 3.15 Speaker to Mic2 Transfer Model and Data Transfer Functions

Figure 3.15 shows the transfer function between the disturbance or top speaker and Mic2, located just under the plate. It is seen that the model and data transfer functions also correlate very well. This transfer function allows us to identify the acoustic modes. The first acoustic mode is located at 136.4 Hz, the second acoustic mode is located at 332.3 Hz and the third acoustic mode is at 483.5 Hz. These are the three acoustic modes that were targeted by the acoustic controller. As before, the other poles that appear in the transfer functions are higher frequency acoustic modes, speaker modes or plate modes that are also picked up by the microphones. Since the actuator and the sensor are not collocated in this case, there are some missing zeros in the transfer functions, as well as frequency roll-off as the frequency increases.

3.4.2 Controller Design

Once the modes of interest, both structural and acoustic, were identified, the structural and acoustic controllers were independently developed and used together using superposition. Figure 3.16 shows the results obtained from each independent controller.

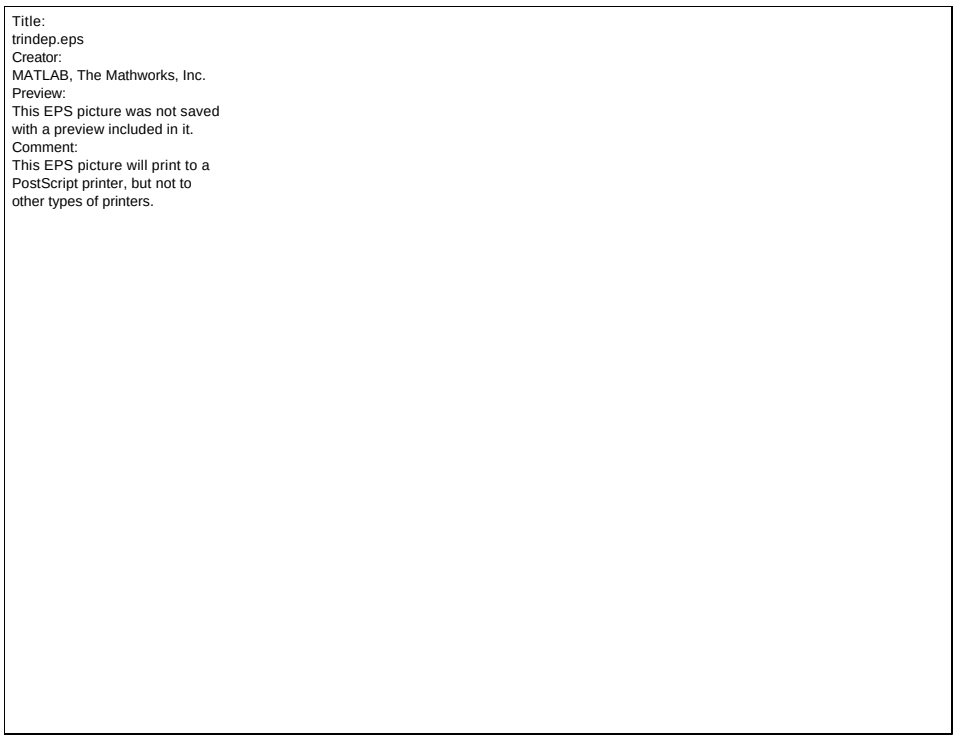

Figure 3.16 Independent Transmission and Reflection Control - Top Speaker to Mic2

The structural controller targets the first three structural modes at 79.7 Hz, 291 Hz and 682.4 Hz, respectively, and the acoustic controller targets the first three acoustic modes at 136.4 Hz, 332.3 Hz and 483.5 Hz, respectively. Table 3.2 shows the attenuation obtained at each of the modes that are targeted as well as the broadband performance from 10 Hz to 1000 Hz.

Table 3.2 Attenuation for Transmission/Reflection Control using PVDF/Mic2

Mode	Attenuation (dB)
Structural1 - 79.7 Hz	8.58
Structural2 - 291 Hz	0.51
Structural3 - 682.4 HZ	-1.13
Acoustic1 - 136.4 Hz	4.137
Acoustic2 - 332.3 Hz	7.17
Acoustic3 - 482.9 Hz	3.48
Broadband (10-1000 Hz)	3.61

Figure 3.17 shows the structural (transmission) controller and Figure 3.18 shows the Nichols plot of the structural loop transmission.

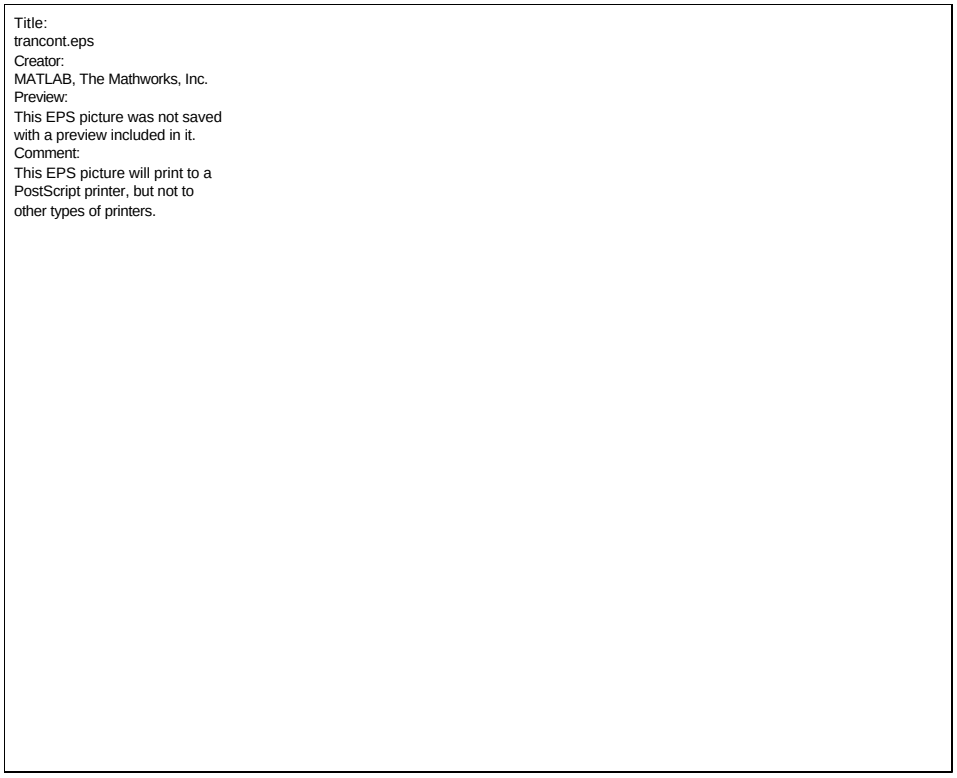

Figure 3.17 Structural (Transmission) Controller

The structural loop transmission was obtained by convolving the structural controller around the open loop transfer function G_{yu}, that is, from the PZT controller to the PVDF. Figure 3.18 shows that there are two loops that have a magnitude greater than

one, which correspond to the first two structural modes that are controlled. The third symmetric mode is targeted but little control effort is spent on it.

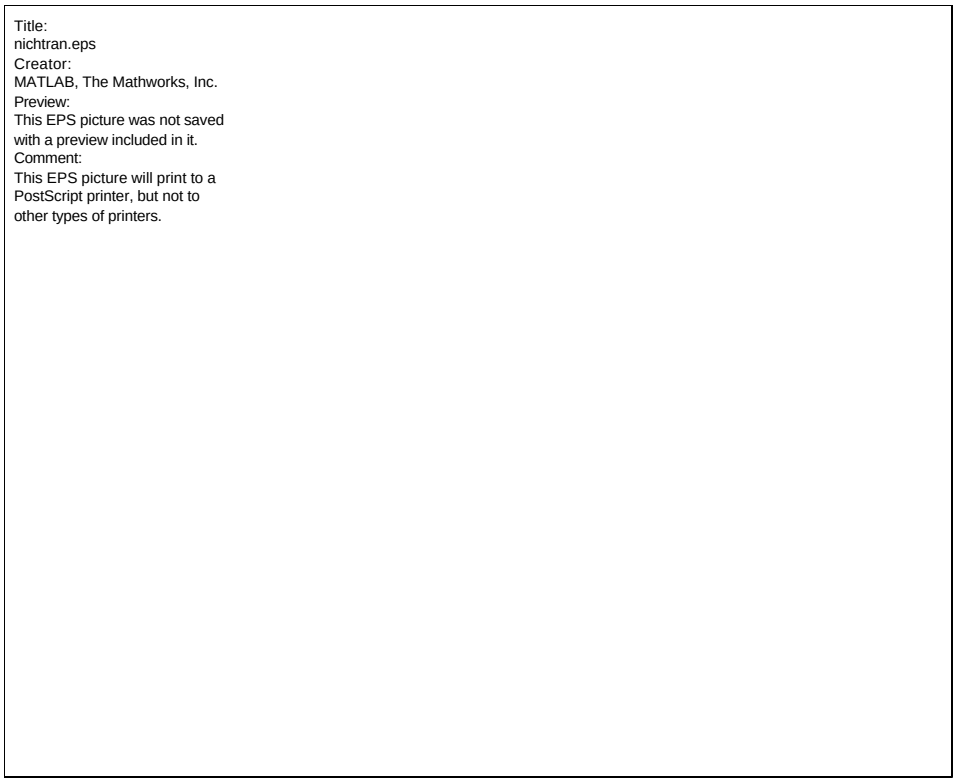

Figure 3.18 Nichols Plot of Structural Loop Transmission

As in Section 3.3, by inspecting the structural loop transmission, it seems that better performance could have been obtained by simply increasing the gain of the controller. For the same reasons, it was therefore preferred to use a stable controller at the expense of lower performance after investigating how much the controller's output could be increased before obtaining an unstable loop transmission.

Figure 3.19 shows the reflection (acoustic) controller, and Figure 3.20 shows the Nichols plot of the acoustic loop transmission. It was obtained as before by convolving the controller with the open loop transfer function G_{yu}, that is, from the PZT controller to the microphone below the plate. Figure 3.20 also shows that only one loop has a

magnitude greater than one, corresponding to the first acoustic mode, which means that acoustic mode is being targeted mostly.

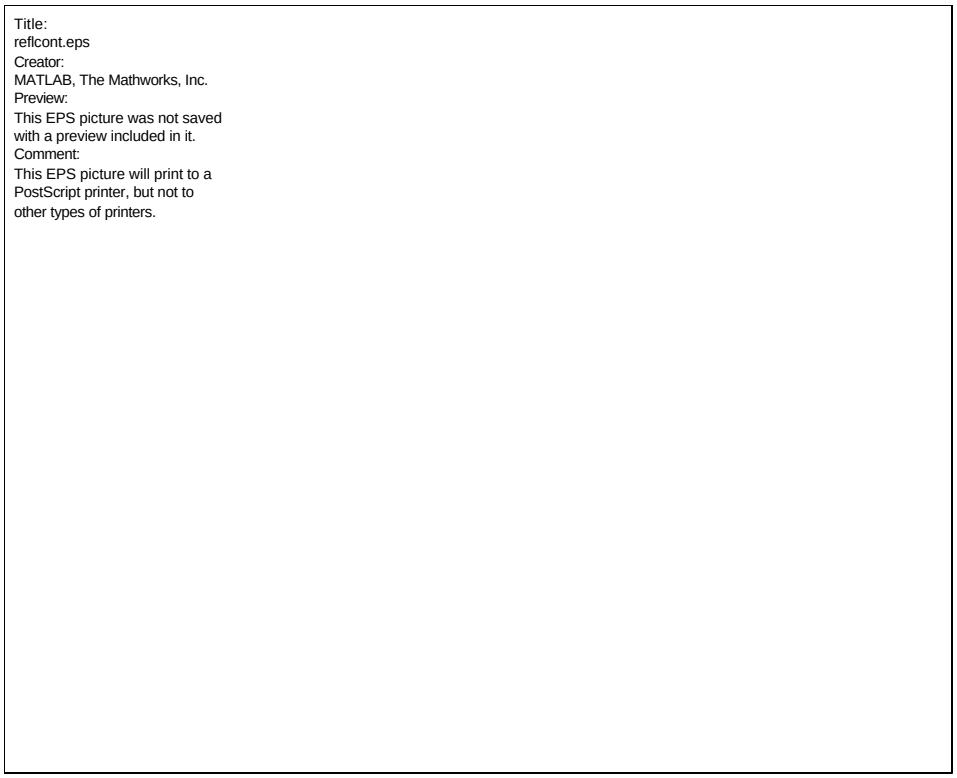

Figure 3.19 Acoustic (Reflection) Controller

As before, it is possible to obtain better performance from this loop by increasing the controller's magnitude at the acoustic modes of interest by changing their penalty in the LQG design but a stable controller with less performance was selected to avoid problems during experimental implementation of the controller.

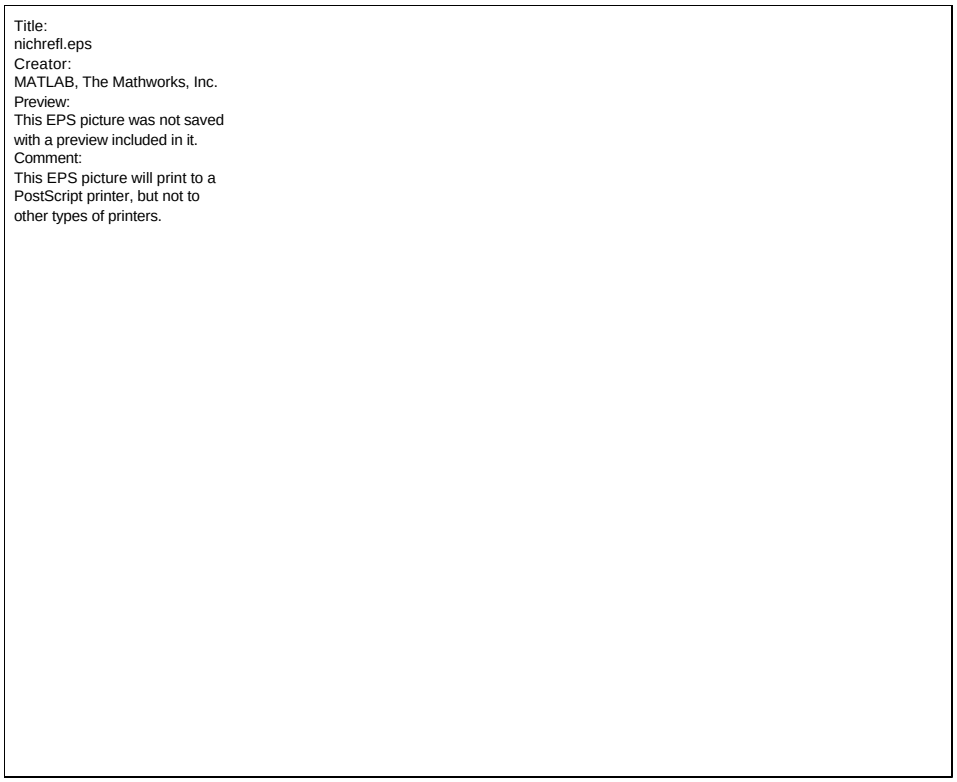

Figure 3.20 Nichols Plot of Acoustic Loop Transmission

3.4.3 System Performance

The following figures show the performance of both controllers as measured by the PVDF on the plate. The actual performance obtained from the PVDF is not of importance, since it is not used as a performance metric. However, the results shown should show a similar pattern of behavior as in Section 3.3.

Both Figure 3.21 and Figure 3.22 show the closed loop performance from the disturbance speaker to the PVDF. The difference is that Figure 3.21 shows the closed loop system formed using the model plant and the controllers, whereas Figure 3.22 shows the results obtained using the measured data instead of the model plant. The same set of equations in Eq. (3.1) was used to calculate these transfer functions.

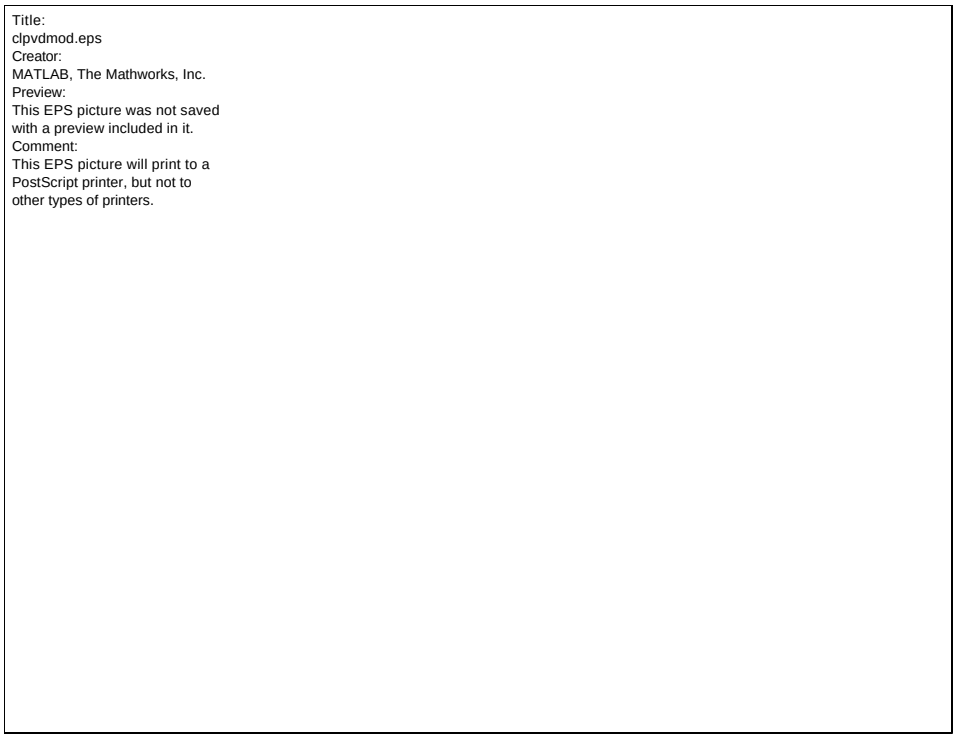

Figure 3.21 Closed Loop Model Performance - Disturbance Speaker to PVDF

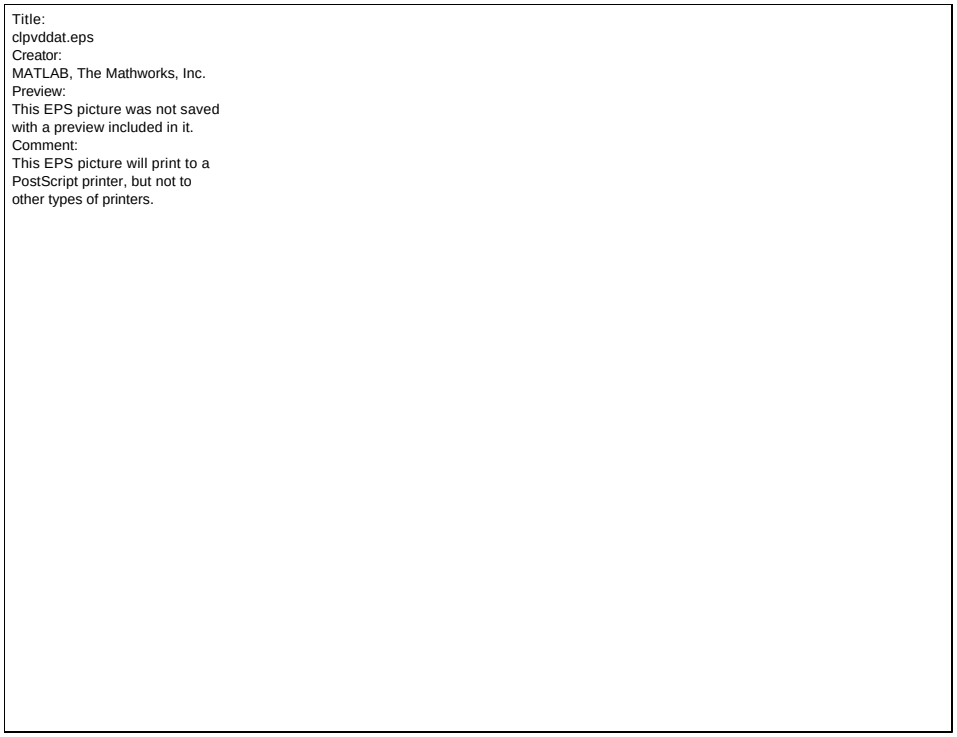

Figure 3.22 Closed Loop Data Performance - Disturbance Speaker to PVDF

The performance shown in both figures is similar, although there are some instances where they differ. They both show the expected behavior of the system as each of the controllers is added. When only the structural (transmission) controller is used, the modes that are attenuated are those at 79 Hz and 290 Hz, the first two symmetric modes of the plate. The mode at 682 Hz, the third symmetric mode, is unchanged even though the controller targets it. The acoustic modes, as expected, are unchanged. The addition of the reflection controller reveals very small changes in the damping of the first acoustic mode at 136.4 Hz, although it appears slightly less damped as it tries to become better coupled with the acoustics. However, the same unexpected behavior for the second acoustic mode that is seen in Section 3.3 is seen here, since it is also attenuated. Also, the second structural mode becomes less attenuated, especially on the plot made using the measured data. Several controllers were designed giving different weights to these acoustic and structural modes, but they all demonstrated similar behavior. The third structural mode at 682.4 Hz showed no change regardless of the controller that was used, and the third acoustic mode at 483.5 Hz showed slight changes, although it appears to behave as expected by becoming less damped.

Finally, Figure 3.23 shows the closed loop performance from the disturbance speaker to the RMS value of the three performance microphones (Mic2, Mic2 and Mic4) inside the bottom chamber. This is the true performance metric of interest, since we are trying to attenuate the acoustics inside this chamber.

Most of the results are as should be expected. The first structural mode at 79.7 Hz is attenuated 8.58 dB. The three acoustic modes, at 136.4 Hz, 332.3 Hz and 483.5 Hz, are attenuated 4.12 dB, 7.17 dB and 3.48 dB, respectively. However, the second structural

mode at 291 Hz is only attenuated 0.51 dB, and the third structural mode at 682 Hz is amplified 1.13 dB.

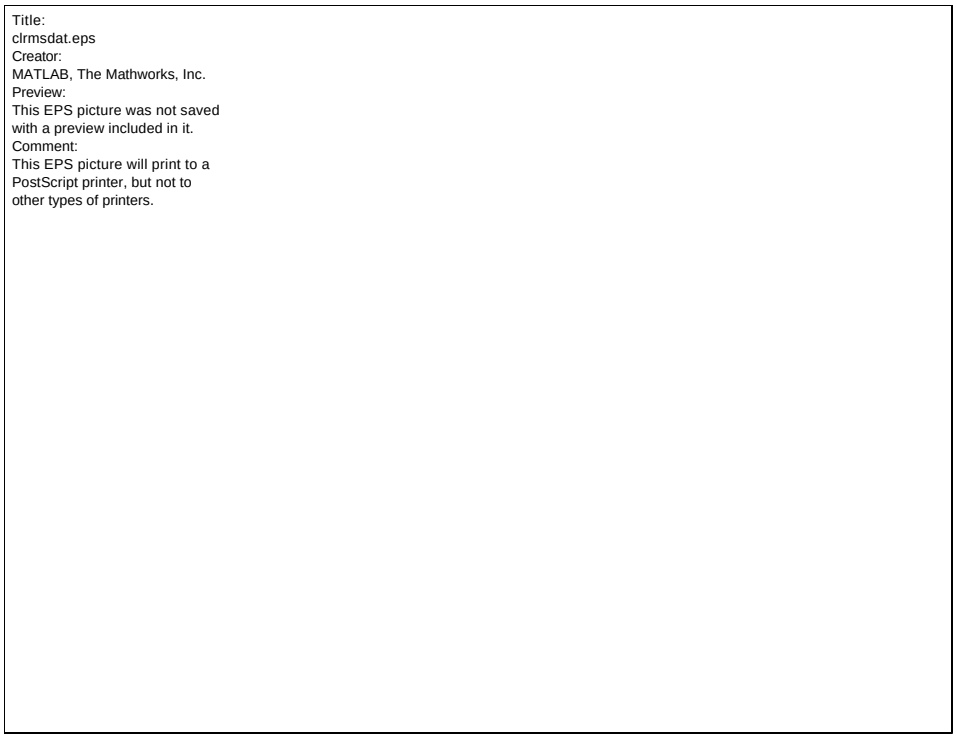

Figure 3.23 Closed Loop Data Performance - Disturbance Speaker to Microphones

As seen in the disturbance speaker to PVDF transfer functions, this unexpected behavior is introduced by the acoustic controller and could not be eliminated by redesigning the acoustic controller. Despite this, a broadband attenuation of 3.61 dB was obtained.

3.5 Summary

In this chapter, two sensor configurations for combined transmission and reflection control were compared. The difference between the two configurations was

the type of structural sensor used: an accelerometer in one case and a ring of PVDF film attached to the plate in the second case.

The performance obtained by both configurations was similar, although the controllers designed with the accelerometer provided better performance and also led to more stable controllers. Despite this, depending on how much the designer desired to push the controller, both sensors can be used to obtain comparable performance. However, the stability of the controller then becomes an issue during actual implementation.

The accelerometer had a couple of undesirable effects that did not show up when using the PVDF sensor. First, the accelerometer showed the electrical resonances in its transfer function. Secondly, since the accelerometer is not designed to filter out higher frequencies, considered as greater than 500 Hz approximately for this problem, the controller designed with this information had a higher bandwidth than the one designed with the PVDF. In this case, since there is interest in only dealing with lower frequencies, the PVDF may be more desirable.

The reflection controller introduced some unexpected behaviors into the system that resulted in lower than desired performance attenuation of the second structural modes. Although several controllers were designed in an attempt to avoid this behavior, the attempts were unsuccessful. It is believed that the proximity of the structural and acoustic modes makes it difficult for the combined controller to target both at the same time. It is also possible that a slight change in the location of Mic2 might have an influence, although this possibility was not pursued due to lack of time.

As expected, the overall performance of this setup is lower than the performance obtained by Asari. However, considering that all the control is being done by the structure, it seems that this is a feasible alternative for transmission and reflection control.

Chapter 4

4. Acoustic Power Diode

An acoustic power diode is a controller that will allow acoustic energy to flow only in one direction while preventing it from flowing in the other. In this chapter, an acoustic power diode designed to target only for the first structural mode is developed and tested. This limitation was imposed by sensor constraints, but performance for that mode showed that it is a feasible alternative.

4.1 Introduction

The concept of a vibration diode was developed by Hyde [5] to obtain active isolation of two structures, referred to as the base and the payload. The goal of this method of active isolation is to prevent base vibrations from flowing into the payload. At the same time, it should reduce payload vibrations caused by the payload itself or other flanking path disturbances. Here, the objective is to extend the vibration diode concept from a structural-structural system to a structural-acoustic system to obtain an acoustic power diode. It should prevent acoustic disturbances from entering the payload through the fairing while at the same time attenuating the internal acoustics. This approach

differs from the one presented in Chapter 3 in that a different set of sensors is used, and the controller takes care of transmission and reflection at the same time, unlike before where two separate controllers target transmission and reflection independently. A detailed description of the vibration diode can be found in Hyde's doctoral thesis [5]. A simple explanation will be given here to understand how the diode works.

In many applications, force feedback alone is used to isolate two structures (base and payload) with high gain. In the limit of infinite gain, the two structures are effectively decoupled. This reduces base vibrations transmitted to the payload from the base. However, it does not provide for an exit path for vibrations originating from the payload. Feedback of the motion of the payload is then used on top of the high gain force feedback to provide an exit path for the payload vibrations. This is achieved by creating an impedance match to the payload.

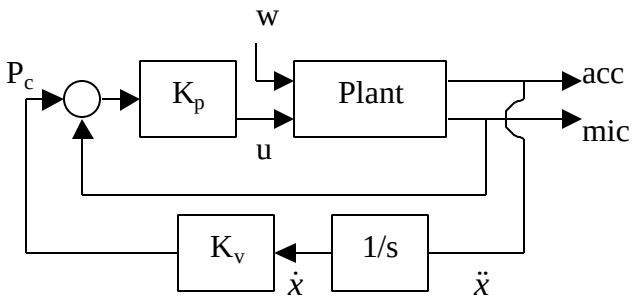

Figure 4.1 Block Diagram of Initial Acoustic Power Diode

Figure 4.1 shows a block diagram of the initial implementation of the acoustic power diode. It is composed of two loops. The inner loop is a force feedback loop, although in this case the force is the pressure measured by the microphone. This pressure is fed back through an LQG (K_p) controller to decouple the structure from the acoustics as much as possible. Simply, this means that the structure is actuated upon so that it has as little effect as possible on the pressure. In the previous chapters, this is what is

referred to as reflection control. However, this loop by itself does not provide a diode effect. Energy can flow from the plate to the acoustics or vice-versa, although it will be more attenuated than in open loop.

The outer loop servos the pressure to a commanded pressure P_c that is a function of the plate motion $\dot{x}$, which is obtained from integrating the accelerometer signal once. K_v in this case is a gain that is selected so the pole-zero excursions of the modes of interest are centered on unity. However, other inertial sensors can be used in place of an accelerometer. The gain of this loop is selected to obtain an impedance match of the acoustic modes of interest with the structure.

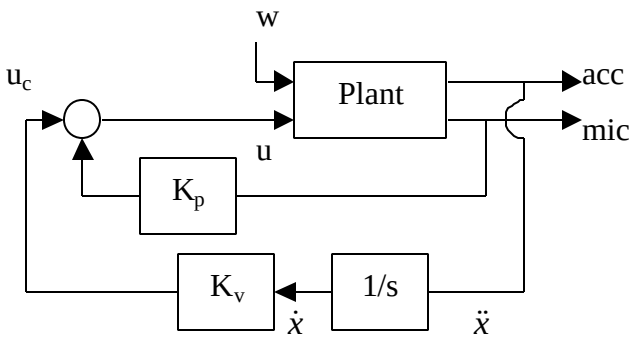

Figure 4.2 Block Diagram of Modified Acoustic Power Diode

However, using this topology, little or no diode effect was observed, so the topology was redesigned as seen in Figure 4.2. Using the initial topology, the motion sensor commands a reference pressure P_c that is added directly to the pressure measurement from the microphone. The controller K_p was designed considering that its input is only the microphone's signal, but in reality it is receiving the sum of the two sensor signals. It is trying to cancel a pressure that is not the real pressure inside the chamber. The modified topology takes this consideration into account, and each controller observes only the signal it is designed for. The final command u into the plant

is now the sum of the two controller signals. The pressure command cancels the pressure at the interface, while the inertial command creates the impedance match between the plate and the acoustics.

The controllers K_p and K_v are the same as in the first design, but now the outer loop commands a reference control u_c instead of a reference pressure.

4.2 Test Chamber Description

The work presented in this chapter also concentrates on computer implementation of modeling and control design methodologies to obtain an Acoustic Power Diode. In order to be familiar with the procedure, a description of the experimental setup will be provided.

For the acoustic power diode control problem, a "symmetric" one-dimensional test chamber was used, as seen in Figure 4.3. It is 30 inches long and is made from 12-inch diameter steel pipe with ¾ inch wall thickness. The bottom end is closed off with flat ½ inch thick steel plates. The chamber is made from several pipe sections. One section is 15 inches long, another section is 7.5 inches long, and the end section is 7.5 inches long and it contains a ten inch dual voice coil subwoofer speaker that is attached to the inner walls of the section with an aluminum ring. Because of the speaker, the effective length of the end section is 3.5 inches, and the maximum length of the waveguide is 26 inches. The joints between each section are sealed tightly with a ring of hardened RTV silicone as well as duct tape to make the joints as airtight as possible. The top of the chamber is not sealed of, but rather open to the atmosphere.

The chamber is made out of fewer sections than the previous experiment since a full waveguide is not required. The main reason to have one open end was to prevent the

acoustic energy from reverberating inside a closed chamber. To demonstrate the acoustic power diode the acoustic energy has to come to the plate from only one side, the side where the speaker is located.

The chamber is divided by a 1/32-inch thick aluminum plate into two smaller chambers, a closed chamber 11 inches long and an open chamber 15 inches long. The closed chamber is lined with acoustic foam to minimize reverberation and simulate an open acoustic field. The speaker is used as a white noise disturbance source.

The plate utilized is the same as in the previous experiment, although the PVDF is not used. An accelerometer is also located at the center of the plate. Four microphones are located throughout the chamber to measure the pressure. Two are located inside the closed chamber, one close to the plate and another flush with the top of the open section. The other two microphones are located inside the closed chamber, one below the plate and the second one near the speaker. All four microphones are located on the longitudinal axis of the chamber. The microphones are either used as sensors for feedback or performance sensors.

The electronics used to measure, power and condition these sensors and actuators is the same as used previously.

In this experiment, the orientation of the plate is important for the symmetry of the problem. Figure 4.3 show two cases where the only difference is the orientation of the plate. This can be seen by the location of the PZT: it is on the top of the plate in Case 1, and on the bottom in Case 2. To show that the acoustic power diode is functioning, a means had to be devised to show that energy did flow in one direction and not in the other. A symmetric configuration of the chamber was selected.

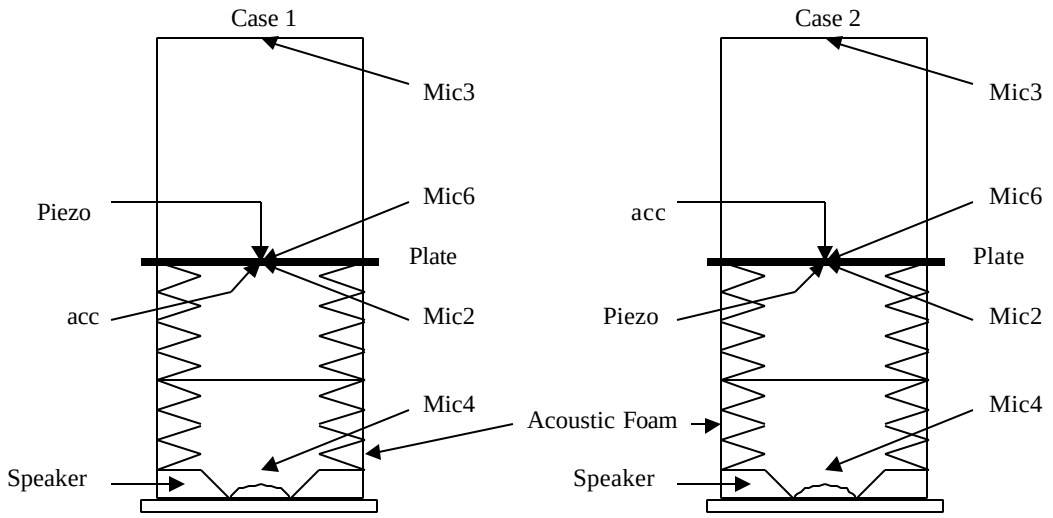

Figure 4.3 Diagram of Test Chamber for Acoustic Power Diode

The symmetry is given by the relative positions of the PZT, the accelerometer and the microphone used as a feedback sensor. In Case 1, the PZT is on the top of the plate, the accelerometer on the bottom and the feedback microphone is Mic2, which is on the same side of the plate as the accelerometer. In Case 2, the PZT is on the bottom, the accelerometer on the top and the feedback microphone is Mic6, which is now on the same side of the plate as the accelerometer. It is important to have the feedback microphone and the accelerometer on the same side of the plate so that their signals are in phase relative to each other.

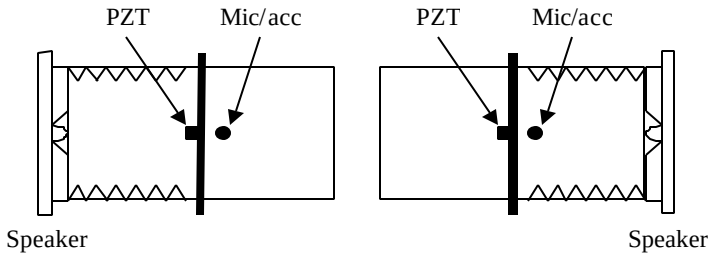

Figure 4.4 Symmetry of the Test Chamber

Figure 4.4 shows how the idea behind this symmetric configuration. As it is seen the chamber remains the same, but the disturbance source changes side. The acoustic

foam was also moved to the appropriate side to attenuate high frequency resonances of the enclosed chamber.

From the point of view of the plate, only the speaker changes side since the PZT, accelerometer and feedback microphone always remain in the same position relative to it.

4.3 Acoustic Power Diode Implementation

The implementation of the acoustic power diode on the experimental setup required that the process be broken into two parts. One end of the chamber was chosen to correspond to the inside of the fairing, and the other end to the outside. The controller for the diode was designed in Matlab considering that the disturbance is located on the "inside" of the fairing. The second part of the process consisted of simply taking the controller and implementing it considering that the disturbance is on the outside of the fairing. The results for both cases were observed and the LQG controller K_p and the gain K_v were varied until the desired results were achieved.

4.3.1 Speaker inside Fairing

A model of the plant was required to develop the LQG controller for the inner pressure loop. This model was obtained from open loop measurements and analysis using the TFID software. The final result was a 52 state model with two inputs (disturbance w and control u) and two outputs (accelerometer and pressure from Mic2).

4.3.1.1 Plant Identification

Figure 4.5 shows the open loop transfer function G_{yw} between the disturbance w and the pressure sensor, Mic2. In this transfer function, the first plate mode at 66.6 Hz and the second plate mode at 257.5 Hz can be observed. Although the plate used in this test was the same used in Chapter 3 tests, the plate modes have changed slightly. This is a result of the destiffening of the plate that is a consequence of an open chamber now being on one side of it.

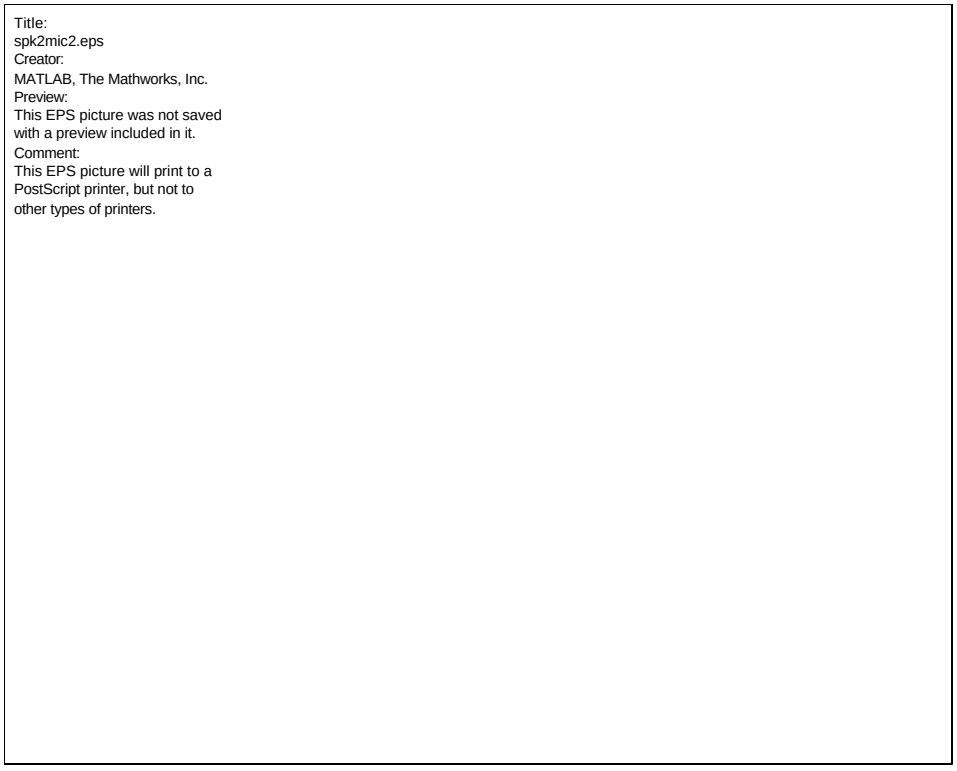

Figure 4.5 Speaker to Mic2 Model and Data Transfer Functions

The speaker mode at 187 Hz can also be observed, as well as the first acoustic mode of the chamber at 536 Hz. This acoustic mode has increased considerably since the chamber is now much shorter. Since only three modes can be seen within the range of

interest (<500 Hz), the two structural modes and the speaker mode, the controller was designed to only target those modes.

A zero can also be seen before the first plate mode. This zero was also observed by Pascal [3]. He observed that the acoustic pressure at the microphone (Mic2) position was close to zero for a coupled modeshape. This zero might decrease the performance of the controller at this frequency, but it cannot be avoided. Moving the microphone only changes the location of the zero, and the microphone cannot be moved too far away from the plate since the pressure of interest is that on the plate's surface.

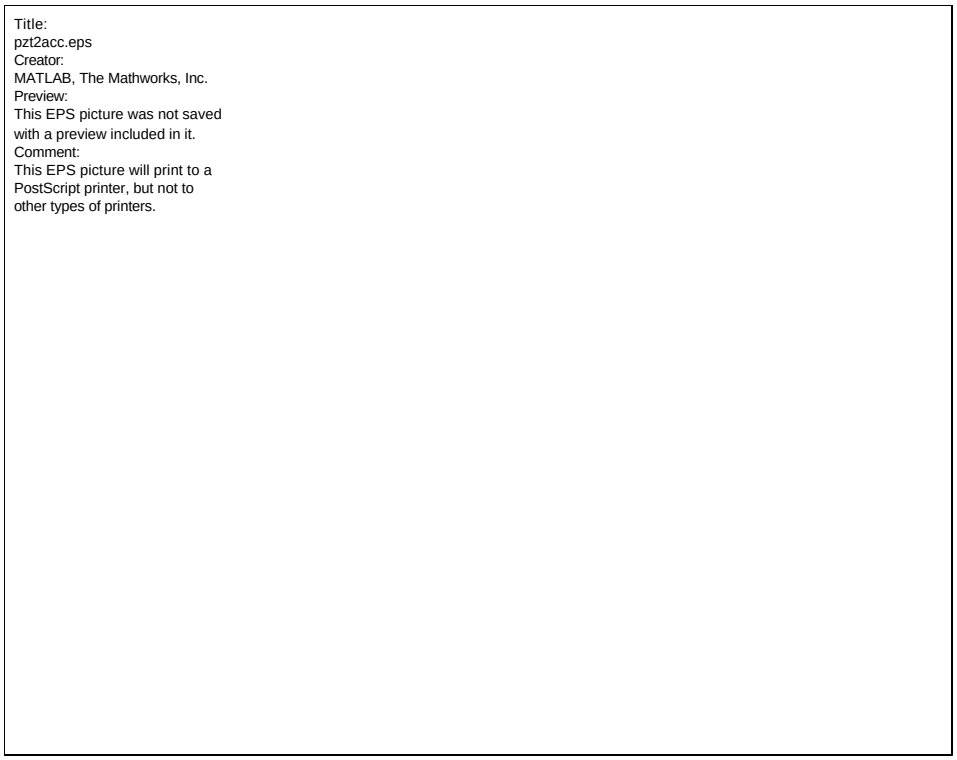

Figure 4.6 PZT to Accelerometer Model and Data Transfer Functions

Figure 4.6 shows the open loop the model transfer function G_{yu} between the control u and the accelerometer. Since the first chamber mode is at 536 Hz, all of the lower frequency modes that are observed are plate modes. The first symmetric plate mode at 66.6 Hz and the second at 257.5 Hz can be observed clearly. However, several

of the asymmetric plate modes are also observed. This is due to the location of the accelerometer, which was slightly off center. However, these asymmetric modes seem not to cause undesired problems for the controller.

4.3.1.2 Controller Design

The controller consists of two parts. The first is an LQG controller designed using the pressure sensor (Mic2) as feedback, and it is connected to the actuator, the PZT on the plate. Figure 4.7 shows the bode plot of the controller, and Figure 4.8 shows the Nichols plot of the pressure loop transmission.

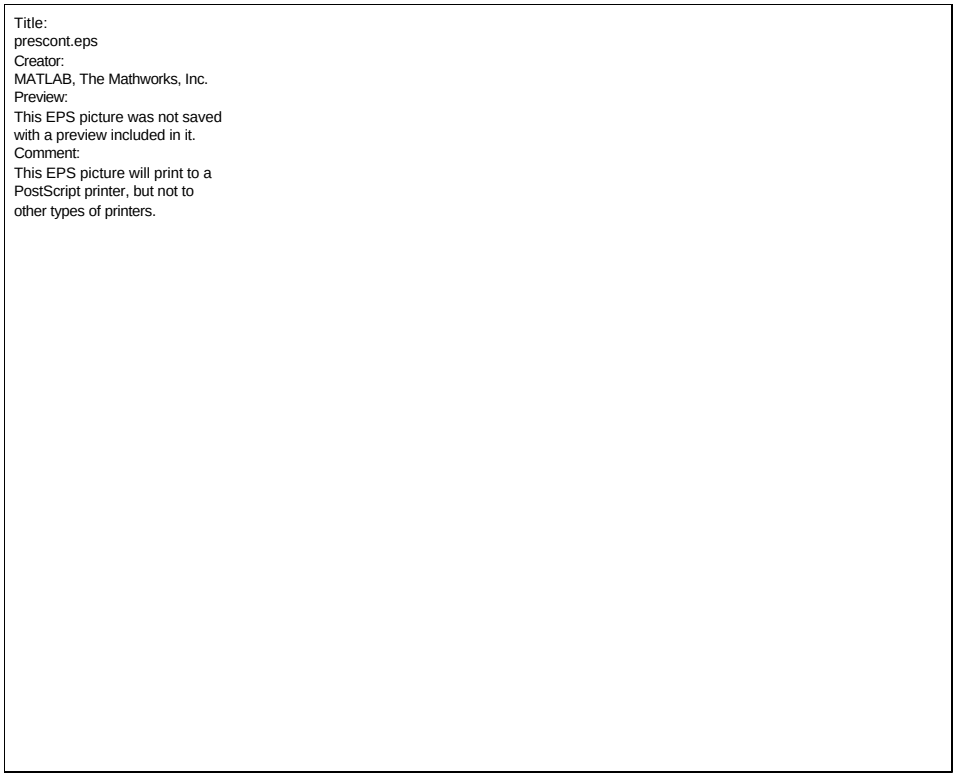

Figure 4.7 Bode Plot of LQG Pressure Controller

To obtain the desired performance, the controller required high gains, and this can be seen in the loop transmission plot. Even though it is stable, the loop transmission has very little phase and gain margin. Reducing the gains did not increase the phase or gain

margins considerably, so it was decided to use this controller for experimental implementation with care not to destabilize the loop. Figure 4.8 also shows that only one loop goes above unity, which corresponds to the first symmetric structural plate mode at 66.6 Hz that is being targeted.

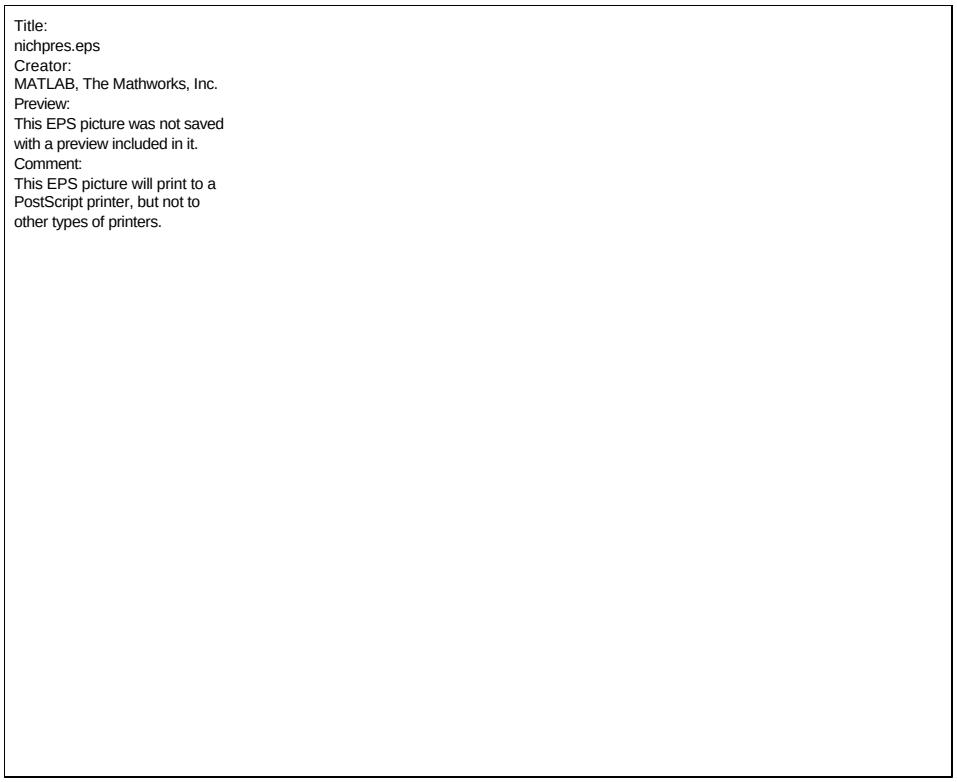

Figure 4.8 Nichols plot of the LQG Pressure Loop Transmission

The velocity signal for the outer loop, the velocity loop, was obtained by integrating the accelerometer signal once. To avoid the infinite energies at low frequencies that result from the integration, a single order low-pass filter with notch frequency at 10 Hz was used to perform the integration, an approach used by Asari in his experiments [2]. Once the velocity signal had been obtained, a gain was added to the loop. The magnitude of this gain was adjusted so that the pole-zero excursions of the velocity loop transmission were centered on unity, as shown in Figure 4.9. Figure 4.10 shows the stability of this loop.

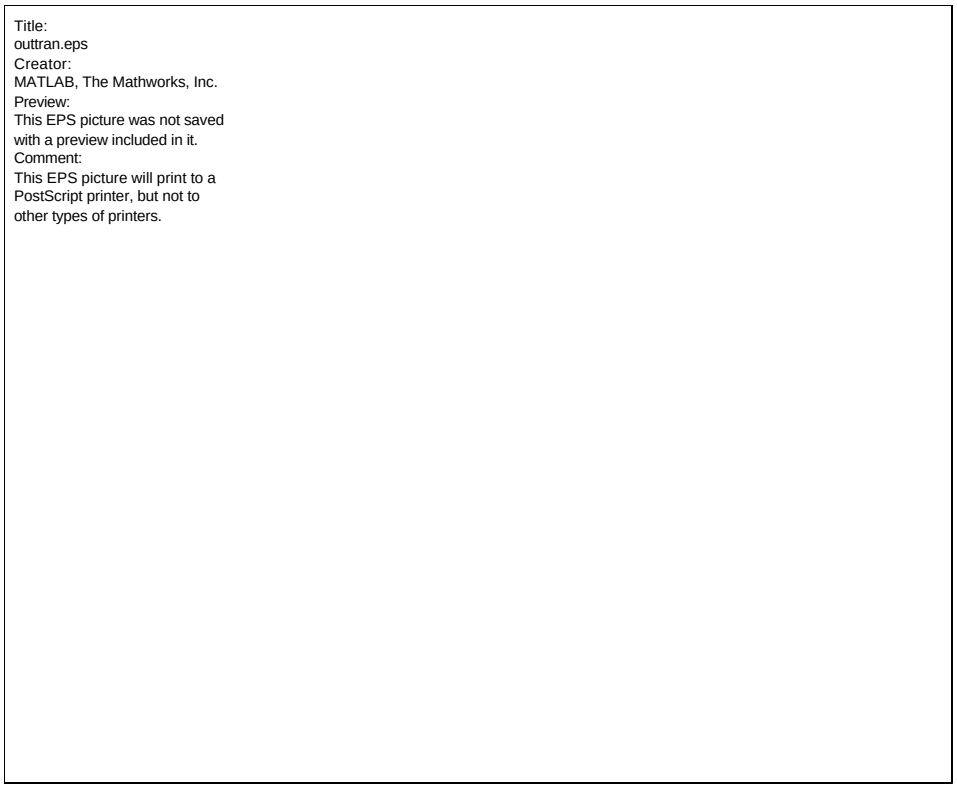

Figure 4.9 Bode plot of the Velocity Loop Transmission

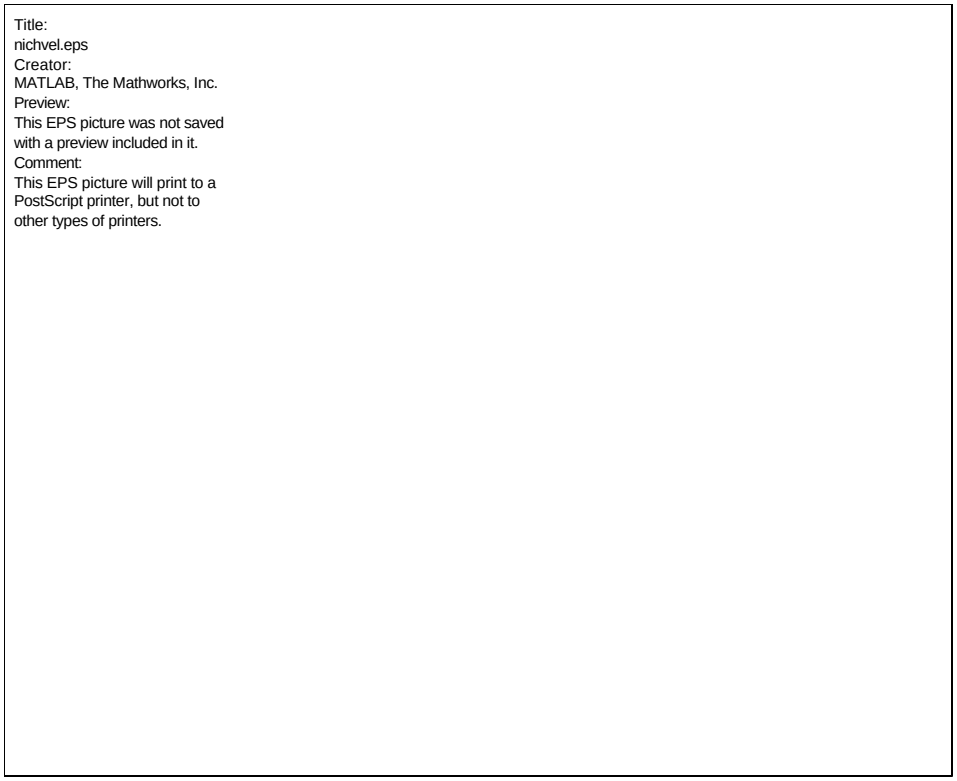

Figure 4.10 Nichols plot of the Velocity Loop Transmission

4.3.1.3 Performance

The following figures show the performance of the power diode. Figure 4.11 shows the bode plot of the closed loop from the disturbance speaker to the pressure sensor, Mic2. The effect of the LQG pressure controller can be best observed in the damping of the first structural mode at 66.6 Hz, where an attenuation of 11.43 dB was obtained. When the outer loop is added, there is a loss in attenuation at this mode of only 1.8 dB. The broadband performance was 1.19 dB for transmission only, and 0.32 dB for the acoustic power diode.

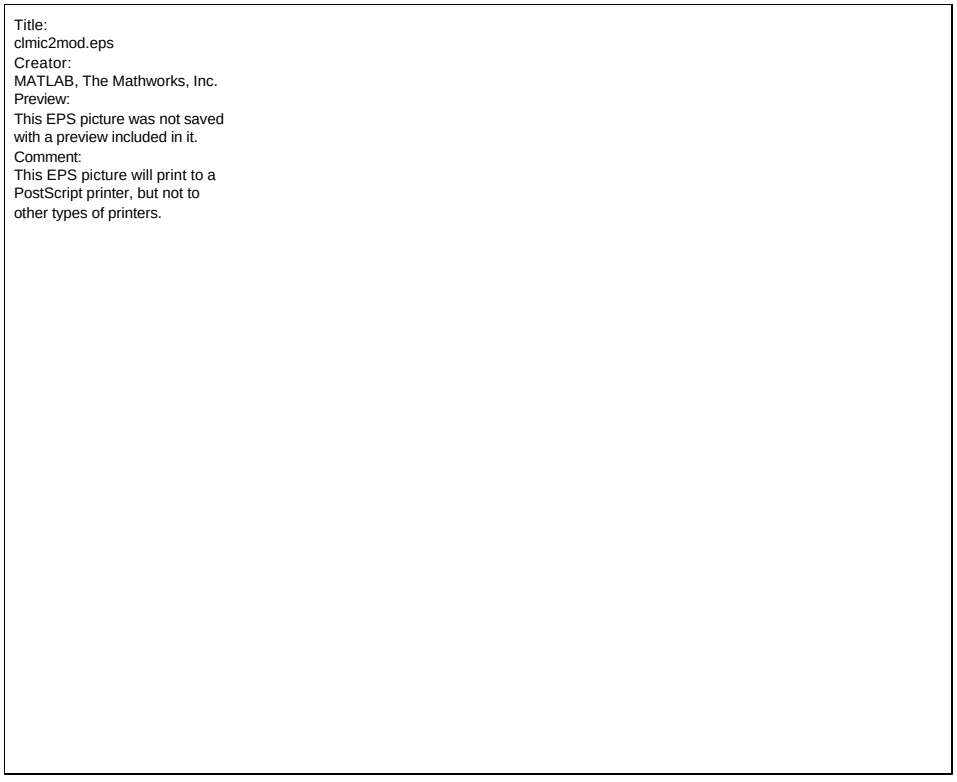

Figure 4.11 Closed Loop Performance - Speaker to Mic2

Figure 4.12 shows the power flow though the plate, which is truly a power flow per unit area measurement since pressure is involved. This power flow was obtained

from the collocated pressure and acceleration measurements using the following equation, given by Hyde [5].

$$P(\omega) = \Re e(F(\omega) * ((j\omega)^{-1}) a(\omega))) \tag{4.1}$$

Here it is seen that the plate no longer irradiates energy in both directions, that is to say, to both of its sides, but rather that it irradiates energy mostly in the direction away from the speaker. In other words, in this configuration, it allows the energy to flow through it from one chamber to another.

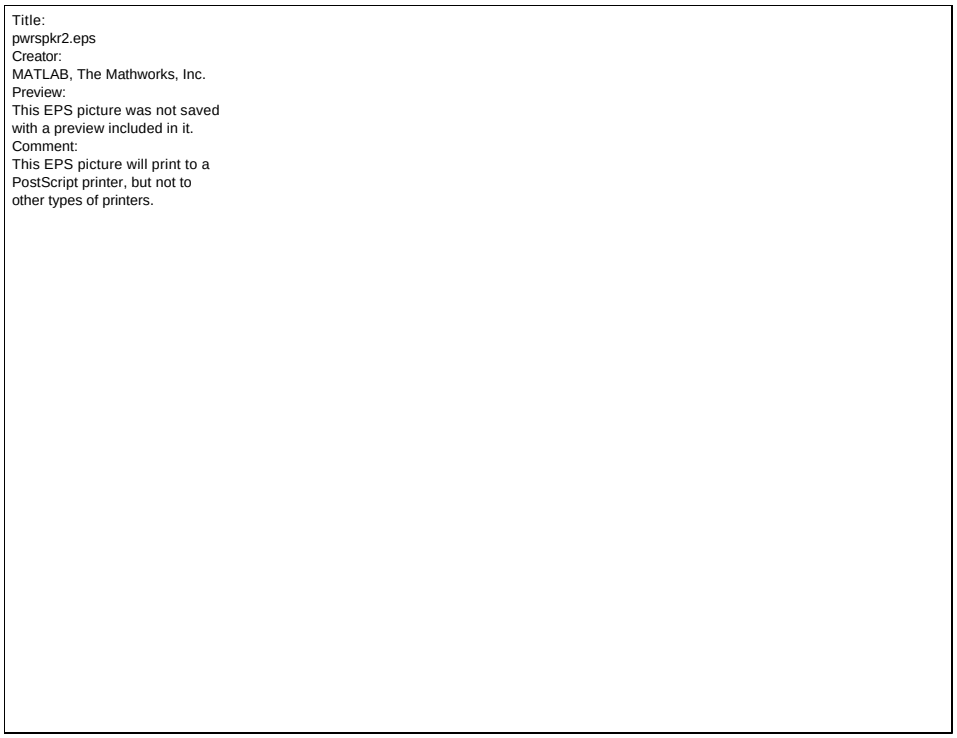

Figure 4.12 Power Flow Through Plate

4.3.2 Speaker outside Fairing

The controller was also implemented for the case where the speaker was located on the inside of the fairing. The model of the plant was obtained from open loop measurements and analysis using the TFID software. The final result was a 54 state

model with two inputs (disturbance w and control u) and two outputs (accelerometer and pressure from Mic6). As is to be expected, this model was very similar to the model developed in the previous section since it was developed from the same chamber and only the plate was turned over.

4.3.2.1 Plant Identification

Figure 4.13 shows the modeled open loop transfer function G_{yw} between the disturbance w and the pressure sensor, Mic6. In this transfer function, the first plate mode at 68.6 Hz and the second plate mode at 257.4 Hz can be observed. These modes are very close to those obtained in the previous section. The speaker mode at 183.2 Hz can also be observed, as well as the first acoustic mode of the chamber at 537.9 Hz.

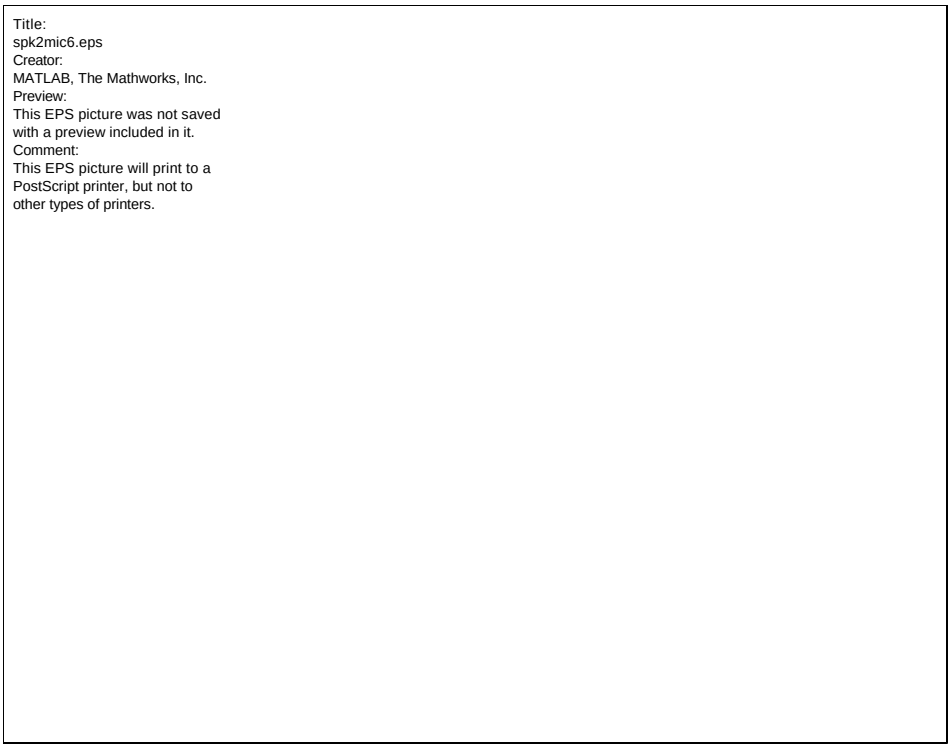

Figure 4.13 Speaker to Mic6 Model and Data Transfer Functions

The zero that was observed in the speaker to Mic2 transfer function is not present here. Since the microphone is located on the side of the chamber that is open to the atmosphere, there are no acoustic resonances in this side of the test chamber, and thus no coupling of the modeshapes as there was in the previous section. This particular measurement shows that the model does not lose phase as fast as the data. Attempts were made to correct this during the construction of the model, but this could not be avoided.

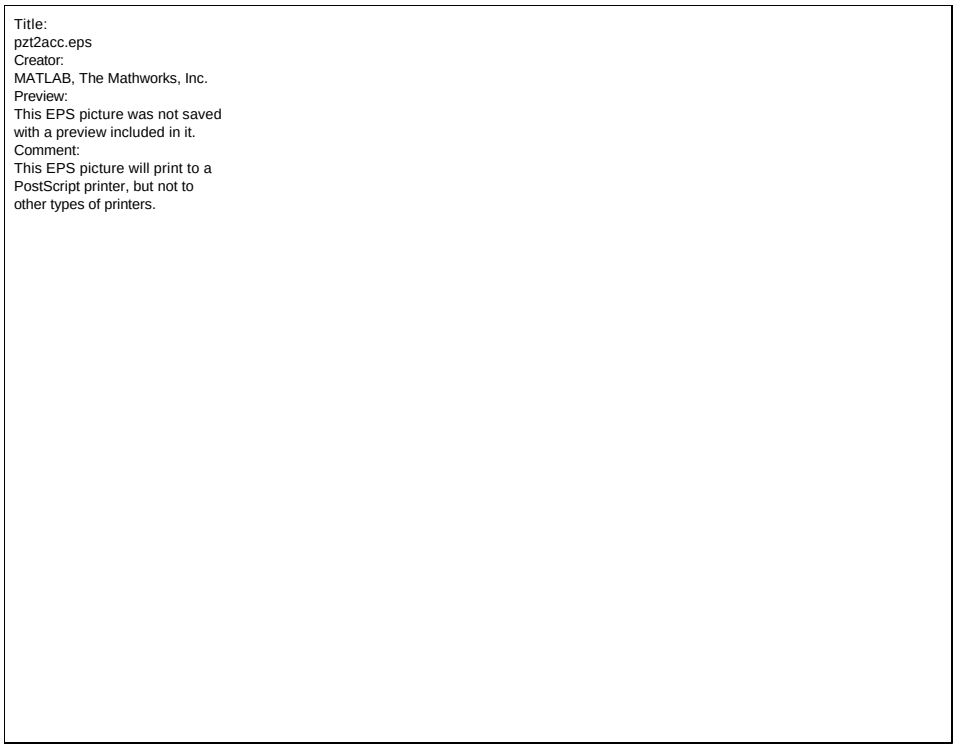

Figure 4.14 PZT to Accelerometer Model and Data Transfer Functions

Figure 4.14 shows the modeled open loop transfer function G_{yu} between the control u and the accelerometer. As before, all of the lower frequency modes (below 536 Hz) that are observed are plate modes. The first symmetric plate mode at 68.6 Hz and the second at 257.4 Hz can be observed clearly. As was previously observed, several of the asymmetric plate modes are also visible. It can also be seen that one of the asymmetric modes was accidentally taken away from the model. A previous model where this mode

had not been taken away was used to observe the mode's influence on performance. It was found that the diode's performance was not affected by the mode, and since this was not a mode of interest for the control design this transfer function was used instead of reconstructing the model from the beginning.

4.3.2.2 Controller Design

The controller used in this part of the experiment was the same used in the previous section, and it can be seen in Figure 4.7. Figure 4.15 shows the Nichols plot of the pressure loop transmission using this same controller.

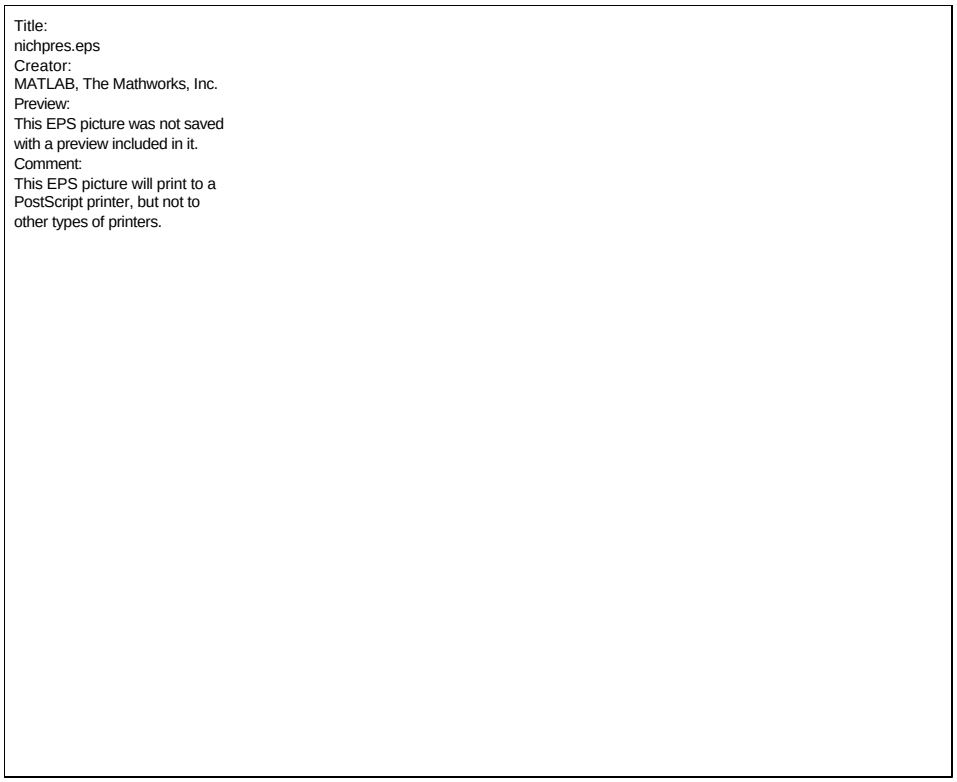

Figure 4.15 Nichols plot of the LQG Pressure Loop Transmission

This loop transmission, unlike the previous one, has better phase and gain margins. It is also seen that only one loop goes above unity, which corresponds to the first symmetric structural plate mode at 66.6 Hz that is being targeted.

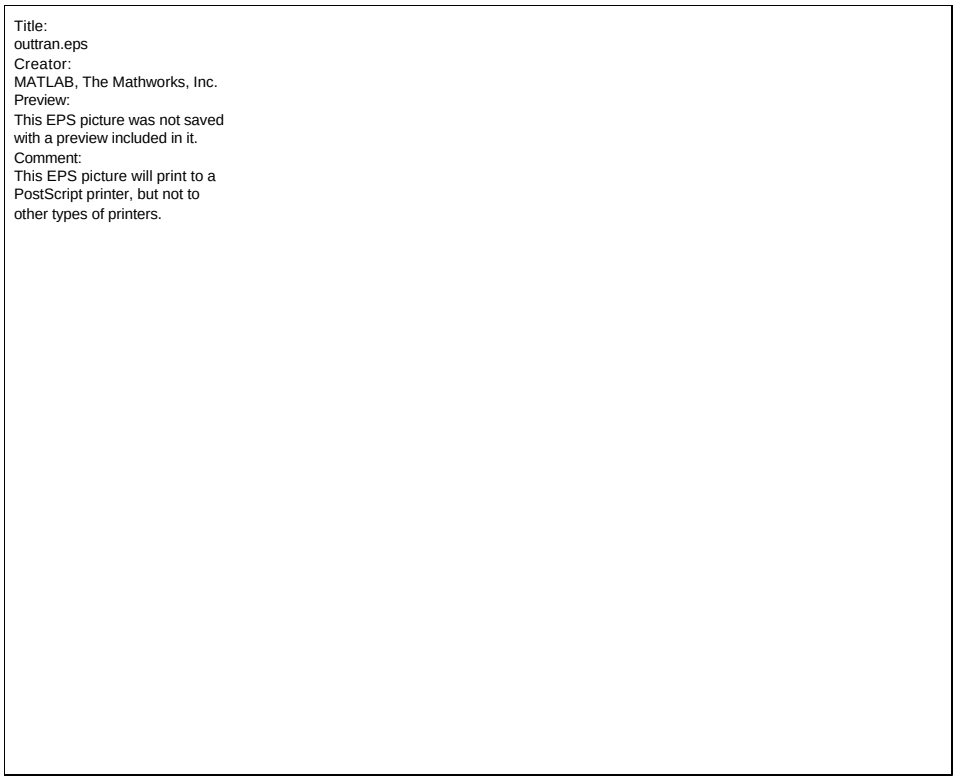

Figure 4.16 Bode plot of the Velocity Loop Transmission

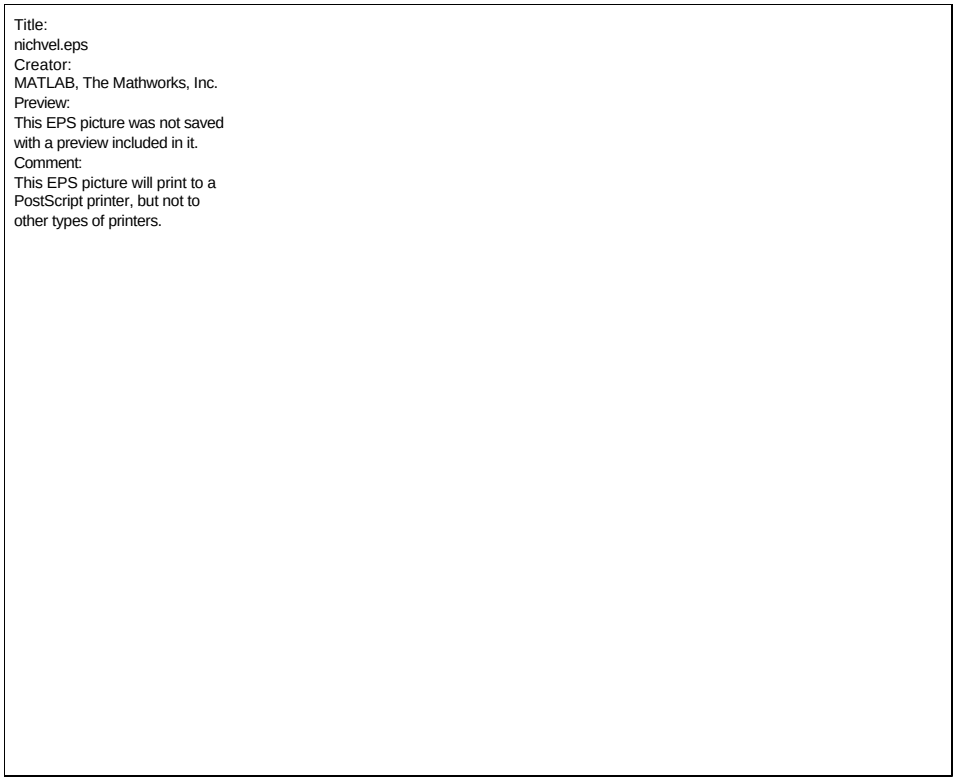

Figure 4.17 Nichols plot of the Velocity Loop Transmission

The velocity loop, or outer loop in the design, requires a velocity signal which was obtained by repeating the process presented previously. The magnitude of the gain for this loop could not be adjusted, since it was already determined in the previous design, and the resulting velocity loop transmission can be seen in Figure 4.16. Figure 4.17 shows the stability of this loop.

4.3.2.3 Performance

The following figures show the performance of the power diode for this configuration. Figure 4.18 shows the bode plot of the closed loop from the disturbance speaker to the pressure sensor, Mic6. The LQG pressure controller gives an attenuation of 2.26 dB for the first symmetric plate mode. Such a performance difference with the previous section is not completely unexpected since the chamber was taken apart, and the models constructed differ slightly as a consequence of this. When the outer loop is added, the attenuation increases to 4.13 dB. The broadband performance was 1.87 dB for transmission only, and 3.3 dB for the acoustic power diode.

Figure 4.19 shows the power flow though the plate, which was obtained from Equation (4.1). Here it is seen that the plate absorbs the energy that it receives without letting it go into the other chamber. In other words, in this configuration, the acoustic power diode prevents the energy from flowing though it.

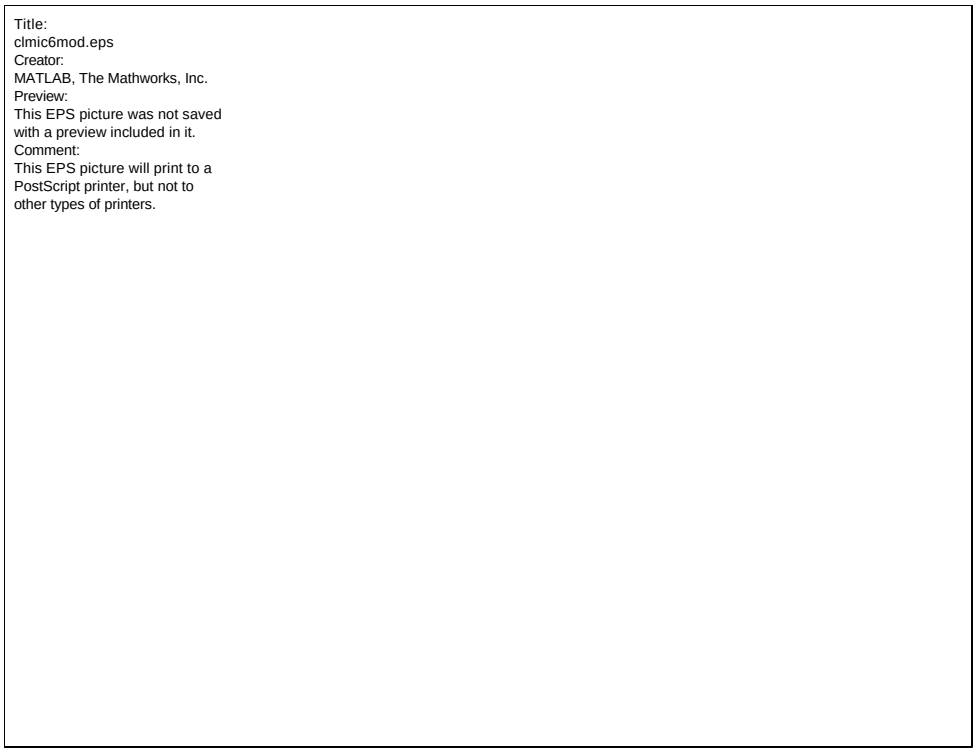

Figure 4.18 Closed Loop Performance - Speaker to Mic6

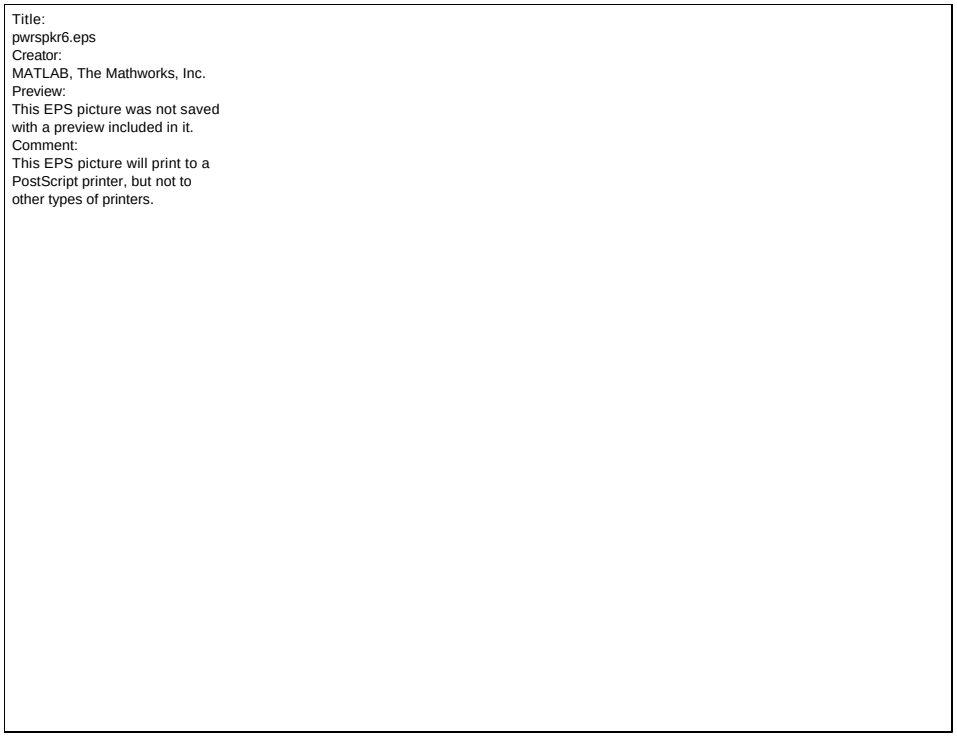

Figure 4.19 Power Flow Through Plate

4.4 Summary

In this chapter an acoustic power diode was implemented on a symmetric chamber. This diode is an extension of the structural vibrational diode designed by Hyde in his doctoral thesis. Its novelty resides in the fact that a single controller is used to take care of both transmission through the fairing and reflection inside the payload fairing, and that it does not require knowledge of the payload.

Performance of the diode was lower than that obtained by using independent controllers to target transmission and reflection, however. It therefore seems that the diode will not provide the best possible performance in its current implementation.

Since all the sensors (microphones and accelerometer) and actuators are located on the longitudinal axis of the chamber, it is at this moment impossible to ensure that the power flows shown in Figure 4.12 and in Figure 4.19 hold for the whole surface of the plate. This can be said only for a small area close to the center of the plate. An array of sensors, both microphones and accelerometers, would be needed to test for the performance over the whole area of the plate. It seems this will be necessary since the microphone performances show that the performance is lower than what should be expected if the power flow were to hold over the whole area of the plate.

Despite these shortcomings, it seems that an acoustic power diode is a feasible alternative that requires further study to obtain worthwhile performances.

Chapter 5

5. Experimental Results

This chapter presents the experimental results of the implementation of the controllers designed for transmission and reflection control on a plate in Chapter 3, and the acoustic power diode of Chapter 4.

The results from transmission and reflection on a plate used two sets of sensors: a microphone and an accelerometer, and a microphone and a PVDF strain sensor. The results from the PVDF/microphone set resembled the predicted data the most whereas the performance using the accelerometer/microphone set was not as high as predicted.

The acoustic power diode, which also relies on an accelerometer, did not perform as well as predicted either, although the diode effect was observed.

5.1 Combined Transmission and Reflection Control on a Plate

The first part of this chapter deals with the experimental implementation and validation of the controllers designed to perform combined transmission and reflection

control on the plate. Two different sensor configurations were implemented, an accelerometer/microphone configuration and a PVDF/microphone configuration.

5.1.1 Accelerometer and Pressure Feedback

5.1.1.1 Controller Implementation

A brief explanation of the electronics used in the experimental implementation of the controllers is given below. All the elements used in the experimental test chamber provide electronic signals (sensors/real time computers) or require electronic signals to operate (actuator/real time computers). Signal conditioners and power amplifiers are used for these tasks.

The electret condenser microphones are powered by a 3-10 Volt DC power supply and their signals are passed by conditioning electronics. The accelerometer's signal is conditioned using an Endevco charge amplifier. A gain box is used to change the gain of the various sensors. The PZT crystal patch and the disturbance speakers are each powered by one channel of a Crown DC-300A series power amplifier.

Time and frequency domain data was recorded using a Tektronix 2630 Fourier Analyzer which is capable of recording time domain and frequency domain data on four individual channels. It was also used as a function generator to drive the disturbance speaker with band-limited random white noise.

The controllers were implemented on two Heurikon digital computers operating at a sampling frequency of 8200 Hz. Since this is a digital implementation of the controllers, a time delay is introduced into the compensator transfer function. To make

the LQG algorithm take this into account, a Padé time delay approximation was added to the plant to ensure the closed loop stability.

Due to limitations of the Heurikon real time computers, the controllers could not be implemented as designed. Full state compensators required a slow sampling rate that caused too much phase lag and thus bandwidth problems of the controllers. To use a sufficiently high sampling rate, a reduced state controller was needed. The 52 state transmission and reflection controllers were reduced to 20 states using a balanced reduction technique in Matlab. Using the 20 state controllers, the sampling frequency was set at 8200 Hz. Before closing the loop, the loop transfer function using the reduced controllers was checked to ensure the closed loop stability of the system. Figure 5.1 shows a comparison of the full 52 state transmission controller and the 20 state reduced controller. Figure 5.2 shows a comparison of the full 52 state reflection controller and the 20 state reduced controller. It can be seen that both reduced controllers capture the dynamics of the original controllers faithfully.

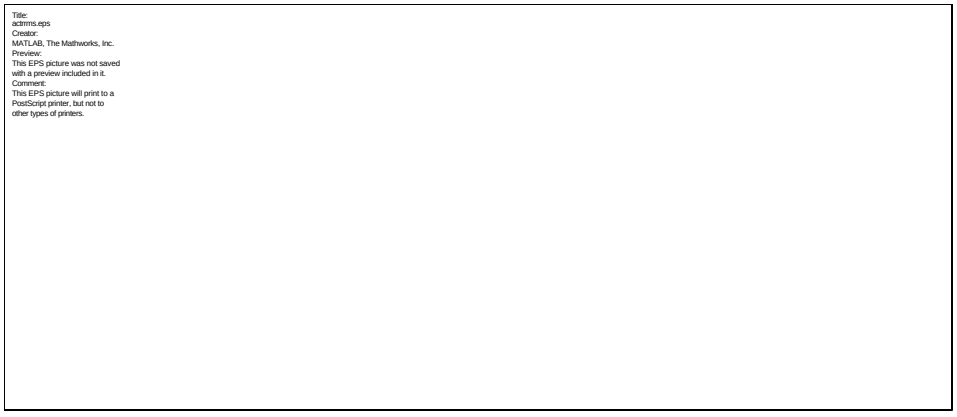

Figure 5.1 52 State and Reduced 20 State Transmission Controller (Mic/Acc)

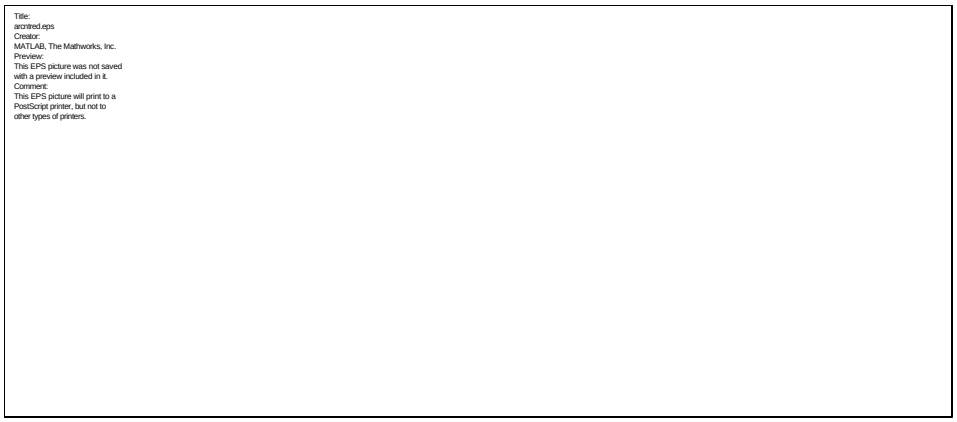

Figure 5.2 52 State and Reduced 20 State Reflection Controller (Mic/Acc)

The two signals coming from the two controllers have to be combined before being sent to the PZT actuator. The combination of the two signals was performed on one of the two real time computers, which was configured to use two inputs. The first input corresponded to the sensor, and the second to the output signal coming from the other real time computer. This signal was added by augmenting the controller and using a feedthrough term in the D matrix. A diagram of this configuration can be seen in Figure 5.3.

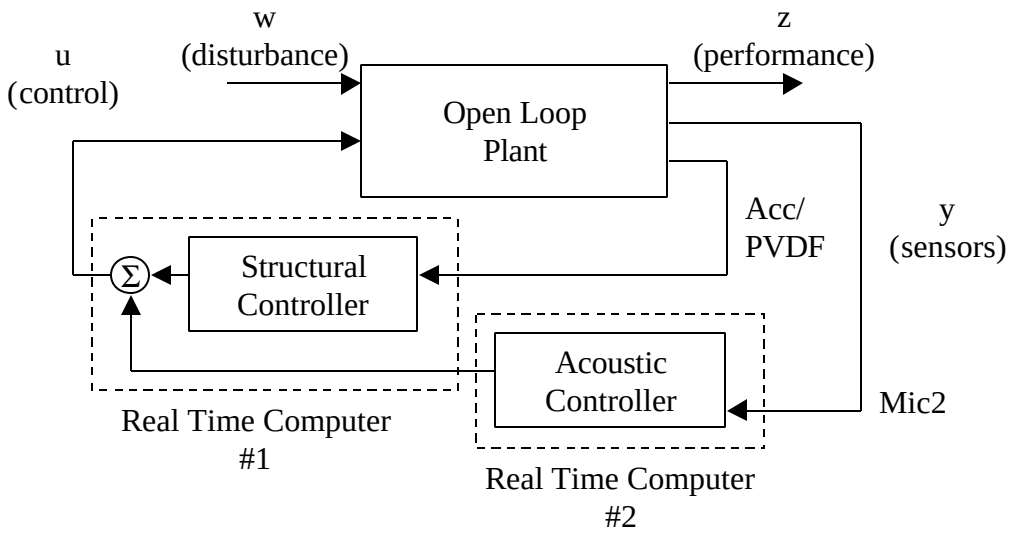

Figure 5.3 Diagram of Real Time Computer Configuration for Combined Transmission and Reflection Control on a Plate

5.1.1.2 Performance

Since two independent loops were used to control transmission and reflection, the first step was to validate each of the individual controllers. The first controller implemented was the transmission controller, which used the accelerometer on the center of the plate as feedback.

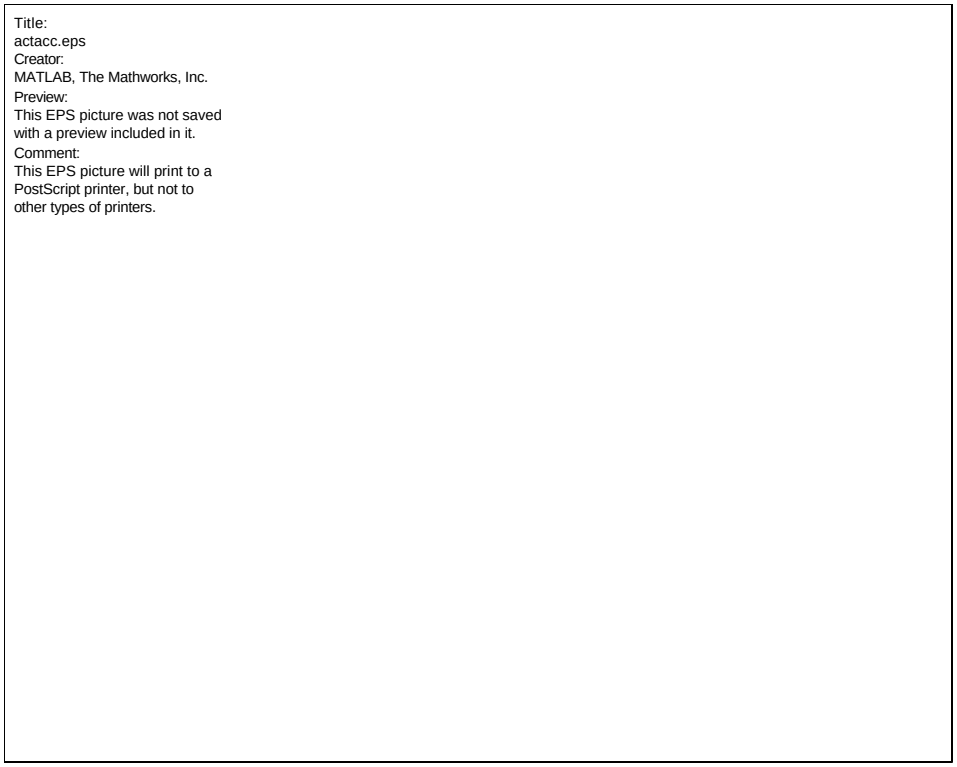

Figure 5.4 Closed Loop Transmission Control on Accelerometer (Mic/Acc)

Figure 5.4 shows the closed loop performance of the transmission controller as seen from the accelerometer. The first three structural modes at 72.9 Hz, 274.4 Hz and 655.7 Hz, respectively, were targeted by the structural controller. The actual performance obtained at each of the modes was less than that predicted. Table 5.1 shows the performance for each of these modes. The 10-1000 Hz broadband performance of the controller was 3.14 dB, which is less than the 3.74 dB performance that was predicted.

Figure 5.5 shows the closed loop performance on microphone 4. It is seen that the predicted performance is also greater than the actual performance of the transmission controller. A 10-1000 Hz broadband predicted performance was 0.36 dB and the actual performance 0.18 dB. Table 5.1 shows the attenuation obtained at each of the targeted modes.

Table 5.1 Performance of Accelerometer (Mic/Acc)

Mode	Attenuation (dB)		
	Transmission	Reflection	Combined
Structural1 - 72.9 Hz	11.72	-	11.17
Structural2 - 274.4 Hz	15.62	-	15.11
Structural3 - 655.5 Hz	7.79	-	8.25
Acoustic1 - 133.3 Hz	-	-3.72	-2.65
Acoustic2 - 325 Hz	-	4.03	4.59
Broadband (10-1000 Hz)	3.14	-1.176	2.22

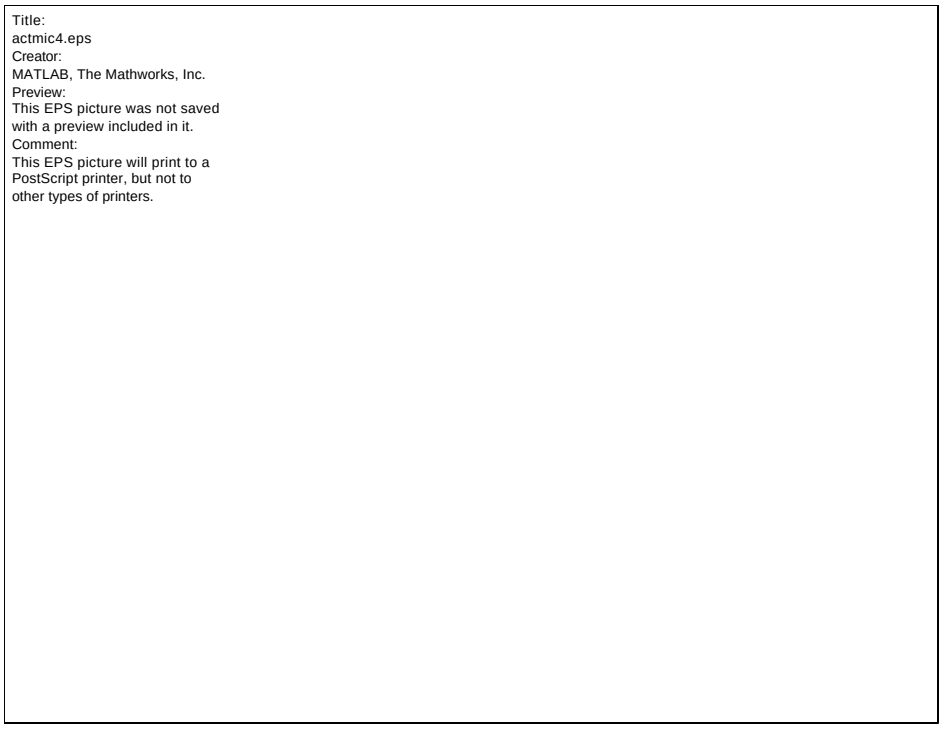

Figure 5.5 Closed Loop Transmission Control on Mic4 (Mic/Acc)

Near 225 Hz there is an amplification that could not be made to disappear by redesigning the controller with different weights. However, the actual amplification is less that the prediction.

The second controller implemented was the reflection controller, which used a microphone located as close as possible to the plate. This controller targeted the first two acoustic modes, located at 133.3 Hz and 325 Hz. During the initial tests, it was observed that targeting these two modes caused a considerable amplification of the speaker mode 188.4 Hz, so the speaker mode was also targeted by the reflection controller.

Table 5.2 Performance of Mic4 (Mic/Acc)

Mode	Attenuation (dB)			
	Transmission	Reflection	Combined	RMS
Structural1 - 72.9 Hz	13.06	-	12.73	7.27
Structural2 - 274.4 Hz	7.719	-	7.36	9.21
Structural3 - 655.5 Hz	3.53	-	3.41	-0.02
Acoustic1 - 133.3 Hz	-	7.85	5.69	3.2
Acoustic2 - 325 Hz	-	2.94	3.48	1.47
Broadband (10-1000 Hz)	0.18	2.37	1.39	2.62

Figure 5.6 shows the performance of the reflection controller on microphone 4. As expected, the first two acoustic modes are attenuated, and the speaker mode is only slightly amplified. The predicted 10-1000 Hz broadband attenuation is 1.82 dB, although the experimental attenuation was somewhat higher, 2.37 dB. The attenuation of each mode can be seen in Table 5.2.

It should also be noticed that the second structural mode at 274.4 Hz is also attenuated by the controller since it is close to the second acoustic mode. This could lead to a decrease in performance of the combined controllers since the second structural mode would receive opposing commands from the transmission and reflection controllers.

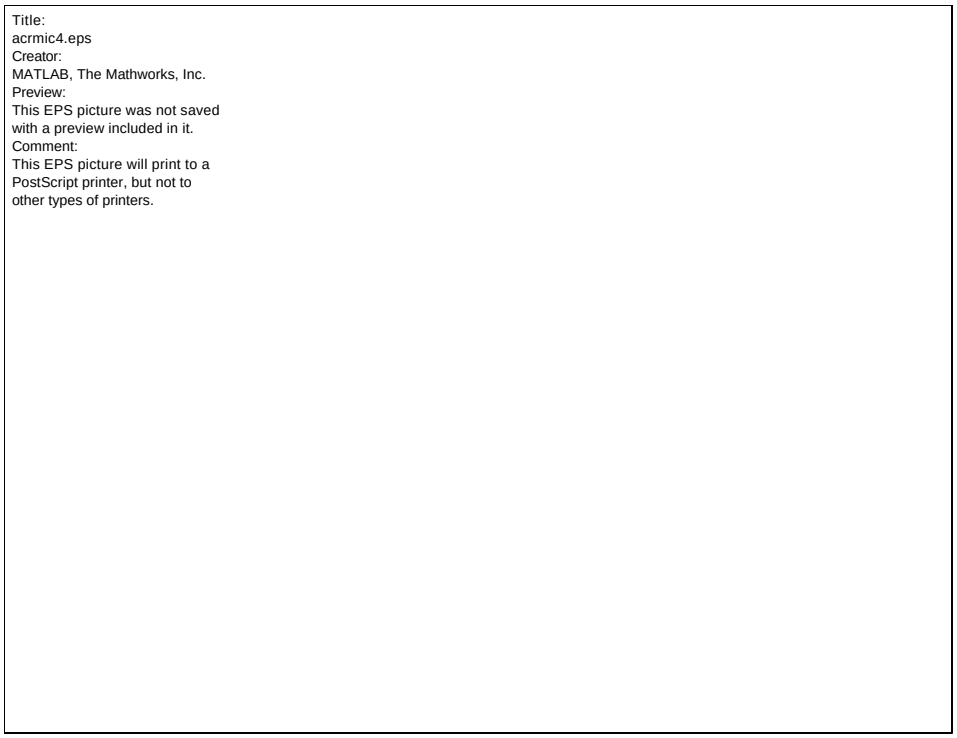

Figure 5.6 Closed Loop Reflection Control on Mic4 (Mic/Acc)

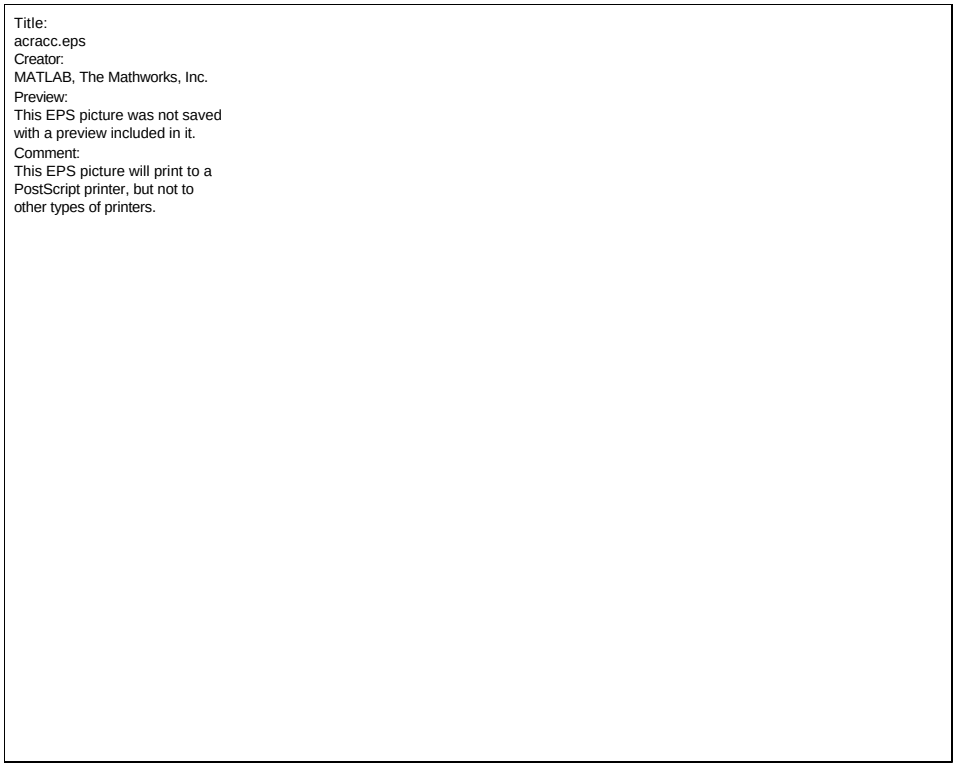

Figure 5.7 Closed Loop Reflection Control on Accelerometer (Mic/Acc)

Figure 5.7 shows the performance of the reflection controller on the accelerometer. The most notable feature in this graph is the amplification around the first acoustic mode at 133.3 Hz. This translates into a broadband amplification instead of attenuation. This shows that the controller is destiffening the plate to obtain a better impedance match with the acoustics. The second acoustic mode at 325 Hz, however, does not appear to show such behavior even though it was targeted. This leads to a broadband amplification of 1.17 dB, less than the 1.53 dB predicted. The attenuation at each mode can be found in Table 5.1.

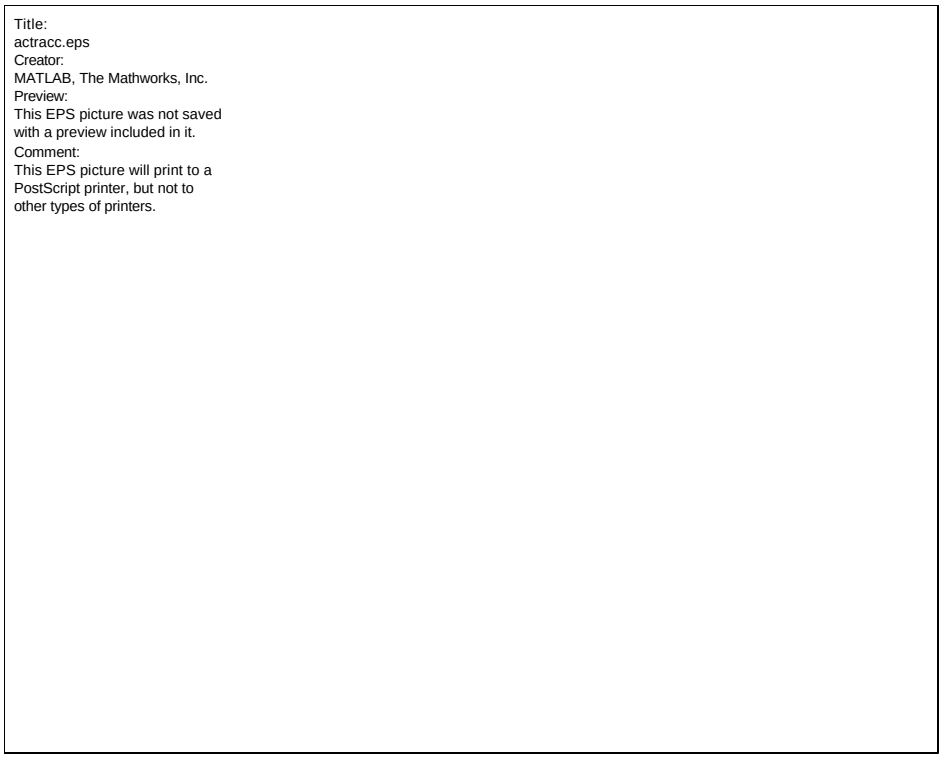

Figure 5.8 Closed Loop Transmission and Reflection Control on Accelerometer (Mic/Acc)

The final step was to implement both controllers together to observe how well they interacted. Figure 5.8 shows the performance of both controllers as observed by the accelerometer. The predicted performance clearly shows that both controllers are

actuating on their respective modes: the three structural modes are being attenuated while the first acoustic mode is amplified. The second acoustic mode is still not amplified, but rather attenuated somewhat. Also, the shortcoming of the transmission controller are also present, that is, the structural modes are not attenuated as much as predicted.

The 10-1000 Hz broadband peformance is an attenuation of 2.22 dB, close to the predicted attenuation of 2.20 dB. This number, however, is not really representative of whether both transmission and reflection are being performed on the plate, since the acceleromter will observe a combination of stiffened modes (structural modes) and less stiff modes (acoustic modes). Table 5.1 shows the attenuation at each mode.

Figure 5.9 shows the performance observed by microphone 4. This measurement is also a performance metric since it is measuring the pressure inside the chamber. It shows how both controllers interact and their effect on the internal acoustics.

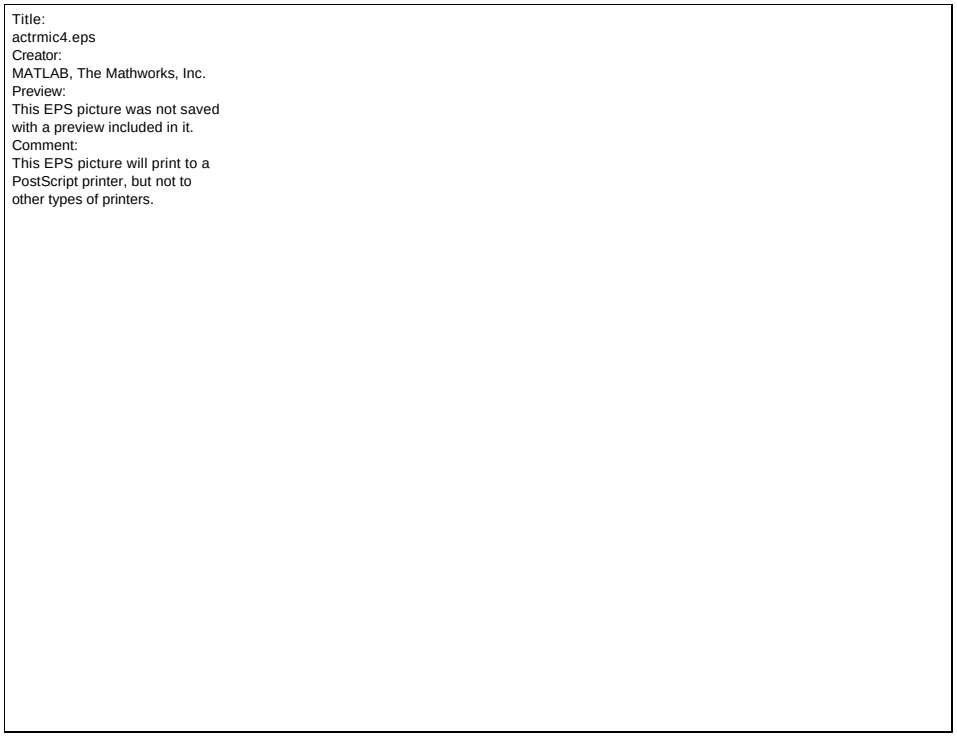

Figure 5.9 Closed Loop Transmission and Reflection Control on Mic4 (Mic/Acc)

The 10-1000 Hz broadband performance was an attenuation of 1.39 dB, somewhat lower than the predicted performance of 1.86 dB. The first acoustic mode was not attenuated as much as predicted, although the first structural mode was attenuated almost as predicted. The same amplification around 225 Hz was present, although it was not as great during implementation. The conflict between the second structural and second acoustic modes at 287 Hz and 325 Hz, respectively, can also be seen, since neither mode is attenuated as much as predicted. Finally, the structural controller attenuated the third structural mode at 665.7 Hz. The attenuation at each mode can be seen in Table 5.2.

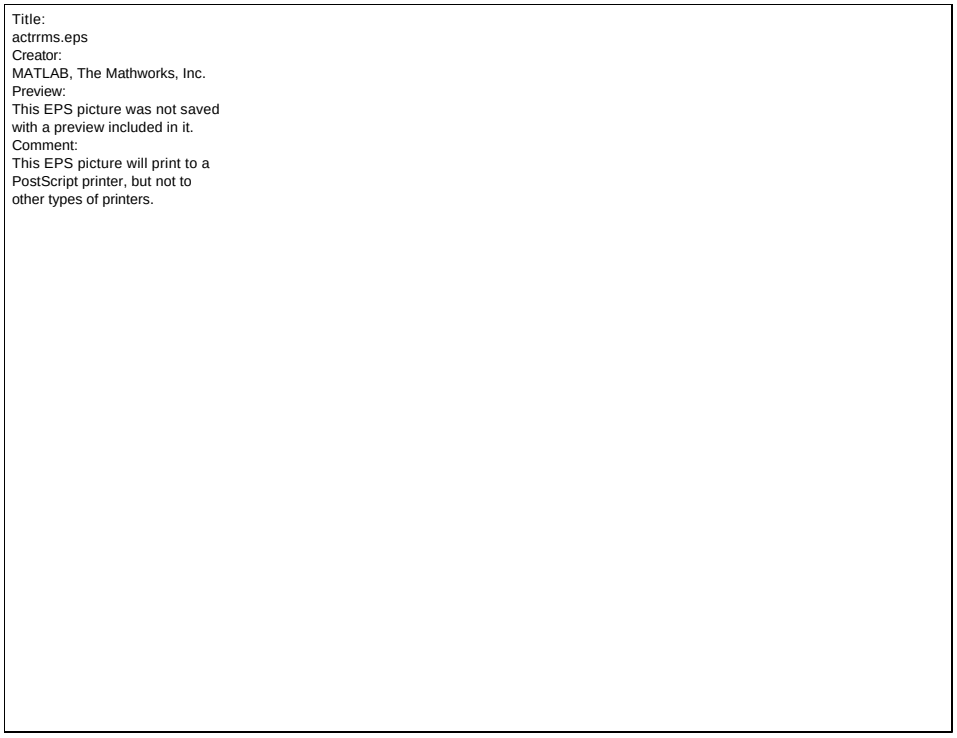

Figure 5.10 Closed Loop Transmission and Reflection Control – RMS Microphones (Mic/Acc)

The final performance of the system was measured by taking the measurements from the three microphones inside the chamber (microphones 4, 1 and 2) and obtaining their the root mean square. This was done to ensure that the acoustic attenuation was

obtained throughout the whole chamber and not only at the location near the plate. Figure 5.10 shows the RMS performance of the three microphones. All the relevant features are also present in this graph: attenuation of the first structural and acoustic modes, although less attenuated than expected; no change in the attenuation of the speaker mode; lower performance at the second structural and acoustic modes due to their proximity; and finally, attenutation of the third structural mode. The attenuation at each mode can be found in Table 5.2.

5.1.2 PVDF and Pressure Feedback

5.1.2.1 Controller Implementation

The implementation of these controllers is exactly the same as the implementation of the controllers of the previous section. In this case, however, the PVDF strain sensor was used instead of the accelerometer. The signal coming from the PVDF strain sensor was conditioned using an operational amplifier to obtain an input impedance of 10MΩ.

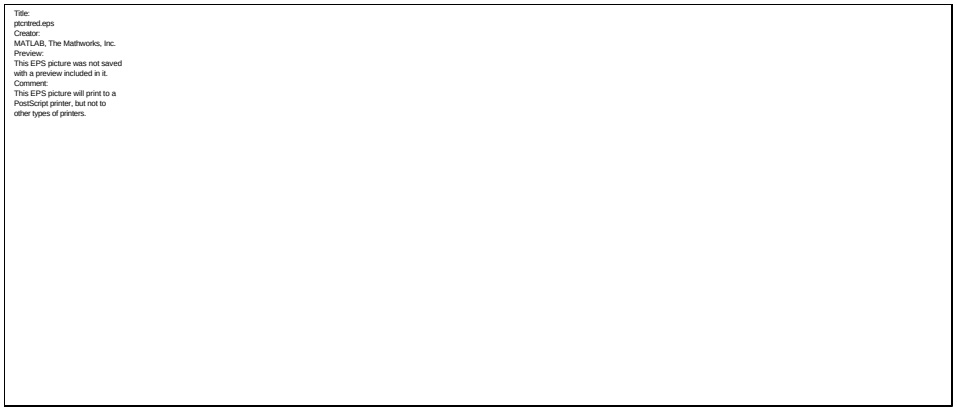

Figure 5.11 52 State and Reduced 20 State Transmission Controller (Mic/PVDF)

As before, the controllers had to be reduced to implement them on the real time computers. Both transmission and reflection controllers were reduced from 52 states to

20 states, allowing the real time computers to run at a sampling frequency of 8200 Hz. Figure 5.11 shows a comparison of the full 52 state transmission controller and the 20 state reduced controller. The same reflection controller of the previous section was used here, shown in Figure 5.2.

5.1.2.2 Performance

The same procedure that was followed in the previous section was used to test the performance of simultaneous transmission and reflection control using PVDF and pressure feedback. The difference is only the type of structural sensor used, which is now the PVDF film on the plate instead of the accelerometer.

Table 5.3 Performance of PVDF (Mic/PVDF)

Mode	Attenuation (dB)		
	Transmission	Reflection	Combined
Structural1 - 72.9 Hz	11.49	-	11.09
Structural2 - 274.4 Hz	11.07	-	10.14
Structural3 - 655.5 Hz	0.79	-	0.86
Acoustic1 - 133.3 Hz	-	-3.56	-3.05
Acoustic2 - 325 Hz	-	4.06	4.2
Broadband (10-1000 Hz)	5.27	-1.13	4.34

Figure 5.12 shows the closed loop performance of the transmission controller as seen from the PVDF. The same three structural modes at 72.9 Hz, 274.4 Hz and 655.7 Hz, respectively, were targeted by the structural controller, although the third structural mode was not highly observed by the PVDF. The actual performance obtained at each of the modes as predicted. Table 5.3 shows the performance for each of these modes. The 10-1000 Hz broadband performance of the controller was 5.28 dB, slightly more than the 5.22 dB performance that was predicted.

Table 5.4 Performance of Mic4 (Mic/PVDF)

Mode	Attenuation (dB)			
	Transmission	Reflection	Combined	RMS
Structural1 - 72.9 Hz	13.23	-	12.89	13.48
Structural2 - 274.4 Hz	6.56	-	5.88	11.36
Structural3 - 655.5 Hz	-0.58	-	-0.05	1.59
Acoustic1 - 133.3 Hz	-	7.31	6.24	6.64
Acoustic2 - 325 Hz	-	2.96	3.12	3.88
Broadband (10-1000 Hz)	0.24	2.013	2.37	4.14

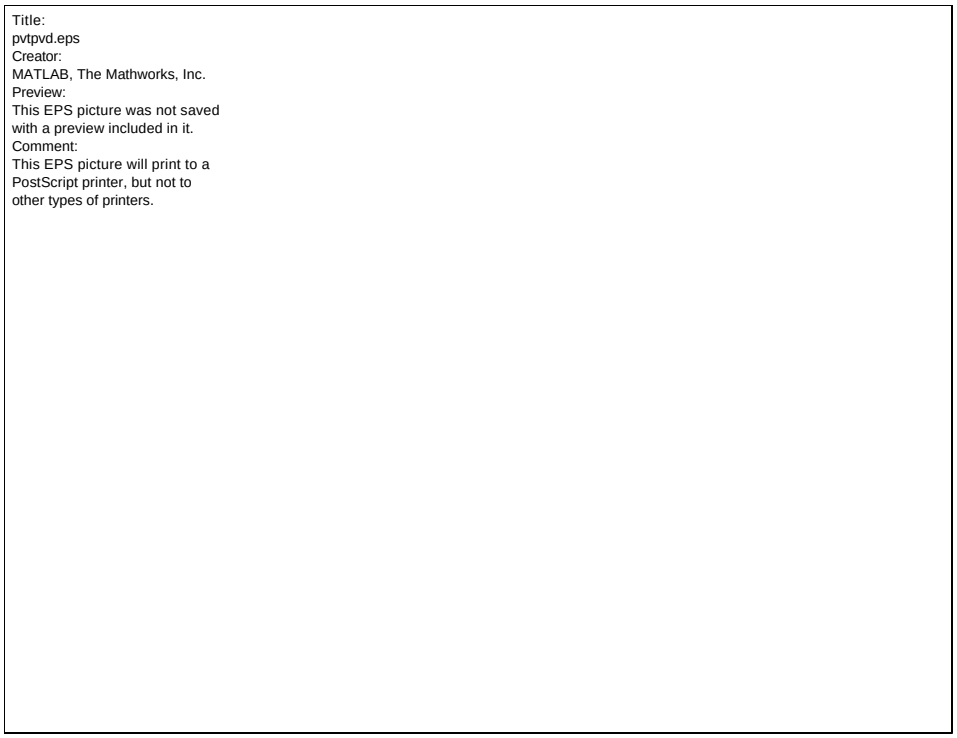

Figure 5.12 Closed Loop Transmission Control on PVDF (Mic/PVDF)

Figure 5.13 shows the closed loop performance on microphone 4. It is seen that the predicted and actual performance of the transmission controller are consistent. The predicted 10-1000 Hz broadband performance was 0.23 dB while the actual performance was 0.24 dB. Table 5.4 shows the attenuation obtained at each of the targeted modes. The same behavior that was observed in the previous section was observed near 225 Hz. The amplification could not be removed.

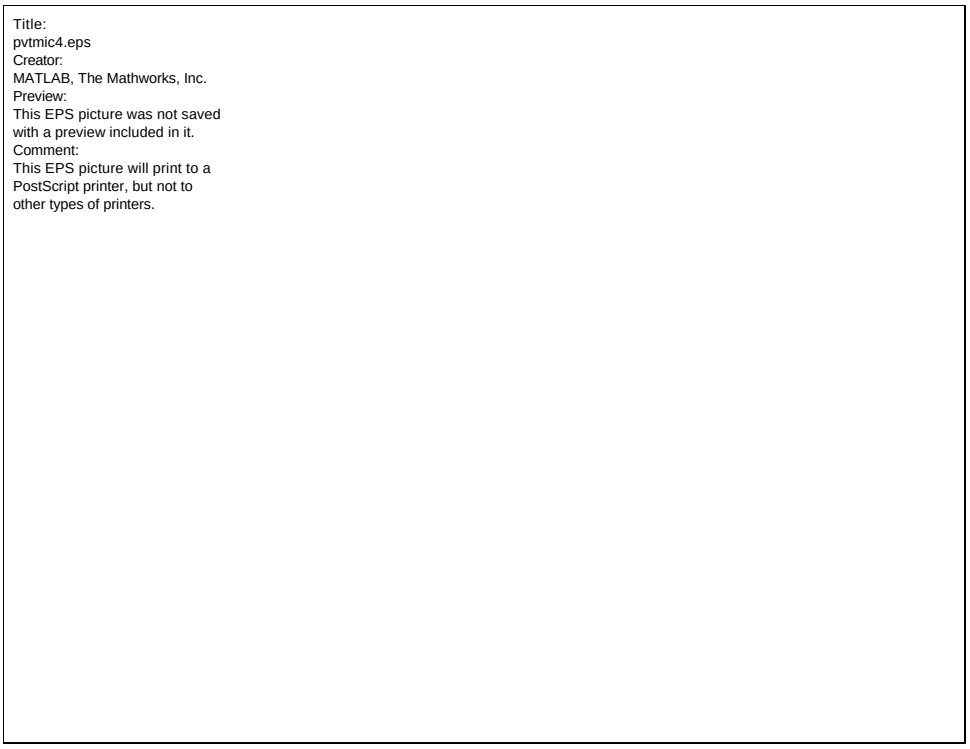

Figure 5.13 Closed Loop Transmission Control on Mic4 (Mic/PVDF)

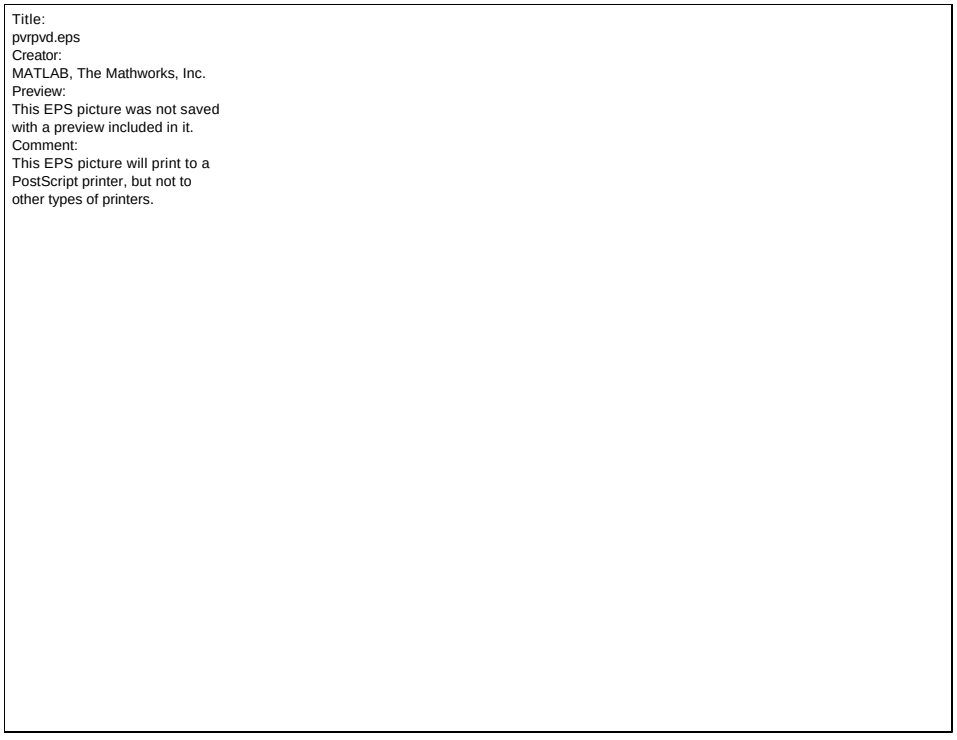

Figure 5.14 Closed Loop Reflection Control on PVDF (Mic/PVDF)

The second controller implemented was the reflection controller using the microphone, which is identical to the one used in the previous section.

Figure 5.14 shows the performance of the reflection controller on the PVDF. The important feature in this graph is the amplification around the first acoustic mode at 133.3 Hz, which was also observed when using the accelerometer. This translates into broadband amplification instead of attenuation where the controller is destiffening the plate to obtain a better impedance match with the acoustics. The second acoustic mode at 325 Hz, however, does not appear to show such behavior even though it was targeted. This leads to a broadband amplification of 1.33 dB, less than the 1.63 dB predicted. The attenuation at each mode can be found in Table 5.3.

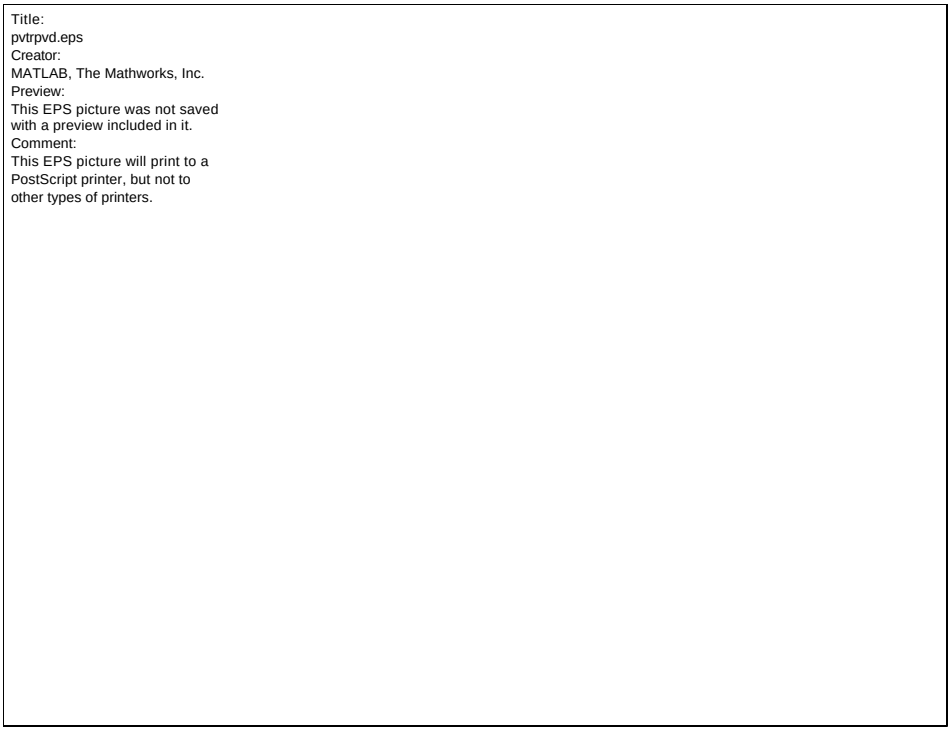

Figure 5.15 Closed Loop Transmission and Reflection Control on PVDF (Mic/PVDF)

The final step was to implement both controllers together to observe how well they interacted. Figure 5.15 shows the performance of both controllers as observed by

the PVDF. The predicted performance clearly shows that both controllers are actuating on their respective modes: the three structural modes are being attenuated while the first acoustic mode is amplified. The second acoustic does not seem to be changed.

The 10-1000 Hz broadband performance is an attenuation of 4.34 dB, slightly above the predicted attenuation of 4.16 dB. As before, this number does not really represent whether both transmission and reflection are being performed on the plate, since the PVDF observes a combination of stiffened modes (structural modes) and less stiff modes (acoustic modes). Table 5.3 shows the attenuation at each mode.

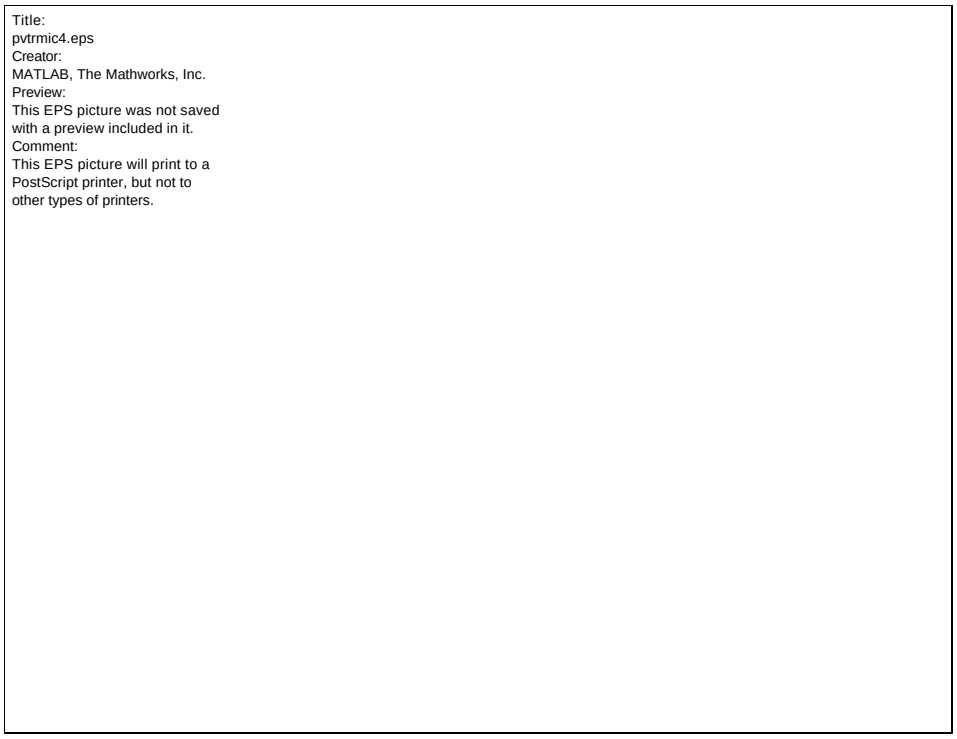

Figure 5.16 Closed Loop Transmission and Reflection Control on Mic4 (Mic/PVDF)

Figure 5.16 shows the performance observed by microphone 4. This measurement is also a performance metric since it is measuring the pressure inside the chamber. The 10-1000 Hz broadband performance was an attenuation of 2.01 dB, close to the predicted performance of 2.05 dB. The first acoustic and structural modes were

attenuated as predicted. The same amplification around 225 Hz was present, although it was not as great during implementation. The conflict between the second structural and second acoustic modes at 287 Hz and 325 Hz, respectively, can also be seen, since neither mode is attenuated as much as predicted. Rather, it seems that the second structural mode is amplified somewhat. Finally, the controllers did not attenuate the third structural mode at 665.7 Hz. The attenuation at each mode can be seen in Table 5.4.

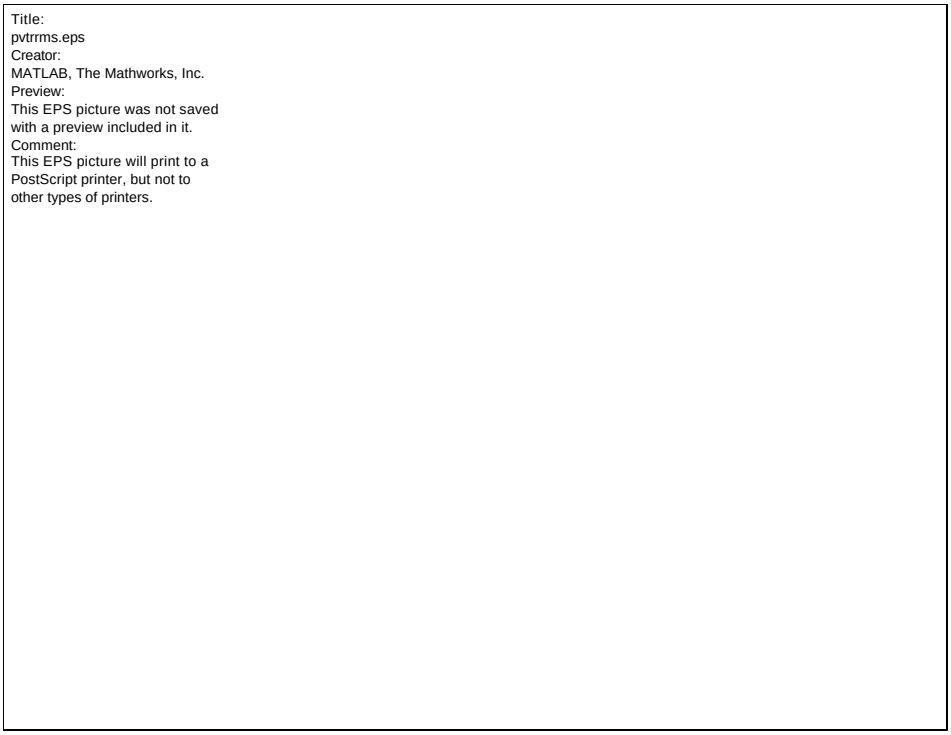

Figure 5.17 Closed Loop Transmission and Reflection Control – RMS Microphones (Mic/PVDF)

The final performance of the system was measured by taking the root mean square of the measurements from the three microphones inside the chamber (microphones 4, 1 and 2). Figure 5.17 shows the RMS performance of the three microphones. All the relevant features are also present in this graph: attenuation of the first structural and acoustic modes as predicted; no change in the attenuation of the speaker mode; lower performance at the second structural mode due to its proximity with

the second acoustic mode; and finally, no attenuation of the third structural mode. The attenuation at each mode can be found in Table 5.4.

5.1.3 Conclusions

In this section, two different sensor configurations were implemented to perform combined transmission and reflection control on a plate. The first configuration consisted of a microphone near the plate and an accelerometer on the center of the plate. The second consisted of the same microphone and a PVDF strain sensor on the plate.

The best performance was obtained from the PVDF/microphone pair, which produced a 10-1000 Hz broadband reduction of the internal acoustics of 4.15 dB. The accelerometer/microphone pair produced a 2.62 dB broadband reduction for the same chamber. It is interesting to notice that the predicted performance of both sensor sets was similar, around 3.6 dB. However, the use of the PVDF proved to be more effective than the accelerometer.

This difference in performance may be due to two reasons. The first is that the PVDF sensor is a distributed sensor, whereas the accelerometer only measures the accelerometer on the center of the plate. Thus, more information on the behavior of the plate is given by the PVDF. Secondly, the PVDF is designed to filter out the third and higher structural modes, and it does not capture the asymmetric modes of the plate well either. Thus, its signal carries only information that is relevant to the controller, whereas the accelerometer picks up all plate modes: the higher symmetric modes as well as the asymmetric modes.

5.2 Acoustic Power Diode

5.2.1 Controller Implementation

The same electronics and basic configuration that were used previously were used to implement the acoustic power diode. In this case, however, the PVDF sensor was not needed, as well as its supporting circuitry.

The controllers were implemented on two Heurikon digital computers operating at a sampling frequency of 8200 Hz. Since this is a digital implementation of the controllers, a time delay is introduced into the compensator transfer function. To make the LQG algorithm take this into account, a Padé time delay approximation was added to the plant to ensure the closed loop stability.

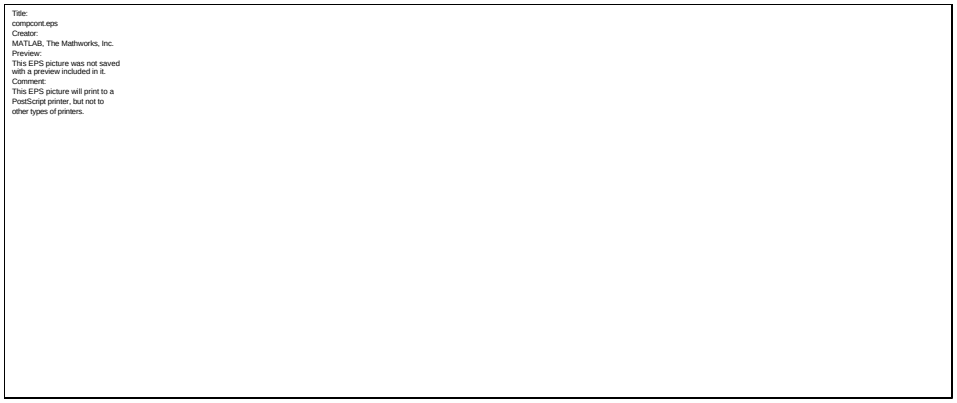

Figure 5.18 54 State and Reduced 20 State Pressure Controller (Diode)

Due to limitations of the Heurikon real time computers, the controllers could not be directly implemented as designed and had to be reduced. The 54 state pressure feedback controller was reduced to 20 states. Using the 20 state controller, the sampling frequency was set at 8200 Hz. Before closing the loop, the loop transfer function using the reduced controller was checked to ensure the closed loop stability of the system.

Figure 5.18 shows a comparison of the full 54 state transmission controller and the 20 state reduced controller. The second controller did not need to be reduced, since it was a gain and an integrator. This requires only one state and the real time computer can handle this with ease at any sampling frequency. However, the same sampling frequency was used in both computers to be consistent.

The two signals coming from the two controllers have to be combined before being sent to the PZT actuator. The combination of the two signals was performed on one of the two real time computers, which was configured to use two inputs. The first input corresponded to the sensor, and the second to the output signal coming from the other real time computer. This signal was added by augmenting the controller and using a feedthrough term in the D matrix. A diagram of this configuration can be seen in Figure 5.19.

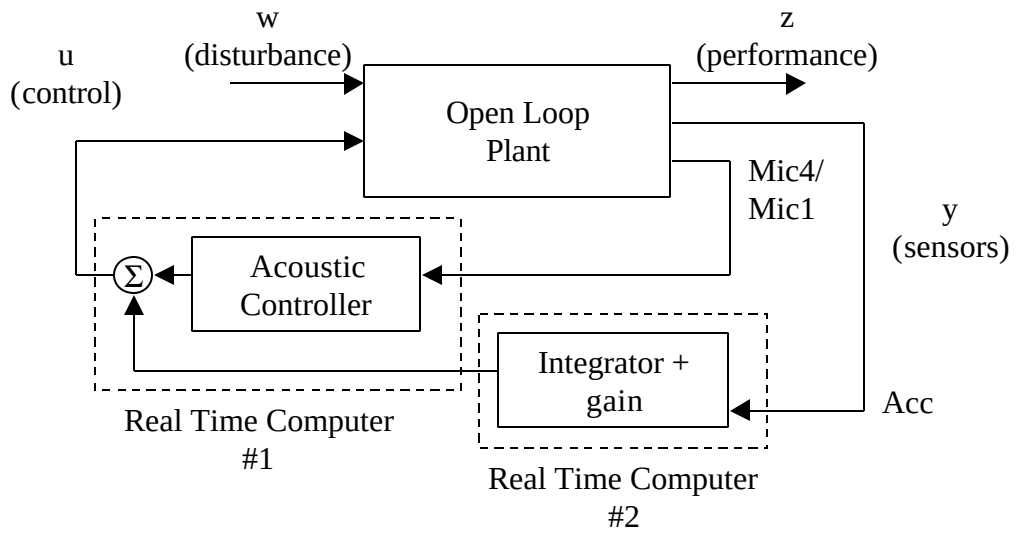

Figure 5.19 Diagram of Real Time Computer Configuration for Acoustic Power Diode

5.2.2 Performance

As was done in the previous section, the first step was to test one loop and then to test both loops. The first loop that was tested was the inner or pressure loop, and then the outer loop was added. This procedure was followed for each of the two cases, the first considering that the disturbance source is inside the fairing, and the second considering that the disturbance is outside of the fairing.

5.2.2.1 Speaker inside Fairing

In this configuration, the disturbance source is located inside the fairing, thus the objective of the acoustic power diode is to attenuate the internal acoustics by allowing energy to flow out of the fairing though the structure.

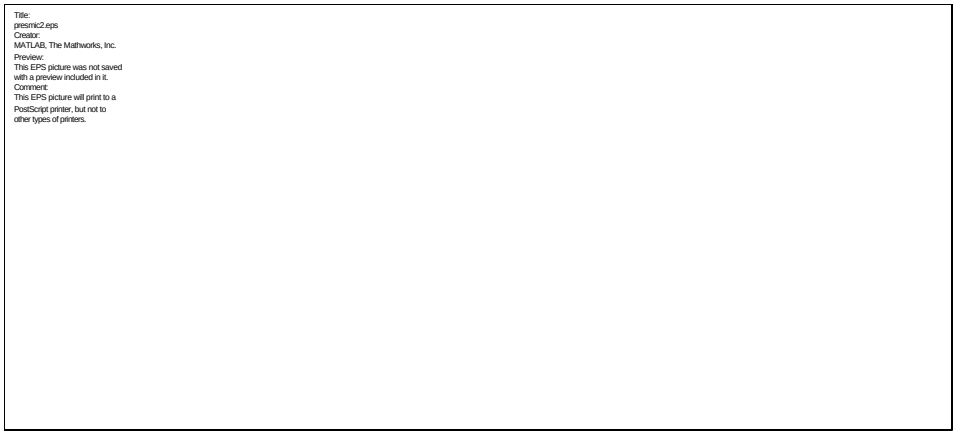

Figure 5.20 Pressure loop performance on Mic2 (Diode)

Figure 5.20 shows the performance of the pressure controller alone. The first plate mode at 71 Hz, the only one that was targeted by the controller, has been attenuated by approximately 11 dB.

The next step was to close the outer loop, which contains the integrator and the gain. Figure 5.21 shows the performance on microphone 2. The addition of the outer

loop seems to cancel out any possible benefits of the controller, since the first plate mode at 72 Hz is not attenuated as before. The other modes, as expected, are not attenuated since they were not targeted by the controller.

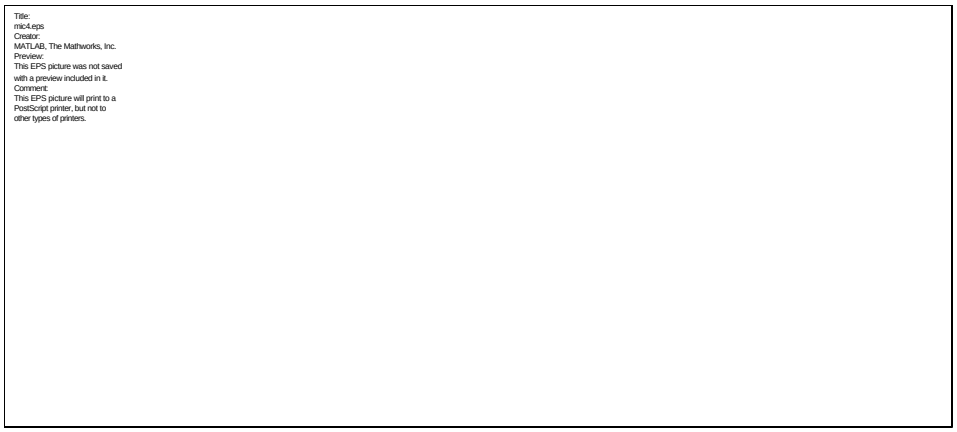

Figure 5.21 Diode Performance on Mic (Mic2)

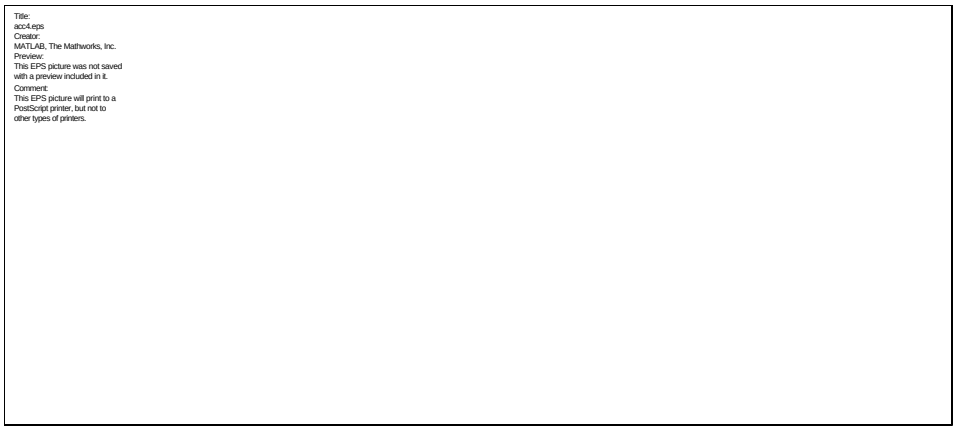

Figure 5.22 Diode Performance on Acc (Mic2)

As Figure 5.22 shows, however, the accelerometer, shows a different response. The first plate mode is not attenuated either, although this is not necessarily unexpected. The purpose of the diode in this configuration is to actuate on the plate in such a manner that will allow energy to flow through it. This means that the plate mode should not be attenuated. It is curious to notice that the second and third plate modes, at 286 Hz and 664 Hz are attenuated considerably, despite not being targeted by the pressure feedback

controller. This attenuation comes from the accelerometer signal, which is used to command the reference input into the controller. However, since the pressure feedback controller is not targeting these modes, the accelerometer commands the plate to stiffen at those modes.

Finally, the predicted performance is somewhat higher than the actual performance, which seems to stem from the accelerometer as was the case in the previous section.

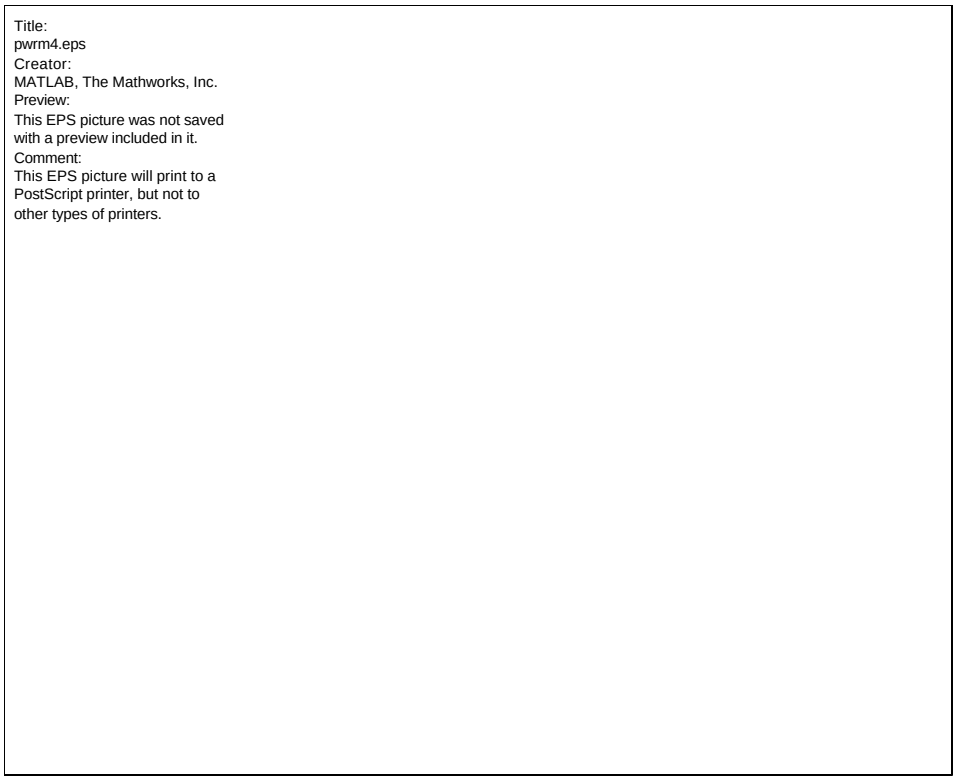

Figure 5.23 Power Flow through the Plate (Mic2)

When considering that the speaker is inside the faring, the objective is to allow acoustic energy to flow out of the fairing with ease. Figure 5.23 shows a plot of the power flow through the plate. It is seen that the acoustic power diode does in fact allow energy to flow in one direction only, as represented by the large negative peaks near the first plate mode at 71Hz. However, the performance of the actual diode was not close to

what was predicted. It seems that the accelerometer is responsible for this since it is only a point sensor and only picks up information on the behavior of the center of the plate.

It is also important to notice that it appears that power only flows through the first plate mode and not through the others. Intuitively it should not be so, but the accelerometer does command the controller to dampen the higher plate modes. Also, since the sensors (microphone and accelerometer) are only located at the center of the plate, with their information it is not possible to show how power is flowing though the other modes. Distributed sensors are needed for this purpose.

5.2.2.2 Speaker outside Fairing

In this configuration, the disturbance source is located outside the fairing, thus the objective of the acoustic power diode is to attenuate the internal acoustics by preventing energy from flowing into the fairing though the structure.

Figure 5.24 shows the performance of the pressure controller alone. The first plate mode at 71 Hz, the only one that is being targeted by the controller, has been attenuated by approximately 6 dB.

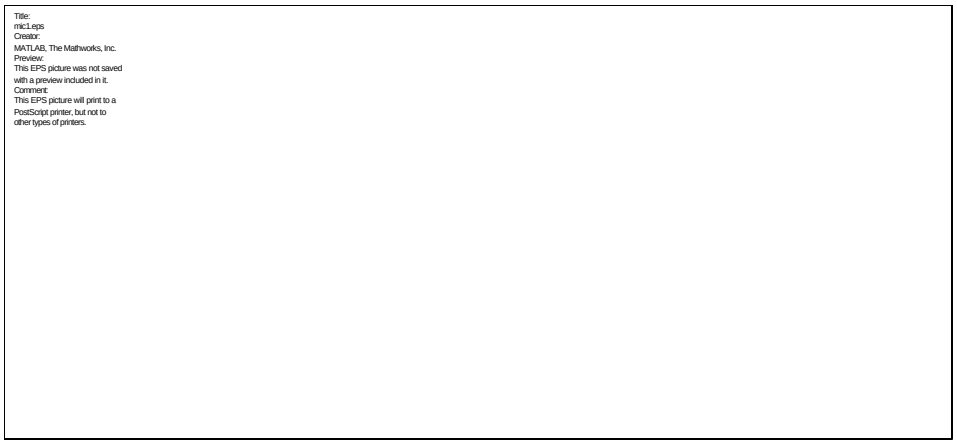

Figure 5.24 Pressure loop performance on Mic6 (Diode)

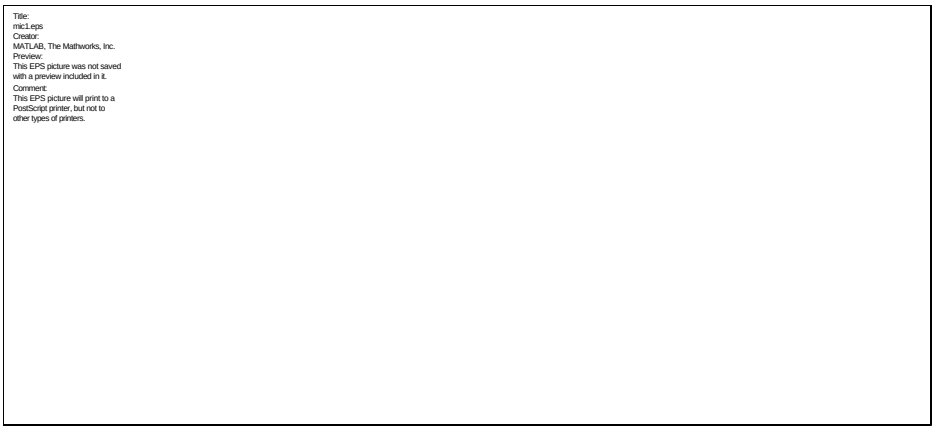

Figure 5.25 Diode Performance on Mic (Mic6)

As before, the next step was to close the outer loop, which contains the integrator and the gain. Figure 5.25 and Figure 5.26 show the performance on microphone 6 and the accelerometer on the plate.

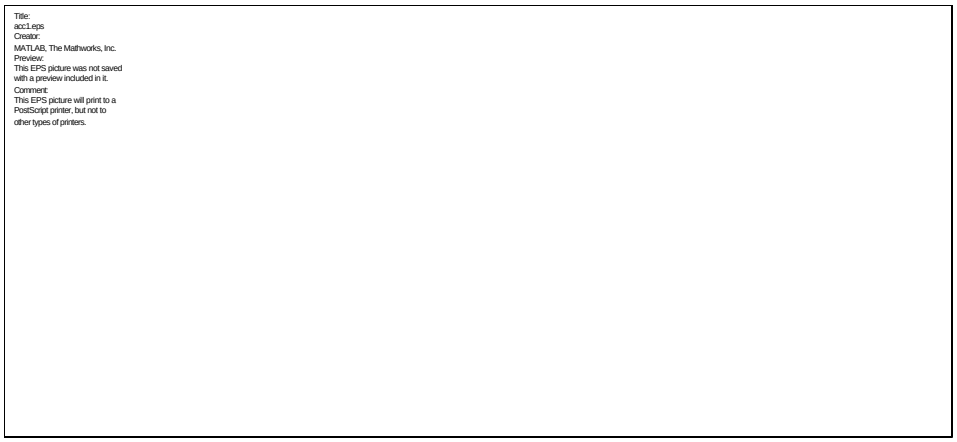

Figure 5.26 Diode Performance on Acc (Mic6)

Contrary to the previous case, the addition of the outer loop does attenuate the first plate mode at 71 Hz. Also, due to the addition of the accelerometer signal, the higher plate modes are also attenuated. This is explained simply by looking at the diode as a transmission controller under this configuration: it prevents energy to flow through the plate, and the information it has to achieve this comes from the accelerometer. Thus, the plate modes are attenuated.

The accelerometer shows a similar response. All the modes are attenuated, which shows that the diode is preventing the plate from vibrating, thus making it act as a transmission controller. The purpose of the diode in this configuration is to actuate on the plate in a manner that will not allow energy to flow through it. As was the case in the previous configuration, this attenuation comes from the accelerometer signal, which is used to command the reference input into the controller.

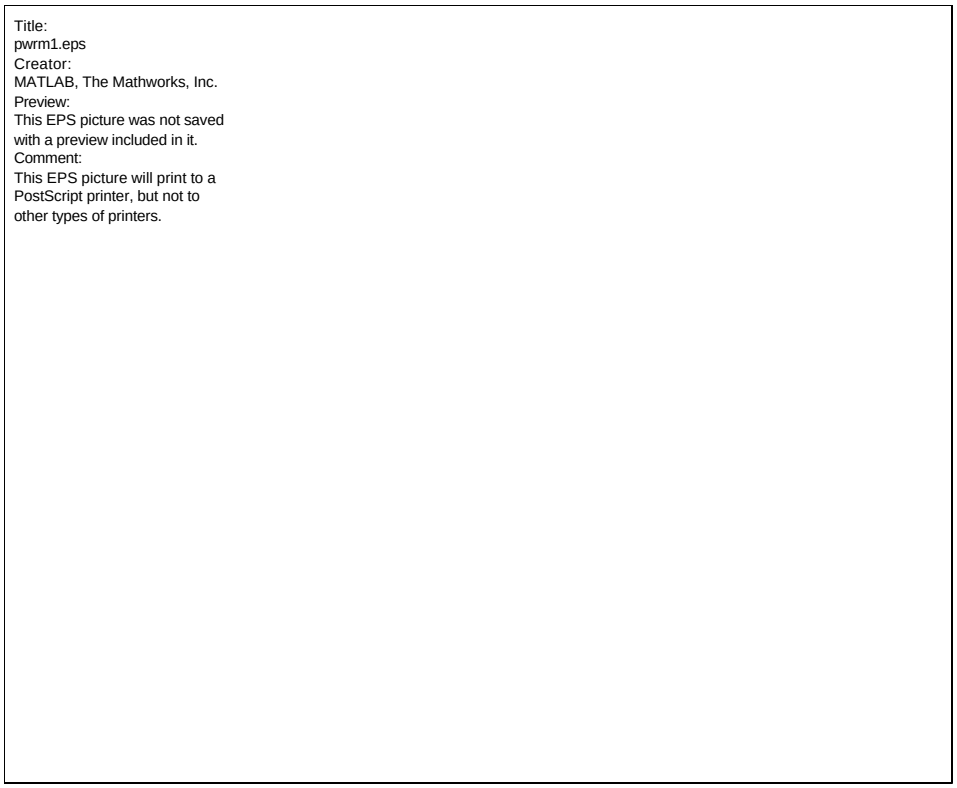

Figure 5.27 Power Flow through the Plate (Mic6)

Finally, the predicted performance is somewhat higher than the actual performance, which again shows that the accelerometer is the cause of the decrease in performance.

When considering that the speaker is outside the faring, the objective is to prevent acoustic energy to flow into the fairing. Figure 5.27 shows a plot of the power flow

through the plate. It is seen that the acoustic power diode does not allow energy to flow into the fairing, as represented by the highly reduced power flows at the first plate mode at 71Hz. The attenuation obtained at this mode was 10.56 dB. The performance of the actual diode seems to be close to what was predicted, but this does not necessarily mean that the accelerometer is not performing below expectations, only that stiffening the plate more using the accelerometer signal requires a non-linear increase in command input.

5.2.3 Conclusions

In this section, the acoustic power diode was implemented on a symmetric chamber to show that the same controller, the diode, would allow acoustic energy to flow in one direction only, attenuating the energy that was coming in the other direction.

The performance of the power diode was not as high as expected, mainly due to the use of an accelerometer. Although it is not known why the accelerometer does not perform as well as expected, it was still possible to observe the diode effect in the two different configurations. In the first, acoustic energy was allowed to go through the plate, and the diode created a path for this energy to flow with more ease than in open loop. In the second configuration, the diode prevented energy from flowing through the plate, thus behaving as a transmission controller. The use of the two sensors (microphone and accelerometer) did show an increase in the performance in transmission control compared to when only the microphone was used. An attenuation of 10.56 dB at the first acoustic mode was obtained, with the possibility of even higher performance were the accelerometer to perform as predicted.

A limitation of the current implementation of the power diode is that only the first structural mode was targeted. Since the microphone is a point sensor, an assumption is

made that the pressure on all the surface of the plate is the same as the pressure at its center. Under this assumption only the first plate mode can be used since it is the only one where an increase in pressure over the whole surface of the plate can take place.

Chapter 6

6. Conclusions

6.1 Summary

Most acoustic disturbances are generated outside of the payload fairing and travel to the inside of the fairing through the rocket shroud or through the rocket structure. It is reasonable to believe that reducing the amount of acoustic noise that is transmitted through the shroud will lead to a reduction of the acoustics inside the fairing (transmission control). However, since some noise will always enter the payload fairing, further reduction of the internal acoustics could be achieved if the acoustic energy inside the fairing could be dissipated (reflection control). A requirement for this procedure is to add as little mass as possible to the existing rocket, and it is also desired to use structural sensors and actuators to the maximum extent possible.

Two independent methods were investigated as possible answers to the problem of vibro-acoustic control applied to launch vehicle shrouds. A simple one-dimensional acoustic study of the two methods was done in lieu of the more complex three-dimensional problem.

The first method studied combined transmission and reflection control on the plate using the acoustic test chamber available at MIT. Transmission control was achieved by adding structural damping to the plate using piezoelectric materials, and reflection control was achieved by removing damping from the plate . In general, damping was added at the structural modes, whereas damping was removed at the acoustic modes.

Two separate configurations were used to implement this type of acoustic control. The first configuration used a microphone to measure the acoustic modes and an accelerometer to measure the structural modes. The second used a microphone for the acoustic modes and a PVDF strain sensor for the structural modes. Two independent LQG controllers, one for reflection and one for transmission, were designed and combined using superposition for each set of sensors and implemented on the acoustic test chamber.

Both sets of sensors showed that transmission and reflection control can be performed on the structure. Using the microphone/accelerometer pair, a 10-1000 Hz broadband attenuation of the fairing acoustics of 2.62 dB was achieved, and using the microphone/PVDF pair, an attenuation of 4.15 dB was achieved. It should be noted that both methods had a predicted attenuation of about 3.6 dB. The choice of structural sensor has considerable importance in the performance of the controllers. PVDF seems to fare better than the accelerometer since it is a distributed sensor, and it was also designed to pick up the first and second plate modes, which are of most interest.

The second method studied consisted in the implementation of an acoustic power diode, whose purpose is to allow acoustic energy to flow in only one direction. In this

case, the diode is set up such that acoustic energy is allowed only to flow from the inside to the outside of the fairing. This method combines both transmission and reflection control into a single controller, and it requires two sensors as well: a structural sensor (accelerometer) and an acoustic sensor (microphone).

It was observed that the transmission and reflection controllers would have lower performance than desired when the structural and acoustic modes that are being attenuated are close together, since the controllers issue opposing commands that reduce their total effectiveness.

The acoustic power diode was implemented on a symmetric chamber to be able to measure the effect of the diode depending on whether the disturbance was located on one end of the chamber or the other. The first case, which considered the disturbance source as being inside the fairing, showed that the controller allowed energy to flow towards the outside of the faring. The second case, which considered the disturbance source as being outside the fairing, showed that the controller prevented energy from flowing into the fairing, obtaining an attenuation of 10.56 dB at the first structural mode. The performance of the diode was not as high as predicted, and it is thought that the use of the accelerometer as a structural sensor is the culprit. Also, a shortcoming of the diode as it was implemented is that due to the point nature of the sensors, only the first structural mode was targeted by the diode.

6.2 Recommendations for Future Work

In the implementation of the two types of controllers it was seen that the accelerometer was the cause for lower than expected performance since it only has

information of the behavior of the center of the plate, and it does not filter out the asymmetric and higher modes of the plate as the PVDF does. An alternative structural sensor, especially in the case of the acoustic power diode, should lead to better performance for both types of controllers.

In the implementation of any control mechanism for attenuation of the acoustic levels inside a payload fairing, it is desirable to add the minimum amount of mass possible to the existing structure. It is for this reason that structural sensors and actuators are preferred. However, due to the weak coupling of the internal acoustics with the structure, the structure cannot be used as an acoustic sensor. A microphone was used in this thesis as an acoustic sensor, but it has the disadvantage of being a point sensor and not being part of the structure.

An alternative to the microphone, which can be attached to the isogrid structure of the payload fairing, is a membrane that will act as an acoustic sensor. This was tested on the acoustic test chamber using a mylar drum membrane with two disks of PVDF film, one on each side, placed ¾ inch apart from the plate. However, it was observed that unless the space between the plate and the membrane was pressurized, the signals coming from the PVDF disks were not clean enough to be used for control purposes. Similarly, actuation on the membrane using the PVDF disks is not possible without this pressurization.

The setup as tested had the drawback that the pressure on one side of the plate changed its boundary conditions, and thus its modes shifted. When the volume between the plate and the membrane was pressurized, the plate became stiffer and its fundamental

mode shifted to higher frequencies. It would be desirable to pressurize the membrane without having to change the plate's properties.

A possible solution for this is to place an identical membrane beside the one mentioned above, sealing them and pressurizing the section between them. This should allow the membrane to act as a distributed pressure sensor without affecting the structural properties of the fairing.

The power diode was only designed to target the first structural mode, although it is obvious that better performance could be achieved if more structural modes could be targeted. For this purpose, a distributed pressure sensor should be used in place of the microphone, such as the membrane configuration mentioned above. Using this new sensor, the power flow at each plate mode of interest should be controllable.

References

[1] Glaese, R.M. "Impedance Matching for Structural-Acoustic Control," Ph.D. Thesis, Massachusetts Institute of Technology, 1997.

[2] Asari, K. "Vibroacoustic Modeling and Control for Launch Vehicle Shrouds," Master's Thesis, Massachusetts Institute of Technology, 1998.

[3] Pascal, R.J. "Actuator and Sensor Design and Modeling for Structural Acoustic Control," Master's Thesis, Massachusetts Institute of Technology, 1999.

[4] Blaurock, C. "PVDF Modal Accentuation Sensor," 1998.

[5] Hyde, T. "Active Vibration Isolation for Precision Space Structures," Ph.D. Thesis, Massachusetts Institute of Technology, 1996.

[6] Jacques, R.N. and Miller, D.W., "Multivariable Model Identification from Frequency Domain Data," *IEEE Conference on Decision and Control*, 1994.

[7] Liu, K. "Identification of Multi-Input and Multi-Output Systems by Observability Range Space Extraction," *Proceedings, 31st IEEE Conference on Decision and Control*, Tucson, AZ, Dec. 1992.

[8] Lublin, L. and Athans, M., "Linear Quadratic Regulator Control" in *The Control Handbook*, CRC Press, 1996.

[9] Gupta, N.K., "Frequency Shaped Cost Functionals: Extension of Linear Quadratic Gaussian Design Methods," *Journal of Guidance and Control*, Vol. 3, No. 6, Nov.-Dec. 1980, pp.529-535.

[10] Eldred, K., "Acoustic Loads Generated by the Propulsion System," Technical Report, NASA SP-8072, NASA, 1971.

[11] Leo, Donald J. and Anderson, Eric H., "Vibroacoustic Modeling of a Launch Vehicle payload Fairing for Active Acoustic Control." *Proceedings, AIAA Structures, Structural Dynamics and Materials Conference*, Long Beach, CA, April 1998, pp. 3212-3222.

[12] Lee, Y.A., "Study of Helium Effect on Spacecraft Random Vibration with VAPEPS Program," *Proceedings, 59th Shock and Vibration Symposium*, Albuquerque, NM, Oct. 1998, pp. 119-135

[13] Weissman, K., M. E. McNelis and W. D. Pordan, “Implementation of Acoustic Blankets in Energy Analysis Methods with Application to the Atlas Payload Faring,” *Journal of the IES*, July/August 1994, pp. 32-39.

[14] Lee, Y. A. and Hendricks, W., “High Level Acoustic Noise Reduction with Helium in Shroud,” *Journal of the IES*, 1990, pp. 539-543.

[15] Nelson, P., Curtis, A., Elliott, S. and Bullmore, A., “The Active Minimization of Harmonic Enclosed Sound Fields, Part I: Theory,” *Journal of Sound and Vibration*, Vol. 117, No. 1, 1987, pp. 1-13.

[16] Nelson, P., Curtis, A., Elliott, S. and Bullmore, A., “The Active Minimization of Harmonic Enclosed Sound Fields, Part II: A Computer Simulation,” *Journal of Sound and Vibration*, Vol. 117, No. 1, 1987, pp. 15-33.

[17] Elliott, S. J., Nelson, P.A., Slothers, I. And Boucher, C.C. , “In-flight Experiments on the Active Control of Propeller-induced Cabin Noise,” *Journal of Sound and Vibration*, Vol. 140, No. 2, 1990, pp. 219-238.

[18] Blaurock, C. “PVDF Modal Accentuation Sensor,” 1998.

[19] Gere, J.M. and Timoshenko, S.P., “Mechanics of Materials”, PWS-Kent, Boston, 1990.

[20] Strang, G. “Introduction to Applied Mathematics,” Wellesley-Cambridge Press, Wellesley, 1986.

[21] Franklin, G.F., Powell, J.D. and Workman, M., “Digital Control of Dynamic Systems”, Third Edition, Addison-Wesley, 1998.

[22] Ogata, K. “Modern Control Engineering,”, Third Edition, Prentice Hall, New Jersey, 1997.

[23] Pierce, A.D., “Acoustics: An Introduction to Its Physical Principles and Applications,” Second Edition, Acoustical Society of America, 1989.

[24] Fuller, C.R. and Jones, J.D., “Experiments on Reduction of Propeller Induced Interior Noise by Active Control of Cylinder Vibration,” *Journal of Sound and Vibration*, Vol. 112, No. 2, 1987, pp.389-395.

[25] Baumann, W.T., Ho, F.S. and Robertshaw, H.H., “Active Structural Acoustic Control of Broadband Disturbances,” *The Journal of the Acoustical Society of America*, Vol. 92, No. 4, 1992, pp.1998-2005.

[26] Fuller, C.R. and Gibbs, G.P., “Active Control of Interior Noise in a Business Jet Using Piezoceramic Actuators,” *Proceedings, Noise-Con 94*, Ft. Lauderdale, FL, May 1994, pp. 389-394.